ANALYSIS OF FLAME IMAGES IN GAS-FIRED FURNACES

A Dissertation Presented to the Faculty of the Graduate School

University Of Missouri-Columbia

In Partial Fulfillment

of the Requirements for the Degree

Doctor of Philosophy

---

by
HANDI COKROJOYO

Dr. Shahla Keyvan, Dissertation Co-supervisor

Dr. Kannappan Palaniappan, Dissertation Co-supervisor

August 2007

The undersigned, appointed by the Dean of the Graduate School, have examined the dissertation entitled

ANALYSIS OF FLAME IMAGES IN GAS-FIRED FURNACES

Presented by Handi Cokrojoyo

A candidate for the degree Doctor of Philosophy

And hereby certify that in their opinion it is worthy of acceptance

_____
Dr. Shahla Keyvan

_____
Dr. Kannappan Palaniappan

_____
Dr. Hongchi Shi

_____
Dr. Ye Duan

_____
Dr. Daopu T. Numbere

ACKNOWLEDGEMENTS

My utmost gratitude for my co-advisor Dr. Shahla Keyvan, for her relentless guidances, inspirations and supports makes this dissertation possible. My sincere thanks for Dr. Kannappan Palaniappan for his insights and advices as my co-advisor. I am very grateful for the numerous assistances from my committee members, Dr. Hongchi Shi, Dr. Ye Duan and Dr. Daopu T. Numbere, thank you very much.

My thanks to my colleagues, Dr. Rodney A. Rossow, Dr. Dong Li, Dr. Hongbing Jiang, Scott Hixson and Huihao Fan for the invaluable time shared together within the research group through the years. Special thanks to the late Dr. Majdi Najm, for his mentoring and providing me opportunities that opened my career path; to Computer Science department secretary, Ms. Jodette C. Lenser, for her timely assistance and Mr. Renjith Stalin for his financial support on my dissertation defense.

I dedicate my work to my father, Mr. Sidius Cokrojoyo, my mother Mrs. Yanti Kurniawan and my sister Ms. Hilda Cokrojoyo. For I am forever grateful and indebted to them. Their love, patience, unending spiritual and emotional support made me who I am today. To God be the glory and may He bless you all.

TABLE OF CONTENTS

LIST OF ILLUSTRATIONS

LIST OF TABLES

ABSTRACT

Combustion is a key issue in gas-fired furnaces in various industries such as glass manufacturing. Its chemical reaction is based on two substances, oxidizer and fuel. Its quality depends on their composition, which are measured in terms of rate of flow and oxidizer to fuel (O/F) ratio by the furnace control system. Monitoring is crucial since improper composition produces hazardous byproducts and may waste expensive fuel.

This research proposes a promising system architecture that provides a method for assessing combustion quality by analyzing two-dimensional furnace flame image and correlates it with its fuel and oxidizer composition as reflected by the furnace control reading. The approach utilizes both image processing and machine learning techniques integrated with artificial intelligence techniques to identify correlations between flame characteristics and fuel flow rate and O/F ratio. Its conceptual design, implementation and evaluation are executed based on a set of experimental runs sampled at nine different composition of fuel and oxidizer flow rates taken from a pilot-scaled glass furnace.

A color CCD camera is used for capturing the furnace flame images. The images are processed using image processing techniques, from de-interlacing, cropping, image segmentation using Otsu's thresholding and image enhancement using proposed intensity suppression. Nine features are used to quantify the flame condition of which four are uniquely introduced in this study. Feature selection process is utilized to identify key features for the classification using wrapper method and decision tree classifiers. Fuzzy logic is then introduced to provide capability in classifying fuel level and O/F ratio beyond the known test data. Membership functions are designed and modeled based on key features output distribution, using generalized bell curve shape with parameters obtained by curve fitting and cubic interpolation technique.

The final architecture is implemented, tested and proven capable to provide insight into the combustion quality in term of its fuel and O/F ratio class within seconds.

1. INTRODUCTION

1.1 Overview

Energy consumption of perishable source such as fossil fuels is a major concern in today's world, for it is still the key source that many industries depend upon. In fact, it is still the primary source of energy that provides relatively 90% of the world's demand [1]. One particular usage of fossil fuels would be for combustion-related industries, where it will remain to be important today and centuries to come [1].

A form of resource management is important for fossil fuel since its consumption always increases and implies economical consequence. Furthermore, inefficient combustion processes have negative outcome to the environment. The study of combustion process therefore becomes necessary and is a growing field of research [1].

This particular study is conducted based on the effort to assess efficient combustion for glass furnaces, focusing on its fuel and oxidizer level intakes relationship with the resulting flame. The main goal is to increase its energy efficiency and reduction of hazardous by-products, by providing an assessment of the flame quality, using machine learning approach.

This chapter will be primarily focused on the brief introduction and overview on the subject, along with the general motivation behind the study itself.

1.2 Combustion and Its Application Overview

The combustion process is also commonly known as burning process. It is a rapid chemical process that involves a pair or more materials, producing both heat and light [2, 3]. In a typical combustion process, two key substances are involved: fuel and oxidizer [2]. For example, when woods are burn in open air, the combustion process here involves woods acting as fuel and air as oxidizer. In this study, the furnace flame is produced using methane (CH4) for fuel and oxygen (O2) is used as the oxidizer.

There are various types of combustion exists based on the characteristic of fluid motion of the flame and how its fuel and oxidizer are mixed. If the fuel and oxidizer are mixed prior to combustion, it is called premixed flame. Otherwise, it is referred as non-premixed or diffusion flame where the mixing occurs during the combustion process. Two types of fluid motion of flames are defined, called laminar and turbulent. Laminar flames have flow motion characteristic that is in parallel layers, following the contours of adjacent solid surface. Another type is called turbulent. It is characterized by having flow motion with irregular fluctuation [2]. Different type of combustion produces different visible characteristic of the flame. Particularly for combustion process in glass furnace, including the ones observed in this study, they are turbulent diffusion flame type.

If the combination of oxidizer and fuel is such a way that they consume each other completely, it is a complete combustion and the resulted flame is defined to be in stoichiometric condition. EQ (1.1) shows a stoichiometric equation by using oxygen as oxidizer and methane as fuel. The chemical reaction from a complete combustion will result carbon dioxide, water and heat [2].

$$CH_4 + 2O_2 \rightarrow CO_2 + 2H_2O \qquad \text{EQ (1.1)}$$

The oxidizer to fuel (O/F) ratio is used to depict the composition of fuel and oxidizer used. The proper composition of fuel and oxidizer is necessary to result the stoichiometric condition with O/F ratio of 2.0. In a condition where there is more fuel than necessary, defined as "fuel rich", the ratio will be lower than 2.0 and pollutants such as carbon monoxide (CO) will be produced. If fuel is less, defined as "fuel lean", the ratio will be higher than 2.0 and results in an increase of nitrogen oxide (NOx) emissions. Both fuel rich and fuel lean conditions imply inefficient combustion with hazardous byproducts that is harmful for the environment [2].

Note that financial saving is an incentive for this study as well. An optimal combustion insures consistent product quality, improved furnace reliability and longer service live of combustion-related subassemblies. Moreover, inefficient combustion clearly has a negative cost implication since fuel is expensive. A typical glass furnace that produces 200 tons of glass daily, consumes approximately 2.4 million dollars worth of fuel [4].

1.3 Combustion Quality Assessment

Conventional approaches monitor the combustion quality in various ways. At the simplest form, there will be a periodical observation by furnace operator on the actual flame through manual operation or by the assistance of video camera. Additionally, pyrometer and thermocouples can be used as well [5, 6], which provide temperature readings on the flames. Their effectiveness is however limited to their physical installation location and observation region. The accuracy is typically low and delay exists between the actual combustion's temperature and their readings.

A more recent approaches implements more sophisticated instruments such as spectrometer [4, 7], ratio pyrometer [8, 9], laser-based [10, 11, 12] and fiber-optic sensor

probes [13] which able to provide a more accurate assessment of the combustion quality based on temperature approximation. These approaches however can only provide observation on a specific and limited region, such as a straight line or a very small surface area [14]. Multiple instruments will be needed depending on the size of the furnace and number of flames to be monitored which may not be an economical solution. Some of the approach also requires the need for object insertion into the furnace which may not be desirable from the furnace maintenance point of view. For example, laser-based method may require the introduction of chemical substances to be added into the flame. In this sense image analysis approach is more attractive since it does not require physical contact with the combustion process. Moreover, a single camera alone has the potential of providing wider area that can be analyzed. Additionally, camera equipments are less inexpensive and have simpler installation and maintenance requirement.

In related to methods using image analysis approach, various different techniques have been proposed in both industry and research field. Typically the investigations are done in the ultraviolet and visible spectrum since the emissions produced by the combustion process can be correlated within their range [15, 16, 17]. Successful or promising results have been shown both in research and industrial area with methods varies depending on the purpose, such as measuring pollutants, fuel intake or combustion stability [18, 19, 20, 21, 22]. The advancement in imaging system also opens more possibility for flame image analysis, such as the utilization of high speed and multi-spectral camera [23, 24].

1.4 Overview of Dissertation

The main focus of this study is in designing a complete system, using machine learning approach and inexpensive equipment to provide combustion assessment tool for gas-fired glass furnace. Physically the system requires two primary devices: a CCD camera to acquire the images from the furnace's interior and a workstation to run the image analysis software. Figure 1.1 shows the proposed general process flow used for the system. The camera is involved in the process for the image acquisition, afterwards the analysis is done using the workstation and it interfaces with the furnace control to provide the flame analysis result.

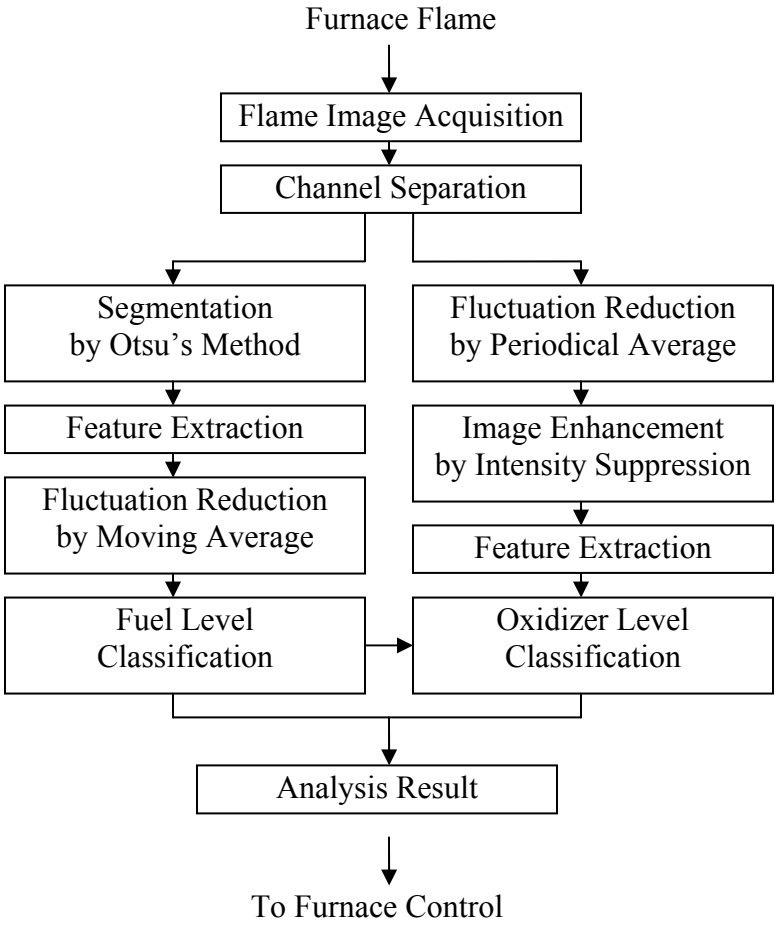

Figure 1.1 Proposed Image Analysis Process

The process flow follows a conventional machine learning process. The acquired digital color images are converted into grayscale images based on its R, G, B, H, S and V channels. Afterwards, two different process and analysis paths are required. One path classifies the fuel level, while the other classifies oxidizer level. As discovered from this study as well, fuel level classification result is needed to classify oxidizer as well.

The flame assessment is based on the fuel level and O/F ratio classification. The idea is that the system will be able to tell whether the combustion is at fuel lean, fuel rich or stoichiometric condition at varying level of fuel and oxidizer. Since the fuel level can be classified, it can provide information on what need to be adjusted if the combustion process is not at stoichiometry.

A preliminary study has been done as well in evaluating the feasibility of using images analysis to assess combustion technique in glass furnace with promising results [25]. This study share and support the same idea but utilizing different strategy to design comprehensive expert system architecture for possible implementation and integration with furnace control. Additionally, unlike previous approach, the design also gives a possibility for a real-time analysis.

This dissertation is organized as follow: Chapter two provides information on the image acquisition process from the CCD camera. Chapter three covers image preprocessing to distinguish the flame region from the background image which is necessary so that features can be extracted properly. Chapter four provides the description of the features characteristics and strategies for analyzing the flame images. Key feature selection and its application for classifying fuel and oxidizer level is discussed and examined in chapter five along with the results based on experiment

conducted on pilot-scaled glass furnace. The assessment of the combustion quality is then discussed in chapter six which proposed ways to build rules using fuzzy logic approach based on the key features thus completing the proposed architecture as shown in Figure 1.1. Conclusion from this approach, future direction and improvement suggestions are discussed in chapter seven.

2. IMAGE ACQUISITION PROCESS

2.1 Overview

Image acquisition process involves several steps which include capturing images from the flame in the furnace, extracting information from the physical phenomena based on the visible spectrum of light scene and converting it into its digital representation in the form of spatial two-dimensional color images. The acquisition process and utilization of Charge-coupled devices (CCD) camera are discussed in this chapter.

2.2 Color Representation

Imaging system works by collecting radiation information that is emitted by the objects and scene [26]. For human eye, the radiation is based on a narrow band of frequencies in the electromagnetic energy spectrum with wavelengths ranging from 360 nm to 800 nm [27]. This range is known as visible light spectrum as shown in Figure 2.1.

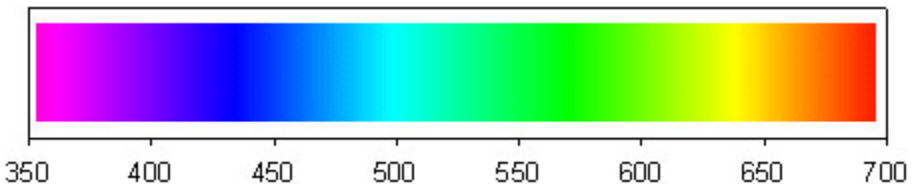

Figure 2.1 Range of Visible Spectrum in Nanometers

The camera utilized in this study is used to capture information emitted by lights in the visible spectrum and produces a visual reproduction for both human observer and image analysis purpose. It is designed particularly for human observer, such that the visual information is acquired mostly from the visible spectrum. The information then can be recreated on other imaging device, i.e., display device such as monitor or printing

device such as printers. This information exchange requires a standardized means of for its representation which is achieved by using color models.

Color models are typically a three-dimensional coordinate system, where each color is represented as a point within the subspace [28]. There are various types of color models available for various purpose and applications, each with their own strength and limitation. In this study, RGB and HSV color models are selected and utilized as discussed below.

2.2.1 RGB Color Model

RGB color model is a type of additive color model that uses three primary color channels or components to describe colors: red, green, and blue [29, 30]. The additive nature means production of colors based on combining any of the three primaries. Combination of the three components with equal maximum intensity yields white color while the absence of all of them yields black. A combination of every two of the three components will yield secondary colors. Figure 2.2 shows the additive nature of RGB color space. Other colors are reproduced based on the variable combination of the three primaries. Figure 2.3 shows a sample of RGB color space with its three axes representing the three primary components ranging from 0 to 1.

Figure 2.2 Additive Nature of RGB Color Model

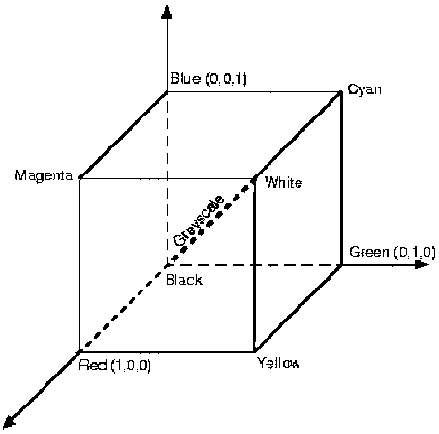

Figure 2.3 RGB Color Model

RGB's color model is related to human's trichromatic visual system. Human perceive colors based on the combination of three primary colors: red (R), green (G), and blue (B). Each of these primary colors corresponds to the three types of conic photoreceptors cells located in human eye [27]. Each type has different sensitivity towards different range in the visible spectrum. They are named as long (L), medium (M) and short (S) according to their wavelength sensitivity [27]. The various combinations of stimulation to the three types of photoreceptors are translated by the brain into what perceived as "colors" in human visual system. The sensitivity of each photoreceptor however is not uniform and varies from one person to another. Hence color perception can be very objective without any available guideline.

In 1931, The Commission Internationale de l'Eclairage or The International Commission on Illumination (CIE) standardized human spectral response and set a specific wavelength values for the three primary colors. These values are: blue = 435.8 nm, green = 546.1 nm and red = 700 nm [26, 28]. Figure 2.4 shows the human spectral response based on the CIE standard. The standard helps in defining the primary components characteristic in imaging devices designed for human observer such as television and monitor display.

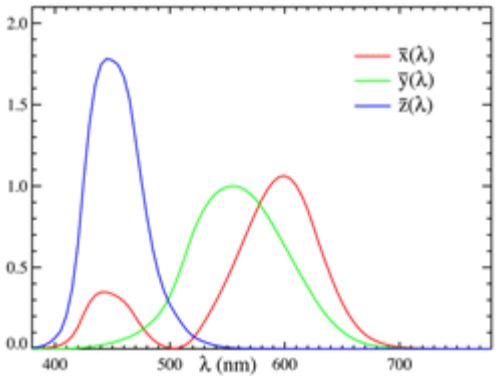

Figure 2.4 Human Color Perception Sensitivity

RGB color model is convenient to use in this study since it is the native color model for image representation in the hardware devices such as the camera and monitor display. In this particular study the native format is 24 bit RGB, where each primary color is represented by an 8-bit integer values. Hence each channel has the range of 0 to 255 with a total combination of approximately 16 millions possible colors.

RGB representation of colors is not perceptually intuitive for human observer. This is due to non-uniform spectral response in human perception. For example, if one doubles the intensity of a color (i.e., R:127 G:127 B:127 to R:255 G:255 B:255), it will not be perceived as twice as bright by human observer [26]. Hence for an analysis that involves human visual judgment, RGB color model may not be sufficient. This is the reason for the inclusion of HSV color model as discussed below.

2.2.2 HSV Color Model

Created in 1978 by Alvy Ray Smith, HSV is a color model that also represents colors using three components as well. The components however designed for describing color the way a human would. The three components in HSV color model are hue (H), saturation (S) and value (V).

Hue is an attribute associated with the dominant wavelength in a mixture of light waves [28, 31]. For example, a light wave with central tendency of 565 to 590 nm will be perceived as "yellow" by human observer. In HSV color model, hue represents the dominant color as observed by the human eye and measured in degree from 0° to 360°.

Saturation measures how vivid or pure a color is. The purity refers the amount of "white" color mixed with a hue. A highly saturated color implies a pure color while no saturation makes the hue appear grey. The degree of saturation is inversely proportional to the amount of white light added. White color has zero saturation.

Value represents brightness of a color. While hue and saturation defines chromaticity, value represents the achromatic notion of its intensity. Pure achromatic colors range from black to white with all the possible gray colors in between.

HSV color space can be represented in various ways. One typical representation is using a conical model as shown in Figure 2.5. Hue is represented by the angular degree of the cone. Saturation is represented by the distance from the center of any circular cross-section of the cone. Value is represented by the distance to the bottom of the cone. The conical shape represents limitation of human vision in differentiating chromaticity at different level of brightness [26].

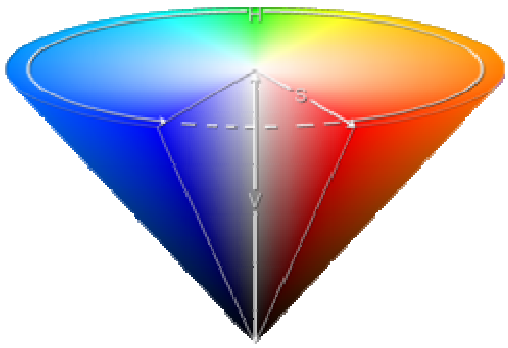

Figure 2.5 HSV Color Space

Since for this study the native color model is RGB, a nonlinear transformation operation is required to express the color in HSV format. Hue parameter has a range of 0 to 359, while both saturation and value have a range of 0 to 255. EQ (2.1) shows the formula for the conversion from RGB to HSV.

$$H = \begin{cases} n/a & if \quad Max = Min \\ 60\dfrac{G-B}{Max-Min} & if \quad Max = R \quad and \quad G \geq B \\ 60\dfrac{G-B}{Max-Min} + 360 & if \quad Max = R \quad and \quad G < B \\ 60\dfrac{B-R}{Max-Min} + 120 & if \quad Max = G \\ 60\dfrac{R-G}{Max-Min} + 240 & if \quad Max = B \end{cases}$$

$$S = \begin{cases} 0 & if \quad Max = 0 \\ 1 - \dfrac{Min}{Max} & if \quad Max \neq 0 \end{cases}$$

$$V = Max$$

EQ (2.1)

where R = Red value from RGB, $R \in [0,255]$
G = Green value from RGB, $G \in [0,255]$
B = Blue value from RGB, $B \in [0,255]$
H = Hue value for HSV, $H \in [0,360]$
S = Saturation value for HSV, $S \in [0,255]$
V = Brightness value for HSV, $V \in [0,255]$
Max = The maximum value of the color's R, G and B components
Min = The minimum value of the color's R, G and B components

Aside for improving visual observation on the image, HSV color model proves to be useful in the image analysis process as discussed in the later chapters.

2.3 Image Acquisition using CCD Camera

Camera plays a very crucial role in the image acquisition process since it affects how the visual information is obtained from the real world scene. For this study, a camera with charge-coupled device (CCD) sensor is utilized. Technical specifications for the camera utilized here are provided in Appendix B [32].

2.3.1 CCD Technology

CCD is a common imaging technology used for image acquisition process in digital photography as well as machine vision application. Invented in 1969 by Willard Boyle and George Smith at AT&T Bell Labs, CCD is an image sensor technology that utilizes integrated circuit (IC) consisting of linked or coupled array of light-sensitive capacitors [33, 34].

CCD has a characteristic of being small in size and very light in weight. It also possesses a very high dynamic range with a near linear correlation between the incoming light energy and the produced electric signal [34].

2.3.2 Measuring Sensitivity

The quality of the visual information captured by CCD can be expressed using spectral response curve. The curve defines its output per incident light energy per wavelength within its operating spectrum range [26]. Different type of CCD has different spectral response depending on the manufacturing technique.

Sensitivity is measured as percentage of photons from the incidental lights that are converted as electrical signal by the device. This sensitivity is wavelength specific. Figure 2.6 shows the spectral response curve of the particular CCD camera used in this study.

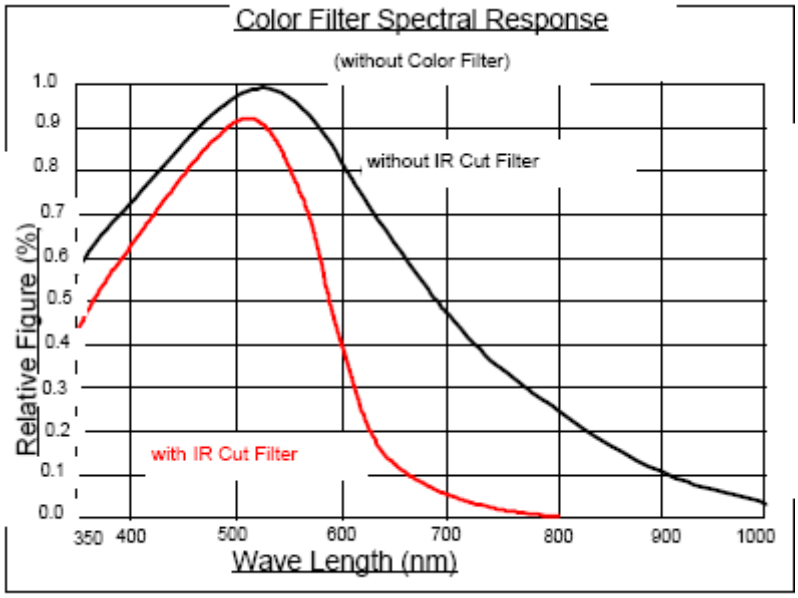

Figure 2.6 Spectral Response Curve

The IR cut filter is installed to remove unwanted information outside the visible spectrum range so that the acquired image remains similar to what a human observer would see. Human observation is used to confirm correctness of the acquired images. As shown in Figure 2.6, with the IR cut filter installed, the CCD image sensor has sensitivity range from 350 to 800nm.

2.3.3 Expressing Color Information with Single CCD

The camera used in this study is a single chip CCD as implicated by the single curve in the spectral response curve as shown in Figure 2.6. Although this indicates that the camera is monochromatic, the actual resulting acquired image is in colors. To depict colors, a color filter array (CFA) is used. It is placed on top of the CCD chip after the IR cut filter as shown in Figure 2.7 [34].

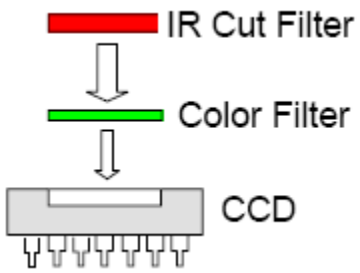

Figure 2.7 Usage of Color Array Filter

CFA is composed of various color filters aimed to specific visible wavelength. The filters are placed to split the incoming colors into its components. The filters are designed in a mosaic pattern, where each filter provides one color component to one capacitor on the CCD beneath it. The total number of filter in the CFA equals to the total resolution of the CCD camera. Figure 2.8 shows the mosaic pattern used for this camera known as CYGM CFA which contains filter for cyan, yellow, green and magenta.

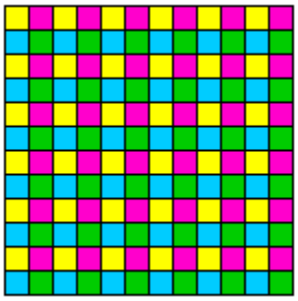

Figure 2.8 CYGM Color Filter Array

The approach implies that each pixel on the image has only one genuine color component extracted from the scene. To obtain the information of the missing components for depicting the color of the pixel, it utilizes estimation algorithm based on its neighboring pixels' information called "demosaicing" [35].

CFA filters are widely used since the camera only need a single CCD chip to produce color images. It makes the camera inexpensive and more affordable with the tradeoff on color fidelity. Alternatively one can utilize a more expensive three chip CCD. However, three chip CCD cameras have lower light sensitivity. Another alternative is X3 technology that enables a single image sensor to detect actual three color components of a single pixel using variable-depth photo detectors [36]. .

Fortunately for this study, based on the experimental results, a single CCD camera is sufficient to achieve the desired goal. The lesser color fidelity effect is suppressed since the image processing and analysis applied to the images are focused more on aggregated image regions rather than on specific individual pixel.

2.3.4 Adjustment in CCD Camera

There are several parameters available to adjust the CCD camera to accommodate various scene conditions, such as shutter speed and gain control. The acquisition rate of the CCD camera is defined at 30 frames per second. That is, the electrical voltage contained within the capacitors on the CCD will be read every $1/30^{th}$ of a second. This rate is not adjustable. To manage the amount of light exposed to the CCD, two parameters can be adjusted within CCD camera, the shutter speed and gain control.

Shutter speed is mechanism that resides on the camera for controlling the rate of exposure time. The shutter speed can be adjusted from 1/60 per second to 1/10,000 per second. For this study the shutter speed is set to be 1/60 per second which is the default setting.

Gain control provides adjustment on the electrical current coming from the CCD chip. Gain adjustment affects both the electrical signal of the actual data and its associated background noise [26,37]. For this particular study, no gain adjustment is made.

2.4 Periscope Components

To protect the CCD camera from high temperature environment in the furnace, it is encased inside a water-cooled steel shell and called borescope or periscope [38] as shown in Figure 2.9. The periscope has an objective lens with a 90-degree view angle so that it can provide a detailed view of the furnace's interior. The lens is kept clean by the purging air at the tip of the periscope.

Figure 2.9 Periscope Components

The periscope is inserted into a port located on the furnace wall. Two additional adjustments can be made on the periscope related to the image quality: iris and focus. Iris affects how much light can enter the periscope, while focus adjusts the focus of the image.

Once the physical setup is complete, the visual information captured by the camera is recorded and prepared for the next step.

2.5 Flame Image Preprocessing Preparation

Before the images are processed further, two additional preparation must be applied to the images which are deinterlacing and image cropping as discussed below.

2.5.1 Deinterlacing

The particular CCD camera used in the study is an interlaced camera. Interlacing technique is originally a technique in video transmission to maintain a good image quality within a limited frame rate or bandwidth. An image is captured in a horizontal direction, row by row from top to bottom. The rows are numbered from top to bottom, starting with number 1, such that they can be defined as odd or even fields according to their row number. As illustrated in Figure 2.10 below, for an image with 6 x 6 pixels resolution, each of the odd and even field has 3 rows. During image acquisition process, one field is filled with the visual information first before the other. For an interlaced mage with acquisition rate of 30 frames per second, it implies that the rate of each field is 60.

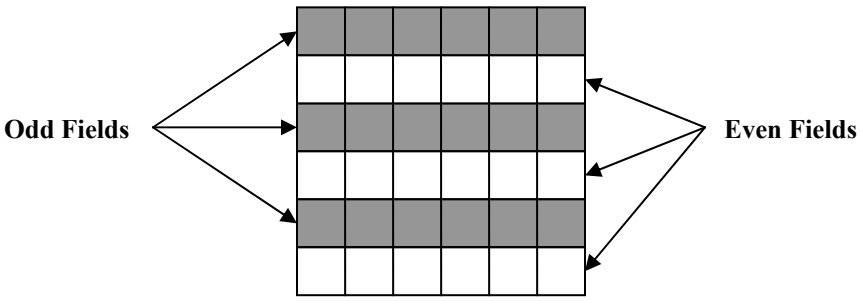

Figure 2.10 Example of Interlaced Image Structure

Images acquired using interlacing can be a problem if the object within the scene moves or changes faster than the acquisition rate. The reason is visual discrepancy between the odd and even field within the same image frame as shown in Figure 2.11.

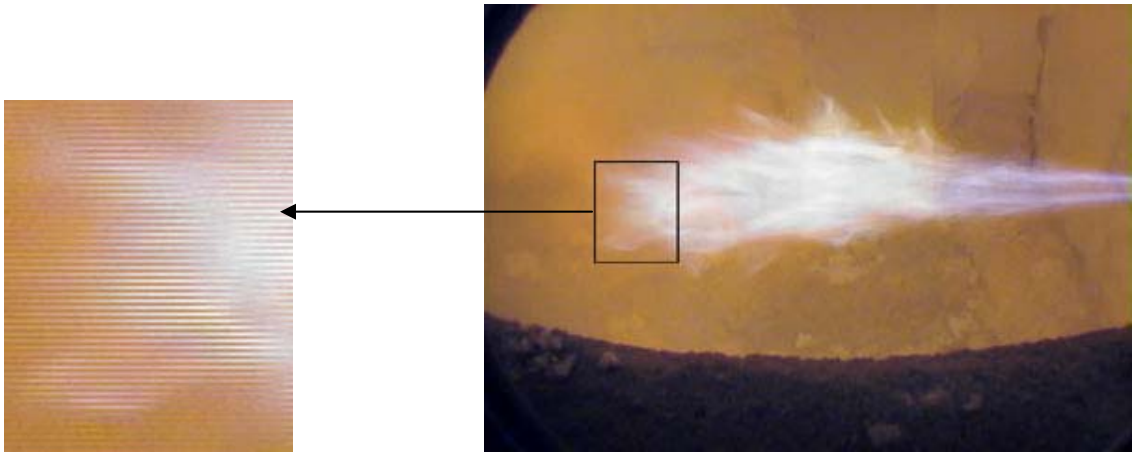

Figure 2.11 Problem with Interlaced Image

Deinterlacing process is needed to remedy the situation. There are various different methods available to do this which usually involves interpolation [39, 40, 41]. In this particular study, the approach taken is to convert the original image into two sub images based on the field group. This approach will reduce the original resolution by half; however it maintains the original image information intact. Figure 2.12 illustrates the deinterlacing process of the original acquired image and also shows the differences in the flame's shape between fields.

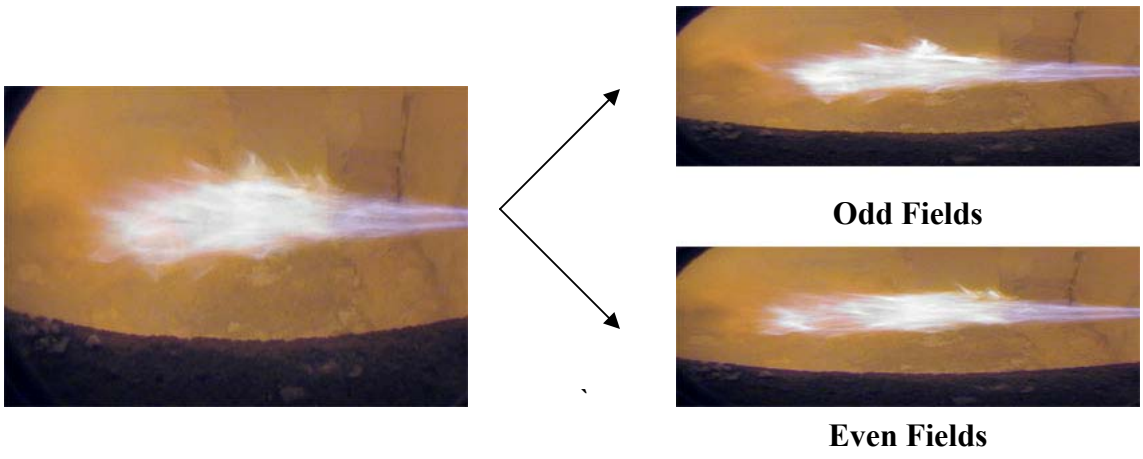

Figure 2.12 Deinterlacing Example of an Image Frame

2.5.2 Cropping

During the image acquisition process, one must divide the image into different regions in order to discard unwanted trivial regions such as port walls as shown in Figure 2.13. The cropping process also reduces the amount of information to be processed in the following step. Further discussion of impact and usefulness of cropping will be provided in the later chapters.

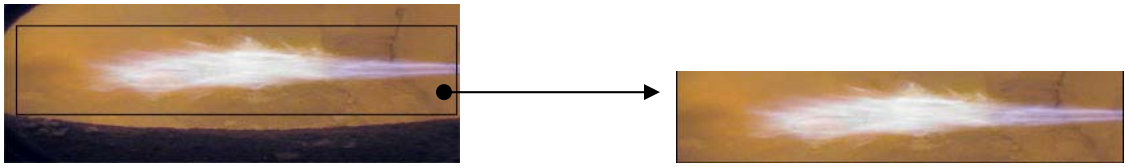

Figure 2.13 Cropping an Image Frame

Once the deinterlacing and cropping processes are completed, the acquired images are ready to be analyzed further as discussed in the next chapter.

3. FLAME IMAGE PREPROCESSING

3.1 Overview

Preprocessing is the first step applied on the flame images such that desired information can be extracted and analyzed on the subsequent stages. The goal is to find a way to minimize the impact of non-flame (background) region on the flame images, such that the image would only contain the flame region. This process is necessary in order to extract the desired information about the flame from its image.

Two possible approaches are proposed in this study. First is through the process of segmentation, which can be defined as a process of subdividing images into desired parts [42]. Particularly in this study, the segmentation process will subdivide the image into two parts, flame and non-flame regions. Another approach is through image enhancement technique, which is specifically designed and proposed for this study. This new approach is based on scaling by power function to emphasize flame region while suppressing background or non-flame regions. Both methods have their own advantages and limitations as will be discussed in this chapter.

3.2 Segmentation Approach

In segmentation approach, one would subdivide the image into sub-images based on certain criteria. For this study, the image will be segmented into two sub-images, the flame and non-flame regions. Figure 3.1 shows an example of a flame image before and after segmentation, with zero (black) pixel intensity is assigned to non-flame region.

There are numbers of possible techniques for segmentation process [43, 44] and Otsu's thresholding technique [45] is selected in this study. The characteristics and implementation of this technique will be discussed in this chapter.

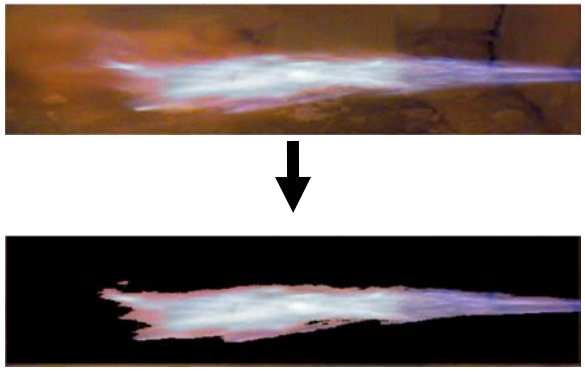

Figure 3.1 Sample of a Flame Image before and after Segmentation Process by Otsu Thresholding Technique

Prior study [25] also utilized a segmentation step as well. Although a different segmentation technique, nevertheless the segmented flame images contain relevant information that strongly correlate with the flame condition regardless of the chosen technique.

The segmentation procedure can be achieved with a rather simple but effective approach due to the favorable condition of the images in this study as explained below.

First, the types of objects that may exist in the images are known. Although the flame moves, its movement is within a boundary that can be approximated well. The

pixels' intensity that constitute to the flames region in the images consistently have higher value or are brighter as compared to the non-flame regions. The non-flames regions mostly depict the furnace wall. As compared to the flame regions; the background pixels' intensity are substantially lower. Therefore, any procedures that can successfully separate between regions with lower pixel intensities and higher ones will provide the desirable segmentation.

Previous study segments the image based on a manually selected set of threshold values beforehand. These values act as thresholds for red, green, blue, hue, saturation and value channel such that any pixel values above the threshold will be left as is and zero otherwise.

Although proven to be effective, the prior segmentation approach has several limitations. First, the selected thresholds are constant values which are determined based on a few selected images acting as the reference or ground truth. This can pose a problem since it might segment the subsequent images incorrectly should the flame behavior differs from the reference. Furthermore there are no clear criteria on choosing the reference themselves. Lastly, the threshold values are picked based on domain expert's view and assessment on how the segmented results should look like which is potentially subjective.

In this regard, a more robust and dynamic method of segmentation is needed. The technique should not require a priori known reference rather it should be adaptively segment each image while providing acceptable confidence on its segmentation quality. Moreover, to make it more practical, segmentation process should be done automatically instead of requiring manual setup.

There are many different methods on how one can segment an image. Particularly for color images, they have varying degree of complexity and sometimes may result more than one segmented object. However, due to the particular image characteristics the separability between flame and non-flame regions is possible as discussed before and the procedure can be simplified to grayscale segmentation.

Each channel of a single image will be treated as a grayscale image that will be segmented separately. Hence for each image, there are six possible segmentation results based on red, green, blue, hue, saturation and value channel. For each channel, now treated as grayscale images, the image will be segmented into flame and non-flame regions. Note that each channel will depict the notion of 'flame region' quite differently as shown in Figure 3.2. Each of the six grayscale images shows consistency of separability between flame and non-flame regions. The degree of separability is different for each channel based on its color space property. Otsu thresholding method is selected and utilized for the segmentation procedure.

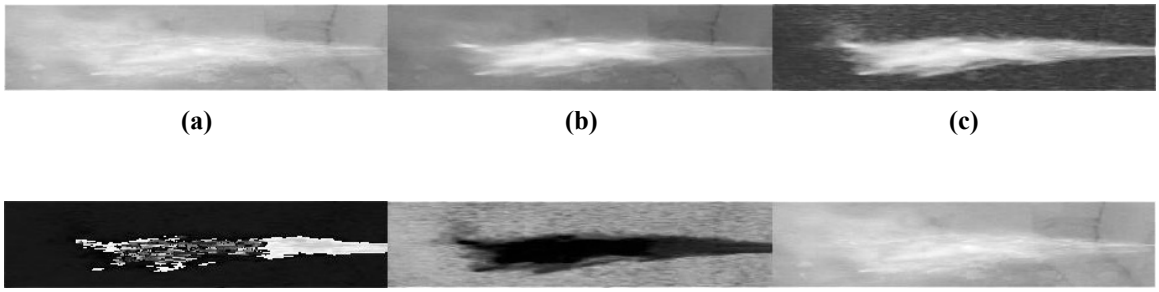

Figure 3.2 Six Grayscale Images Derived from Image in Figure 3.1 Depicting (a) Red, (b) Green, (c) Blue, (d) Hue, (e) Saturation and (f) Value Channel

3.2.1 Otsu Thresholding

Otsu threshold is a segmentation technique based on finding the optimal threshold T that would separate an image into two classes (e.g. black and white). The optimal threshold in this case is defined as the intensity value that would maximize the uniformity within each class or minimize the within class variance of its pixel intensity distribution [45]. The assumption is that the image can indeed be separated into two classes, which fits well to the flame image segmentation task.

Once the threshold T is selected, image's pixels will be grouped with one class for all values below or equal to T and another class for greater than T. The characteristic of the segmentation can be better understood by analyzing on how the thresholding technique works.

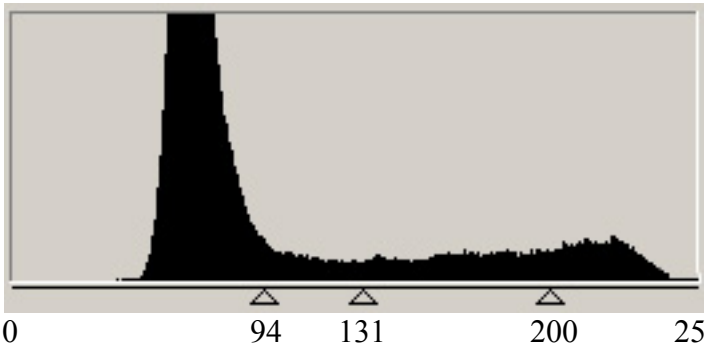

Figure 3.3 A Sample Pixel Distribution for The Blue Channel of a Flame Image

A sample pixel distribution is shown as histogram in Figure 3.3 that is derived from the blue channel of the flame image depicted in Figure 3.2. The pixel intensity value ranges from 0 to 255, with 0 being pure black and 255 pure white. The threshold T thus has a range from 1 to 254. There can be many possibility of choosing the threshold T to achieve the desired segmentation.

Figure 3.4 shows a sample of segmentation results, using two different manually selected thresholds at 94 and 200. Using Otsu's method, the threshold would be calculated as 131.

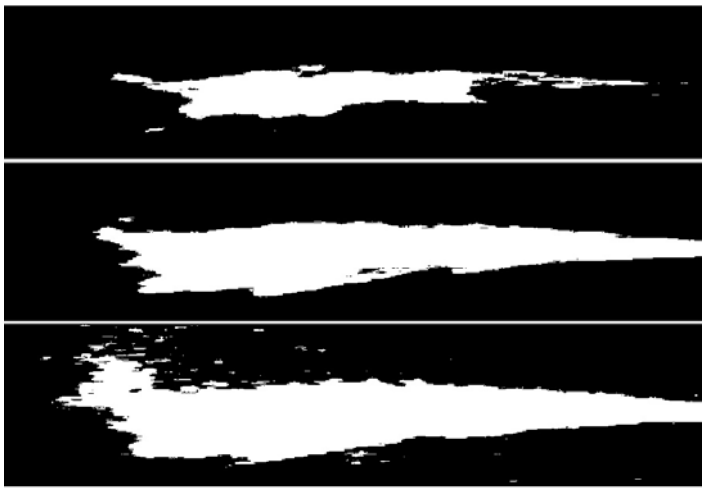

Figure 3.4 Segmentation Results using Threshold at 200, 131 and 94 (Top to Bottom)

Using the image from the blue channel for an example, as shown in Figure 3.4, the flame regions are classified as white pixels. A different threshold value yield a different size of the flame regions. As shown in this example, lower threshold will classify soot as white. Soot regions do contain useful properties according to some studies for other combustion condition [46, 47] but still unknown for the combustion observed in this study. At higher threshold, the flame regions shrinks since some part of it are classified as non-flame region or black pixels. Hence, by changing the threshold one can change the size of the flame regions. The key question is how to obtain the optimal threshold.

Otsu's thresholding is a method which attempt to find the threshold T that separates the image into two classes by maximizing the cost function σ (See EQ 3.6)

through iterative process. The two classes in this case would group the image pixels based on their intensity values, representing the flame and non-flame regions.

There are two general types of Otsu threshold methods, global and local. Global method calculates threshold T that classifies the entire pixel in the image and segment it into two classes. On the other hand, local method computes more than one threshold T, each of them segments some parts and subsets of the whole image. The size of the subset is predetermined manually. Local method is preferable if the image is expected to contain or can be separated into more than two classes. Since the flame image is expected to have only two classes, global method is chosen for the task. The method's algorithm utilizes a set of equations as shown in EQ (3.1) to EQ (3.6).

The Otsu algorithm can be summarized as follow:

1. Set threshold = 1, $\sigma' = 0$.
2. Iterate from x = 1 until 254 do step 3 to 6:
3. Compute $q_1(x)$ and $q_2(x)$
4. Compute $\mu_1(x)$ and $\mu_2(x)$
5. Compute σ.
6. If $\sigma' < \sigma$, set σ' to σ and threshold to x

$$0 \le i \le 255,\ 0 \le P(i) \le 1,\ \sum_{i=0}^{255} P(i) = 1 \qquad \text{EQ (3.1)}$$

where P(i) = Total number of pixels with intensity value i

$$q_1(x) = \sum_{i=0}^{x} P(i) \qquad \text{EQ (3.2)}$$

where $q_1(x)$ = Total number of pixels with intensity 0 to x

$$q_2(x) = \sum_{i=x+1}^{255} P(i) \qquad \text{EQ (3.3)}$$

where $q_2(x)$ = Total number of pixels with intensity x to 255

$$\mu_1(x) = \frac{1}{q_1(x)} \sum_{i=0}^{x} \frac{i}{255} P(i) \qquad \text{EQ (3.4)}$$

where $\mu_1(x)$ = Average pixels intensity for pixel intensity 0 to x

$$\mu_2(x) = \frac{1}{q_2(x)} \sum_{i=x+1}^{255} \frac{i}{255} P(i) \qquad \text{EQ (3.5)}$$

where $\mu_2(x)$ = Average pixels intensity for pixel intensity x to 255

$$\sigma = q_1(x) q_2(x) \left[\mu_1(x) - \mu_2(x)\right]^2 \qquad \text{EQ (3.6)}$$

where σ = cost function

The method can be understood by examining the formula and algorithm above. To begin with, it is an iterative method that attempts to find the maximum σ, such that both class' averages, $\mu_1(x)$ and $\mu_2(x)$, will have maximum dissimilarity for some $q_1(x)$ and $q_2(x)$. This implies that the two classes are optimally separated.

The summation of $q_1(x)$ and $q_2(x)$ is equal to 1, thus they can be considered as probability of $q_1(x)$ and $1-q_1(x)$ ("Not" $q_1(x)$) given pixel intensity x. The product of both components $q_1(x)$ and $1-q_1(x)$ will find T such that the resulting variance will be minimum for each class. In other word, each class will contain pixels with most similar intensity values.

Thus the method can be summarized as an attempt to find a threshold T that will minimize variance within the same class and maximize variance between the two classes.

A flame image always can be segmented into two classes. This is because pixels' intensity from the flame region is always different from that of non-flame. At the same time, pixel intensities within the flame region, are very uniform with relatively little variance. This situation will guarantee a low variance for 1 class. However the non-

flame region's pixel intensity might not necessarily be uniform as previously shown in Figure 3.4. Since this is a two-class classification problem, fortunately by successfully classifying one class, it will indirectly classify the others into one. This is reflected by the $q_1(x)$ and $1-q_1(x)$ component in Otsu's method.

One special condition need to be taken care of with the automated thresholding method. This is a condition when the flame is shut off, thereby creating a situation where the threshold T value will be meaningless. Fortunately the condition can be detected based on the range of threshold T value. Without the flame, the pixel intensity of the entire image has little variance and relatively dimmer which lead to lower range of threshold T values compared to when flame exists in the image. This range can be determined through experiments.

3.2.2 Segmentation Result

Based on the experimental results, Otsu's method applied on the six channels consistently yields good segmentation quality. The quality of segmentation do differs for each channel, some better than the other. In general, they are able to separate the flame regions as shown in Figure 3.5. Blue channel in particular has a very good segmentation quality. This is due to the fact that the flame region in the original image is significantly more saturated and brighter than its surrounding as visually apparent from the grayscale images shown in Figure 3.2.

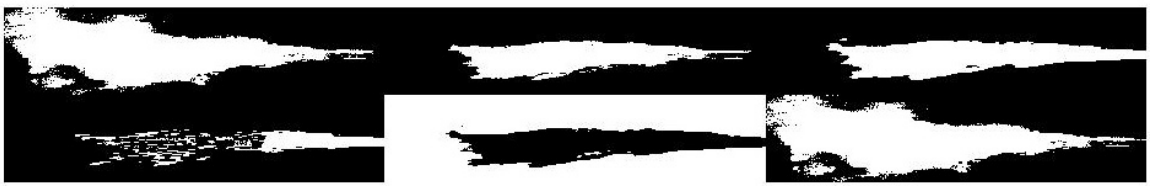

Figure 3.5 Sample of Otsu's Threshold Results on Red, Green, Blue, Hue, Saturation and Value (Left to right, top to bottom)

There is no guarantee however, whether Otsu's method would outperform or as good as manual segmentation done in the previous study. Nonetheless it has the advantage of providing automated segmentation and the computation is adaptive, i.e. it takes into account the nature of the images. Based on the experiments in this particular study, it works very well for this particular study.

The method has its disadvantage nonetheless. Compared to manual thresholding, it is much more expensive to calculate, thus affects the entire system performance substantially. However based on the experiments, the performance is still quite acceptable. With a more powerful hardware and resources, eventually this will not be a problem.

Once segmentation is applied to the images, six different results will indicate the flame regions in black and white, as shown in Figure 3.5. Except for saturation channel's result, white region represents flame regions. For the other channel, higher pixel intensity in the image indicates pixels that represent the flame region. For saturation, lower pixel intensity represents the flame regions since zero saturation implies least saturated pixel. Least saturated implies the 'whitish' regions in the original image which corresponds to the flame region.

These black and white images shown in Figure 3.5 are also called 'masks'. The system would use them to determine where the flame region would be. Information will be extracted only from the flame region as indicated by these masks as white pixel. The masking process is shown in EQ (3.7).

$$P'(x,y) = P(x,y) \times M(x,y) \qquad \text{EQ (3.7)}$$

where P'(x,y) = pixel intensity on the masked image at coordinate (x ,y)
P(x,y) = pixel intensity of the original image at coordinate (x ,y)
M(x,y) = pixel intensity of the mask at coordinate (x ,y) which is either 0 for black or 1 for white

A sample of a masked image result is shown in Figure 3.6 which is the result of the mask created by applying Otsu threshold method on the blue channel.

Figure 3.6 Masked Image based on Segmentation Mask derived from the Blue Channel

3.2.3 Segmentation Limitation

Aside from the advantages of incorporating Otsu method, there are several limitations that need to be addressed and discussed as well.

One possible drawback in using Otsu method is its dependency upon the size of the crop window. The crop size will completely include the flame region by default, however there are flexibility in determining how much non-flame regions is needed in order to exploit Otsu's thresholding property in achieving the two-class segmentation goal. Based on the experiments, incorrect crop size will lead to incorrect segmentation due to possible non-uniform pixel intensity on the non-flame region.

Figure 3.7 shows various possible crop window to generate a sub-image that contains both flame and non-flame regions. The crop size will directly affects the shape of the pixel intensity distribution and finding the optimal size is not trivial.

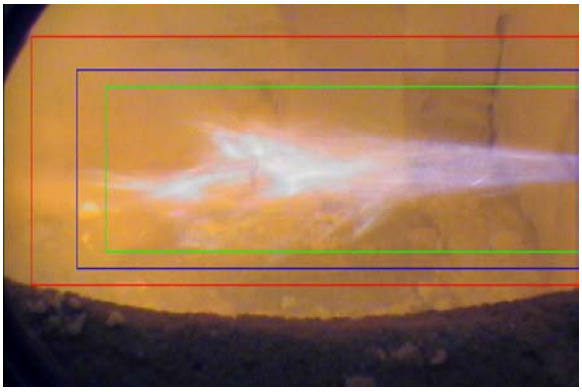

Figure 3.7 Various Possible Crop Size Windows Shown in Red, Green and Blue Borders

Figure 3.8 shows one possible incorrect segmentation should the crop size is too big. The error is caused by the non-uniform non-flame region. The non-flame region in this case, includes the furnace's interior and also the hole on the wall where the camera is placed. The intensity difference between the furnace interior and hole on the wall is more substantial than the difference between flame and non-flame region, hence the incorrect segmentation.

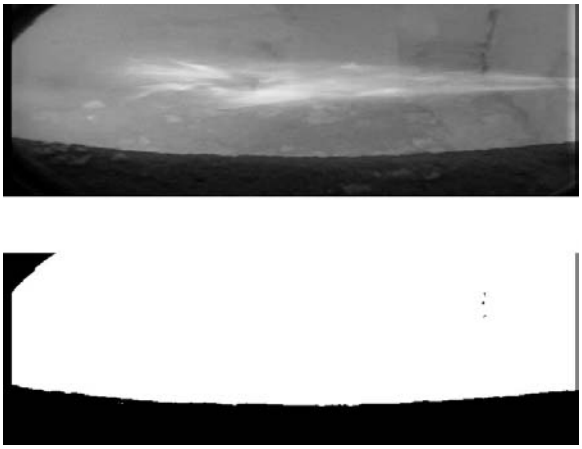

Figure 3.8 Incorrect Mask Due to Incorrect Crop Size using Green Channel

Another possible drawback is due to the fact that the lighting property of t he scene in the image is affected by the flame itself. The hotter the flame, the brighter the overall image will become. Moreover, the hotter flame will also heat the furnace wall

more which in turns cause them to glow brighter. Figure 3.9 shows such situation due to a high flow in fuel and air.

Figure 3.9 Incorrect Mask Due to Glowing Furnace's Interior Wall using Green Channel

The non-uniform background region is also channel dependent. The severity of the segmentation error is different for each of the color channels. Figure 3.10 shows the mask that is created based on segmentation on blue channel. Since blue pixel intensity is apparently very low unless around the flame region, the resulted mask is still correct even with the wrong crop size or non-uniform background.

Figure 3.10 Correct Mask with Incorrect Crop Size and Non-Uniform Background using Blue Channel

Non-uniform background implies a difficulty in detecting non-flame region due to a possibility of having more than two distinctive groups of pixels in their distribution. The groups usually can be reflected by the number of local maxima in the distribution. Hence, the pixel intensity distribution of the image to be segmented may not reflect the desired two classes as shown in Figure 3.11. This is a well known problem in two-class segmentation [42] and Otsu's method certainly affected by it. The impact in real case is not as severe as the simulated image of Figure 3.11, otherwise Otsu's method would have

failed completely. However the existence of this limitation still need to be addressed and it leads to the second strategy of using different approach in achieving the desired flame image preprocessing.

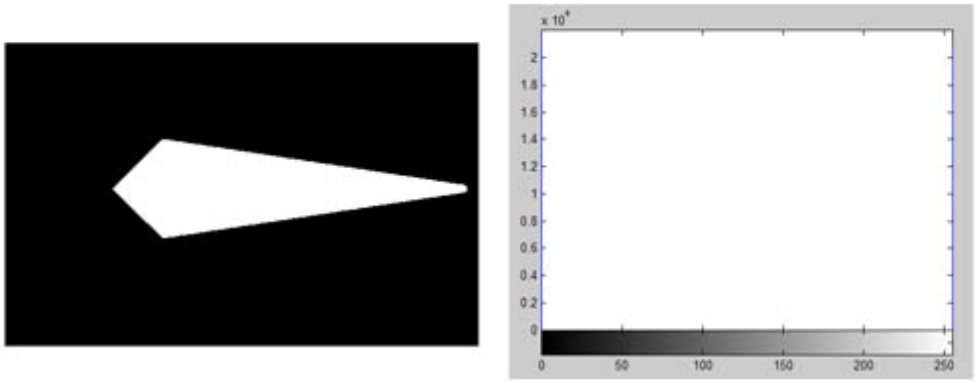

a. Uniform Background

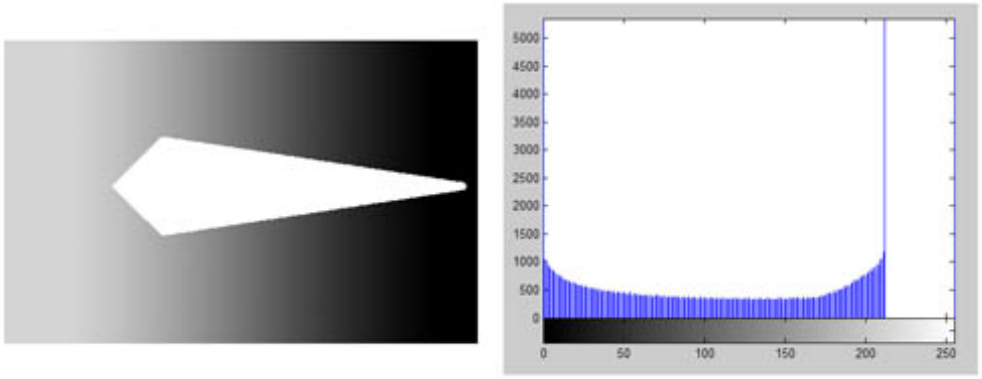

b. Non-uniform Background

Figure 3.11 Sample of Uniform and Non-Uniform Background with their Pixel Intensity Distribution

3.3 Image Enhancement Procedure

Segmentation technique divides an image into separate sub-images, whereas image enhancement utilizes a function to convert an image into a processed image with more desirable characteristics. There are many varieties of functions in image enhancement technique for various applications [48].

An image enhancement technique is designed specifically for this study to overcome the limitation of Otsu's method discussed previously. The goal of the proposed technique is to suppress pixels' intensity in the non-flame region such that the impact of the background on the image analysis will be insignificant. This is achieved by using a function defined as "*Intensity Suppression*" method as proposed and applied here.

3.3.1 Intensity Suppression Method

Intensity suppression method is a type of image enhancement requiring 2 steps: 1) Transformation of the range of the pixel intensity between 0 and 1, and 2) Modifying the pixel intensity of the original image using a selected magnitude of power.

The first step is achieved by dividing the pixel intensity by the maximum intensity, which is 255 in this particular study. This step would not be necessary should the original image have its pixel intensity range from 0 to 1. The transformation is necessary so that the resulting processed image will have pixel intensity value from 0 to 1 as well. In addition, the range of 0 to 1 is useful for both displaying and feature extraction process.

The second step is depicted in EQ (3.8), which is the proposed formula as implemented in this study.

$$P'(x,y) = \left[P(x,y)\right]^n \qquad P(x,y) \in \left[0,1\right] \qquad \text{EQ (3.8)}$$

where P(x,y) = pixel intensity of the image at coordinate (x ,y)
P'(x,y) = pixel intensity of the new image at coordinate (x ,y)
n = the degree of power applied to P(x ,y)

Similar to Otsu's method, the image conversion will be applied separately for each color channel. The method is relatively simple to compute but sufficiently practical in achieving the desired goal as shown in Figure 3.12. Note that the image in Figure 3.12 is the same image that Otsu's method incorrectly segments as shown in Figure 3.9.

Figure 3.12 Sample of Intensity Suppression using n = 4 using Green Channel

An exponential function has a property of reducing pixel intensities with the range of 0 to 1, such that lower intensities will be reduced more than higher ones as shown in Figure 3.13. Hence, the method is appropriate for this study since the lower background intensities could be substantially reduced as the power of the exponential function increase.

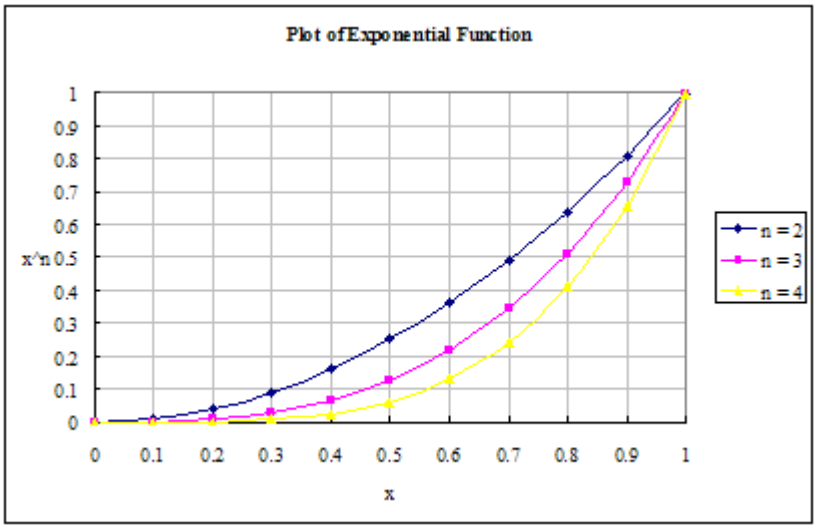

Figure 3.13 Sample plot of Exponential Function with Varying Degree of Magnitude

3.3.2 Intensity Suppression Result

Based on the experiment, the resulted processed images have intensity reduction on the non-flame region that is more significant that they become relatively more uniform. At the same time, for the relatively higher pixels intensity of the flame region, their intensity is less reduced if not retained. Furthermore, even for flame pixels with not very high intensities, their reduction will always be much less compared to the non-flame region.

Figure 3.14 shows results based on the images shown in Figure 3.9 and 3.12 with various magnitude of power n and corresponding pixel intensity distribution. The higher the power n the more pixels will be converted to lower intensity, hence, shifting the distribution shape towards the lower range. Note the change of the scale in the distribution plot of Figure 3.14.

The lower range of the distribution depicts the non-flame region while flame pixels are at a higher range compared to the background region. Intensity suppression when applied to the non-flame region pixels causes them to have intensities even lower

and closer to zero; hence their intensity values are closer to each other than before thereby generating a more uniform background. The intensity values of the flame region are also suppressed, however, since their intensity values are always higher than the non-flame regions, the degree of reduction is much less than the background. The resulting processed image will then have the non-flame regions more uniform while keeping the flame region separable from them.

A uniform non-flame region makes this particular method not dependent on the crop window size since different crop sizes will only add or remove non-flame pixels with a more or less similar intensity values.

As the power n increases the size of the flame is reduced further to the point only the brightest flame region remains. Hence one would need to be careful in selecting the parameter n to avoid losing desired information.

Unlike segmentation method which uses mask, with proposed image enhancement method there is no additional step. The intensity suppression generates a weighted image based on its own pixel intensity while masking process in segmentation method, as depicted in EQ (3.7), weights each pixel with either a 1 or 0 constant.

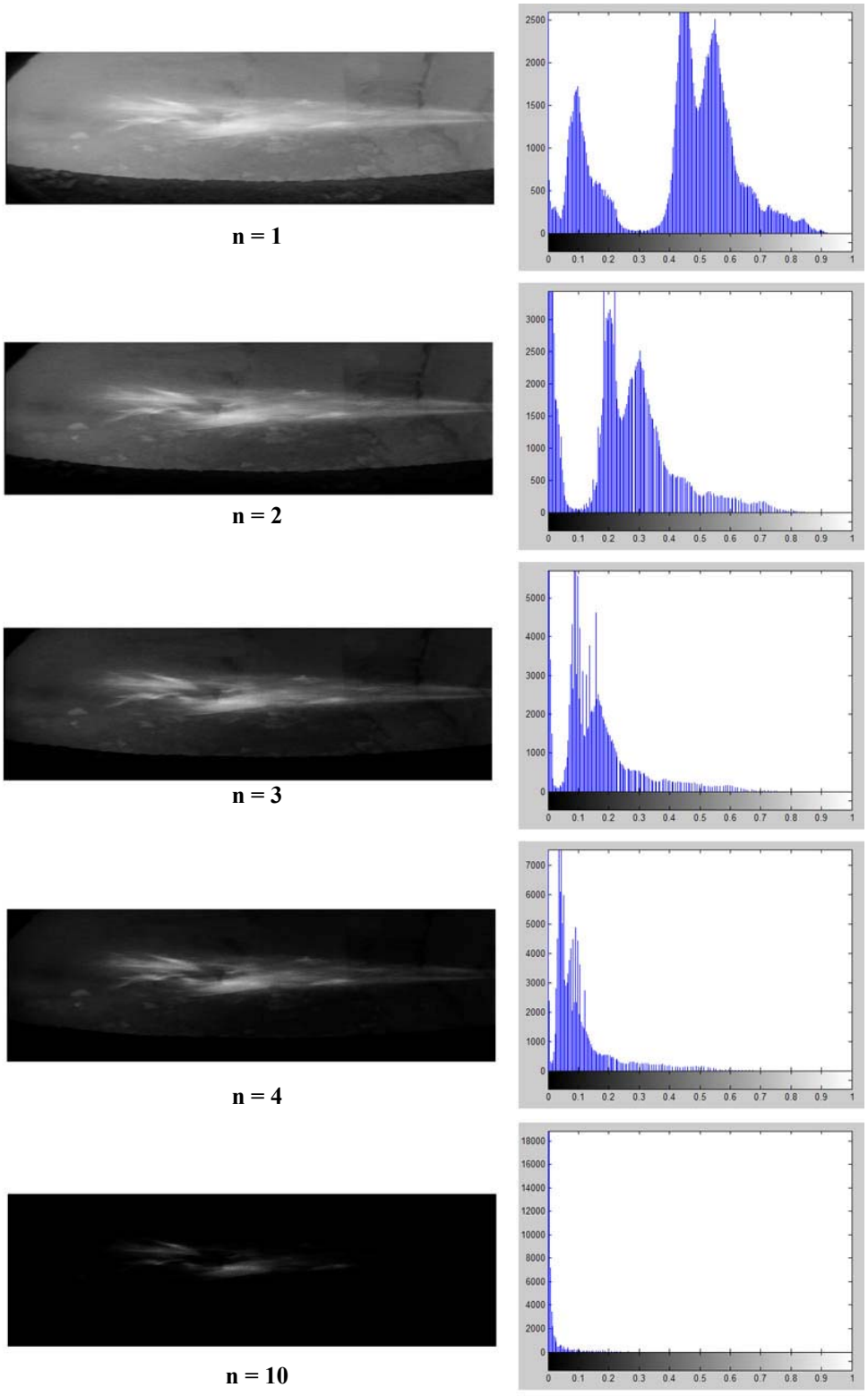

Figure 3.14 Sample of Intensity Suppression Results on Green Channel with The Corresponding Intensity Pixel Distribution

3.3.3 Image Enhancement Limitation

Even though the proposed method addresses certain drawbacks with Otsu method such as crop window size dependency and non-uniform background, it still possesses certain limitation.

As shown in Figure 3.14, there are many possible values of n to select with varying degree of results. It is treated as an independent parameter in the system and its adjustment varies depending on the furnace under study. The selection of the power n is very crucial and needs to be chosen properly in every furnace application. In this study, the selection of the value of n is based on experiment and is set to 4.

In this study both the Otsu's segmentation and the proposed image enhancement are adopted in the strategy for flame image preprocessing. The resulting processed images then will be ready for feature extraction process as discussed in the next chapter.

4. FEATURES DESIGN

4.1 Overview

This chapter is dedicated to definition, design and explanation of "features" and feature extraction techniques.

After the flame images are segmented, the next step is to obtain the essential information from them. This information, called features, is a set of numerical data calculated from the flame image on which the flame analysis will be based upon. The process of deriving these features from the image is called the feature extraction process.

Features are extracted from the flame image in several ways. Some of the features are statistical measurement based on the pixel intensity of the flame image while others are based on geometrical or structural aspect of it. At the present, there are five feature examined in prior study [25] and also four new ones are proposed and explored in this study. Their design, characteristic and formulization will be discussed in detail in this chapter.

4.2 Feature Definition

Features are essentially algorithms based on mathematical formulas. The choice and possibility in designing one can be very complex. In this particular study, some of the important aspects to consider are simplicity to minimize calculation time, robustness to minimize impact of other variables on their values, and high sensitivity in order to maximize their detection in all operation condition.

Simplicity is important because the flame analysis system is designed to be a real-time application. At the same time, one would need to be able to correlate the feature to the actual physical phenomenon as close as possible. Robustness is in reference to a feature that will be reliable and consistent from one experiment to another and easily applicable to various different types of furnaces. Finally sensitivity is very important as the features must not only be able to reflect the characteristic of the flames but also to detect the changes in an acceptable time frame.

Based on each channel of RGB and HSV color space, there are six different kind of segmented flame images. Thus, for each type of feature there will be six measurements generated based on each channel. There are a total of nine feature types in this study; hence the total number of possible features output is 54 given one image frame.

To calculate the value of each feature, one needs to establish a coordinate system to identify each pixel location. EQ (4.1) will be used to represent pixel intensity of a flame image or frame at position (x, y). The two-dimensional coordinate system used to reference a pixel position in an image is shown in Figure 4.1. Given the flame image with size w x h, its top left corner coordinate will be set as (0, 0) and bottom right corner as (w-1, h-1).

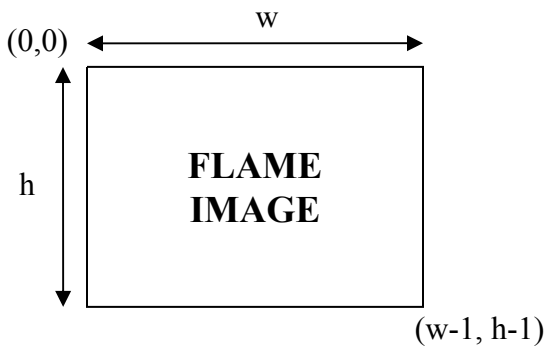

Figure 4.1 Coordinate System Configuration

P(x,y) = pixel intensity value at position (x,y)

$$x \in [0, w-1] \ , \ y \in [0, h-1] \text{ and } P(x, y) \in [0,255] \qquad \text{EQ (4.1)}$$

4.2.1 Previously Implemented Features Set

This section describes the mathematical representative of several features from prior related study on flame image processing [25] that are utilized here, as well as the four new features designed in this research work. Five prior features are also utilized here because they show good sensitivity toward changes in air and fuel level. These features are named area, average, variance, skew and kurtosis.

4.2.1.1 <u>Area</u>

Area refers to the total number of non-zero pixels in a given image. The idea is that the visible size of the flame would correlate directly with how both air and fuel intakes change. The increase in the level of either one would constitute to bigger flame size and vice versa. EQ (4.2) shows the formula used to compute area. It is one of the simplest features to compute and is extracted first because it is used by other features as part of their calculation.

$$A = \sum_{i=0}^{w-1} \sum_{j=0}^{h-1} I_{ij} \quad \text{with } I_{ij} = \begin{cases} 0 & if \quad P(i, j) = 0 \\ 1 & if \quad P(i, j) > 0 \end{cases} \qquad \text{EQ (4.2)}$$

$$\text{and} \quad A \in [0, w \times h]$$

where A = area
I_{ij} = unit measure for pixel at location (i, j), 1 being flame pixel and 0 being background pixel
P(i, j) = pixel intensity at location (i, j)

4.2.1.2 Average

Average, with its formula as shown in EQ (4.3), measures the average pixel intensity of the flame region in the segmented flame image. It is one of the best features according to previous study [25] in detecting changes in flame characteristic.

$$\mu = \frac{1}{A}\sum_{i=0}^{w-1}\sum_{j=0}^{h-1} P(i,j) \ , \ \mu \in [0,255] \qquad \text{EQ (4.3)}$$

where μ = average
A = area
P(i, j) = pixel intensity at location (i, j)

It should be mentioned that since the image is segmented; its regions that are considered to be non-flame have pixel intensity of zero. Therefore average feature can be considered as computing the average intensity of non-zero pixels in the image.

Average computation requires area as one of its parameter. Thus its output would be available after area has been computed. In turns, average's output will also become a parameter for other features calculation such as variance, skew and kurtosis.

Based on the experiments, the pixels intensity values in the flame region are relatively homogenous. Hence its average could be a reliable source in reflecting the changes in flame region and its condition.

4.2.1.3 Variance

Similar to average, variance also suggested to be a good feature based on previous study [25]. Measuring variance of the pixel intensity in the flame region reflects the magnitude of fluctuation or non-uniformity of the region.

Variance computation has the same order of complexity as area and average. It requires both area and average for its computation as shown in EQ (4.4). Variance is

computed following the average. Its output in turn becomes a parameter for both skew and kurtosis feature calculation. Since the numbers of pixel are relatively large, the biased version of variance is used in EQ (4.4).

$$V = \frac{1}{A}\sum_{i=0}^{w-1}\sum_{j=0}^{h-1}\left[P(i,j)-\mu\right]^2 \ , \ 0 \le V < \infty \qquad \text{EQ (4.4)}$$

where V = variance
μ = average
A = area
P(i, j) = pixel intensity at location (i, j)

4.2.1.4 Skew

Skew is a feature for measuring the degree of unevenness of a distribution. Skew's value will be more negative for a distribution that is skewed to the left, positive for skewed to the right and zero for normal. As a feature, it is used to measure the skewness of the pixel intensity distribution of the flame image. EQ (4.5) shows the formula used in this study to compute skew.

$$S = \frac{1}{AV^{3/2}}\sum_{i=0}^{w-1}\sum_{j=0}^{h-1}\left[P(i,j)-\mu\right]^3 \ , \ S \in Q \qquad \text{EQ (4.5)}$$

where S = skew
V = variance
μ = average
A = area
P(i, j) = pixel intensity at location (i, j)

Skew is a good feature as well, in particular since the original image in this study is segmented using Otsu Threshold method that takes into account the overall pixel intensity distribution. Hence, skew measurement can be very sensitive to visible changes of the flame's condition. The only drawback, as shown in the equation, is that it can be

computationally intensive to measure. Moreover, its calculation has to wait until area, average and variance have been computed.

4.2.1.5 Kurtosis

Similar to skew, kurtosis is also originally a statistical measurement representing shape of a distribution. In this case, a small value means a distribution that is very narrow and concentrated around the mean, while large value implies a broad distribution. EQ (4.6) shows the formula incorporated to measure kurtosis. Its inclusion is also important since it reflects the intensity distribution. Like skew, it is computationally intensive. Similarly, its calculation has to wait until area, average and variance have been computed.

$$K = \frac{1}{AV^2}\left[\sum_{i=0}^{w-1}\sum_{j=0}^{h-1}\left[P(i,j)-\mu\right]^4\right]-3,\ K \in Q \qquad \text{EQ (4.6)}$$

where K = kurtosis
V = variance
μ = average
A = area
P(i, j) = pixel intensity at location (i, j)

4.2.2 New Feature Set

Aside from the above features introduced in the previous study, four new ones are designed and examined as well. Based on the experimental results they contribute in further improvements for real time flame analysis. These are otsu threshold level, image entropy, average flame temperature and center of mass. Their description and corresponding mathematical equations are explained below.

4.2.2.1 Otsu Treshold Level

Otsu threshold level, as discussed in the previous chapter, refers to the pixel intensity value derived using Otsu method to obtain the flame region in the image. Naturally, it would be the first feature to be computed and its output will affect the other features.

The Otsu threshold value inclusion as a feature along with its reasons is already explained in the previous chapter.

4.2.2.2 Image Entropy

In image compression, one would like to reduce the data size of an image as much as possible without losing the important information contained in it. Image entropy, as typically used for image compression [49], is a method to measures the amount of information an image contains.

The term “information” is a representative of how homogenous the pixel intensity values are. The more uniform the pixels intensity, the less informative the data carried by the image. This uniformity measurement further implies the likelihood of one’s ability to aggregate them, thereby reducing the image’s data size.

In this study, image entropy is anticipated to provide some measurement of uniformity of the pixels intensity of the flame region. Entropy has a relatively similar goal as variance, although with a different way of expression. Its computation is less taxing compared to variance. It does require that pixel intensity distributions be available beforehand. Fortunately, during the feature extraction process, they are available for Otsu threshold computation for image segmentation. Additionally, unlike variance, image entropy can be computed as soon as the segmented flame image is available. Its inclusion therefore is not only to improve the flame analysis, but also to provide a possibility of replacing another feature that is more taxing to calculate. EQ (4.8) shows the formula used to compute entropy [50]. Note that its input value are not normalized to simplify and expedite its computation.

$$E = -\sum_{i=0}^{255} h_i \log_2 h_i \ , \ E \in Q \qquad \text{EQ (4.8)}$$

where E = image entropy
h_i = number of pixels with intensity i, $i \in [0,255]$

4.2.2.3 Average Flame Temperature

Flame color is a well known indicator for flame condition and has been one of the conventional means for the furnace operator to monitor furnace flame. Flame color is directly related to its temperature; therefore temperature is a very good feature that is sensitive to the flame condition. Fortunately it is feasible to measure temperature based on the flame image using technique called two-color method.

Two-Color method is a well known technique for measuring temperature using total radiation from luminous gas flame in a furnace, as pioneered by Hottel and Broughton [51]. The method selects two wavelengths of its radiation spectrum and its

conceptual formulation is based on Planck's Law of blackbody radiation [52]. It has been used by scientists for measuring temperature in coal burner, steel furnace, and combustion engines [15, 17, 53, 54].

The two color based temperature information can be obtained in many ways [55]. A one dimensional flame temperature can be obtained by using a spectrometer which is explained in a prior research activity [56]. Furthermore, a two dimensional flame temperature measurement can be obtained from images taken by a CCD camera based on proportionality of radiation energy to image pixel intensity [57]. Therefore, it is possible to measure flame temperature based on the flame images and use them as feature.

EQ (4.9) shows the original formula to measure pixel temperature at position (x, y) in the image. The equation involves several known constants and coefficients that need to be computed or known beforehand. C_2 is one of the constant for Planck's radiation law. λ_R and λ_G are the wavelength of red and green channel, 700nm and 546nm respectively. C_A is a correction coefficient required because pixel intensity is used instead of radiation energy. It is also influenced by factors such as spectral sensitivity of the CCD camera, sensor noise, etc. ε_R and ε_G are emmisivity constant for red and green channel respectively.

$$T(x,y) = \frac{C_2\left(\frac{1}{\lambda_G} - \frac{1}{\lambda_R}\right)}{\ln\frac{P_R(x,y)}{P_G(x,y)} + C_A - \ln\left(\frac{\varepsilon_R}{\varepsilon_G}\right) - 5\ln\left(\frac{\lambda_R}{\lambda_G}\right)} \qquad \text{EQ (4.9)}$$

where T(x,y) = temperature for pixel at position (x,y), in K.
C_2 = Second Planck's constant
$P_R(x,y)$ = Image's pixel intensity of Red channel at position (x,y)
$P_G(x,y)$ = Image's pixel intensity of Green channel at position (x,y)
λ_R = Constant of Red channel's radiation wavelength
λ_G = Constant of Green channel's radiation wavelength
C_A = Correction coefficient
ε_R = Emissivity constant for Red channel
ε_G = Emissivity constant for Green channel

One technique used to measure the temperature is based on utilizing a known temperature from external independent temperature measurement device such as IR Gun or thermocouple, and calculating a comprehensive correction C'_A which contains both C_A and the emmisivity approximation as well. The formula for C'_A is given in EQ (4.10) [57].

$$C'_A = \frac{P_G(x,y)}{P_R(x,y)} \exp\left(\frac{C_2\left(\frac{1}{\lambda_G} - \frac{1}{\lambda_R}\right) + 5T_{known}\ln\left(\frac{\lambda_G}{\lambda_R}\right)}{T_{known}}\right)$$

EQ (4.10)

where C'_A = Comprehensive correction coefficient
$P_R(x,y)$ = Image's pixel intensity of Red channel at position (x,y)
$P_G(x,y)$ = Image's pixel intensity of Green channel at position (x,y)
λ_R = Constant of Red channel's radiation wavelength
λ_G = Constant of Green channel's radiation wavelength
T_{known} = A known reference temperature

With a measurable C'_A as the comprehensive correction coefficient, one can measure the temperature on a given location (x, y) on the image based on EQ (4.11) [57]. Using this temperature one can measure the new feature μ_T, which is the average temperature of the flame region in the segmented flame image as shown in EQ (4.12).

$$T(x,y) = \frac{C_2\left(\frac{1}{\lambda_G} - \frac{1}{\lambda_R}\right)}{\ln\frac{P_R(x,y)}{P_G(x,y)} + C'_A - 5\ln\left(\frac{\lambda_R}{\lambda_G}\right)} \qquad \text{EQ (4.11)}$$

where T(x,y) = temperature for pixel at position (x,y), in K.
C_2 = Second Planck's constant
λ_R = Constant of Red channel's radiation wavelength
λ_G = Constant of Green channel's radiation wavelength
$P_R(x,y)$ = Image's pixel intensity of Red channel at position (x,y)
$P_G(x,y)$ = Image's pixel intensity of Green channel at position (x,y)
C'_A = Comprehensive correction coefficient

Table 4.1 Constants Values Used for Temperature Feature

Constant Parameter	Value
C_2	0.0143875
λ_R	700E-9
λ_G	546E-9
C'_A	5.6874

$$\mu_T = \frac{1}{A}\sum_{i=0}^{w-1}\sum_{j=0}^{h-1} T(i,j) \times I_{ij} \quad , \ \mu_T \in Q \qquad \text{EQ (4.12)}$$

where μ_T = Average temperature of the flame region
T(i, j) = Temperature for pixel at position (i, j), in K.
I_{ij} = unit measure for pixel at location (i, j), 1 being flame pixel and 0 being background pixel
A = Flame area as computed using EQ (4.2)

Although temperature is probably the most relevant feature to correlate with the furnace flame, it has its own challenge of identifying the level of accuracy of the measured temperature. Due to the sensitivity of the correction coefficient used in the temperature equation, it must be calculated for the same flame under study otherwise the calculated value could be off from the actual temperature. Its inclusion as a feature in this study however is valuable beyond its accuracy because the trend of its output is very useful. That is, its rate of change and sensitivity toward the physical changes in the furnace flame is indeed more important for this study than the absolute temperature measurement itself.

4.2.2.4 Flame's Center of Mass about Y Axis

The visual appearance of the flame is not made of uniform pixel intensity even though they are brighter than the background. Part of its region is particularly brighter then the rest and located relatively around the same region in the flame as shown in Figure 4.2. Its existence is the reason for incorporating center of mass computation as a feature in this study. This bright region is proven to be useful for locating a common flame region as it will be discussed later in this chapter.

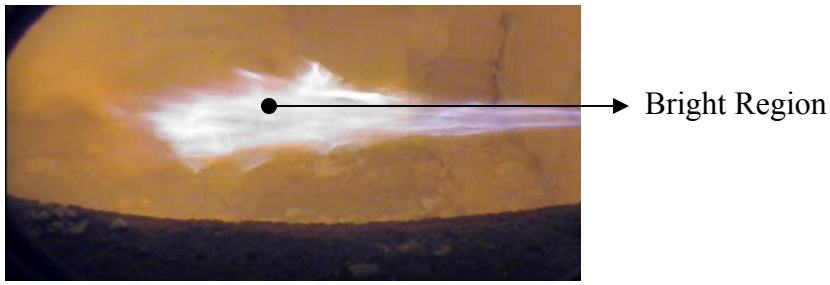

Figure 4.2 Location of Bright Region in a Flame Image

Center of mass is considered a moment-based shape feature that treats pixel intensities as mass [4, 25]. In this particular study, the flame region is considered as a two-dimensional object with pixels intensities representing its total mass. Since brightest region on the image are typically located at the center of the flame as shown before, thus computing center of mass will track the location of the flame's brightest spot at any given time.

For this study, the computation for center of mass is with respect to Y axis. The reason is that the flame movements are more apparent in the horizontal direction. The formula for calculating the flame's center of mass about Y axis is given in EQ (4.13).

$$C_X = \frac{\sum_{x=0}^{w-1}\sum_{y=0}^{h-1} xP(x,y)}{\sum_{x=0}^{w-1}\sum_{y=0}^{h-1} P(x,y)} \quad C_x \in [0, w-1] \qquad \text{EQ (4.13)}$$

where C_X = Center of mass about Y axis
w = Width of the flame image
h = Height of the flame image
P(x,y) = Pixel intensity of the flame image at coordinate (x, y)

4.3 Challenges and Solutions

In summary, the feature extraction process will produce a set of numerical values derived from the features' formulas for each flame image. This set of values is defined as a set of feature output, which will consist of 54 numerical values in total based on the nine features for each of the six color channels.

Note that since the original images used in this study are interlaced, every one of them will be de-interlaced first into two separate flame images. Hence, two sets of feature outputs are derived from a single original image. In another word, 60 flame images need to be processed per second due to the 30 fps acquisition rate.

In the feature extraction process, there are several challenges that need to be addressed. This is related to the large fluctuations on the feature output values due to flame movement, as well as the high volume of data that needs to be processed and analyzed due to the number of features and the image acquisition rate.

4.3.1 Stabilizing Feature Output

With an image acquisition rate of 30 frames per second, flames are still perceived as blurry object since the actual chemical reaction and turbulence speed is much faster than this acquisition rate [1, 2]. As a result, the shape of the flame can be quite different even between subsequent flame images as shown in Figure 4.3. This is the reason for large fluctuations on the feature output values thereby making it harder to do flame classification at the next analysis stage.

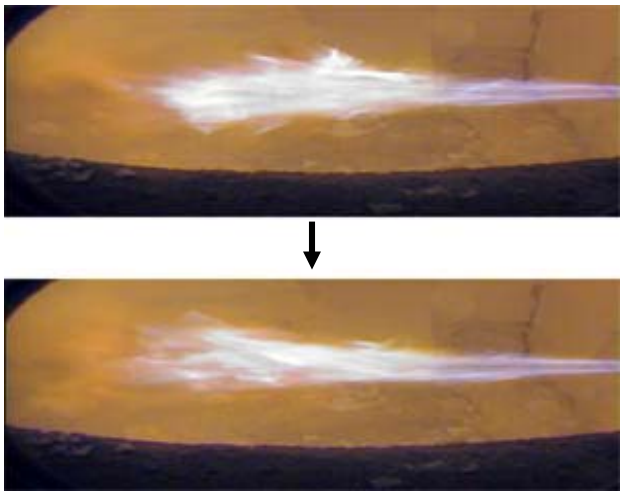

Figure 4.3 Sample of a Flame Image and Its Changes in Subsequent Image

One strategy to solve this is to use aggregation technique in some fashion so that the feature outputs are not based on one individual flame image, rather on a group of images. Thus at any given time during the image analysis, the extraction process yields an aggregated set of feature output that is impacted by the trend of the flame region. An

aggregated feature output not only reduces the amount of fluctuation, but also makes the feature analysis process more reliable and coherent. The number of feature output sets to be aggregated and how the corresponding procedure has to be carefully planned to insure that the changes in flame characteristic due to oxidizer and fuel flow variation can be analyzed and detected properly.

Observing trend is also a preferred strategy because there would be a certain degree of correlation for any flame image with images before and after it. Thus if one only observe at the level of individual flame image, this correlation with the other images will be missed.

Two aggregation methods are proposed in this study in the form of statistical average operation. One method is a moving average process which is applied to the feature output sets. The second method is a periodical average process which is applied to the flame images themselves. The aggregation applied to feature output sets results in a set of averaged numerical values. Aggregations to the flame images results in averaged flame images and are referred to as "flame profiles". Both methods are described below.

4.3.1.1 Moving Average

Moving average is originally a statistical technique for analyzing time series data. It is used to smooth short-term fluctuations so that patterns on a longer-term would become more visible.

In this study, moving average operation is applied to the periodically generated set of feature output values. In any given time it will compute a set of average values, one for each feature, based on the N most recent extracted feature output sets. Hence

moving average will produce a set of 54 numerical values corresponding to the 9 features and 6 channels.

The formula used to apply moving average is shown in EQ (4.14). In this study the parameter N is set to 60. Thus at any given time, 60 of the most recent sets of feature output will be averaged. The value 60 is chosen based on image acquisition of 30 fps which produces 60 flame images per second after de-interlace operation. Hence, the moving average output will always contain the most recent one-second worth of feature extraction process.

$$M_j(t) = \frac{1}{N} \sum_{t=t-N}^{t-1} F_j(t) \qquad \text{EQ (4.14)}$$

where t = a unit of time when one set of feature output is extracted, t > N
$j \in [1, number \quad of \quad features]$
N = number of feature output sets to be averaged
$F_j(t)$ = feature output value at time t for the j^{th} feature
$M_j(t)$ = moving average value at time t for the j^{th} feature

Note that as indicated by the formula, its computation requires keeping information on the feature output sets produced from time t – N to time t - 1. In this study it implies that one needs to store current feature output set along with 59 most recently extracted sets. It also means the first moving average operation starts after N numbers of feature output sets have been extracted and stored. Hence for this study, using moving average means there is a one second delay at the beginning before the analysis process can start.

Moving average as a method to measure trend in the feature outputs has several advantages. It is a relatively simple method that can be incorporated in a real-time system without extensive additional demand for computational process and resource.

Moreover, based on the experiments, it proves to improve the stability in flame image classification and analysis as well by suppressing fluctuation and outliers.

In the implementation, this method would indeed require resource that depends on parameter N. Each set needs to be stored in order to compute subsequent moving average operation, hence requiring computational resource.

4.3.1.2 Periodical Average

Another aggregation approach to suppress the fluctuation is computing an average periodically. The equation to compute periodical average is shown in EQ (4.15). In terms of the computation procedure, it is identical to moving average operation. The difference is in the periodical nature of the operation. Unlike moving average, the periodical average is only computed at a specific time interval, and applied to the flame images.

The parameter N is set to 60 for current implementation, so at any given time the output from periodical average is based on averaging 60 flame images or 1 second worth of acquired images. The period for computing the periodical average is also set at 1 second, such that all 60 flame images are utilized in exactly one periodical average operation. Therefore, an output from this method is produced once for every second.

$$A_j(t) = \frac{1}{N} \sum_{t=t-N}^{t-1} F_j(t) \qquad \text{EQ (4.15)}$$

where t = a unit of time when one set of feature output is extracted
$j \in [1, number \quad of \quad features]$
N = number of feature output sets to be averaged
$F_j(t)$ = feature output value at time t for the j^{th} feature
$A_j(t)$ = periodical average value at time t for the j^{th} feature

Using this method implies longer waiting time before an output can be analyzed as compared to using moving average method. This approach however still has an advantage over moving average when it comes to flame images aggregation. Had moving average been used, each of the 60 flame images would need to be stored individually which can be taxing for both computational operation and resource requirement. For periodical average, the flame images are not stored individually. Only their combined summation is stored at any given time, thus requiring less computational resource as compared to moving average computation.

As revealed from the experiment, applying periodical average to the flame images is proven to be useful for analysis. The resulting images based on averaging flame images, which is called flame profile in this study, help in providing insights in the correlation between the visible structure of the flames and its characteristic.

Figure 4.4 shows an example of a flame profile. This profile is a single periodical average generated using 600 flame images, or 5 seconds worth of image acquisition. Note that flame images shown in Figure 4.3 which are included in the aggregation process no resemblance to Figure 4.4. There is a distinctive shape that can be seen on the resulting image whose flame bears little resemblance to the individual flame images that generate it. This is the main reason for incorporating center of mass computation as mentioned earlier in this chapter. The flame profile is proven to be distinctive for different flames according to the changes in fuel and oxidizer levels. This result is fully explained in the next chapter.

Figure 4.4 Sample of Flame Profile

4.3.2 Managing Amount of Computation

Using conventional 720x480 resolution 30fps CCD camera, about a megabyte of data is available for processing and analysis for every $1/30^{th}$ of a second. Further improvements in the image acquisition technology will more likely increases the resolution and the frame rate as well. Hence, there is a need for a strategy to keep the amount of computation tasks manageable such that the system performance is fast enough to be considered real-time without sacrificing reliability. Three strategies are proposed as described below.

4.3.2.1 Configuring Crop Windows Size

The utilization of crop windows helps in reducing the amount of data hence minimizing the computation cost. In this study, the size is particularly optimized as the smallest window size without losing valuable flame information. Detailed explanation and implementation of this strategy is provided in chapter 5.

4.3.2.2 Observation Rate Reduction

It is also possible to have the observation rate less than the actual acquisition rate. For example, even though there are 30 images acquired by the camera per second, it is possible to only process every other image and reducing the observation rate to 15 per second. The observation rate reduction to 15 frames per second is proven to be sufficient

for the purpose of fuel and oxidizer classification as described in detail in the next chapter.

4.3.2.3 Features Reduction

There are a total of 9 features that could be extracted from the six channels (red, green, blue, hue, saturation and value) for every frame. It would take a considerable amount of time to compute all of them. Feature selection is necessary in order to select the least number of features for classifying the flames belonging to various operational conditions. A feature selection strategy is used in order to find the most sensitive features that meet the objectives and to reduce the amount of computation. The technique used for feature selection and the performance evaluation of the selected features is discussed in the next chapter.

4.4 Feature Extraction Procedure

The methods proposed for image preprocessing along with the solutions to its challenges provides various possible configurations for the feature extraction process. Two configurations are proposed in this study as shown in Table 4.2.

Table 4.2 Feature Extraction Procedure

Criteria	Configuration 1	Configuration 2
Preprocessing Method	Otsu's Thresholding	Intensity Suppression
Fluctuation Reduction	Moving Average on Feature's Output	Periodical Average on Input Flame Image
Maximum Rate of Output	$1/30^{th}$ of second	1 second

Configuration 1 is designed for feature extraction that can provide faster output rate thus creating a system that is more responsive to flame changes. On the other hand, configuration 2 is designed to provide output rate that is slower but more robust due to using flame profiles as its input flame image. The robustness is due to a more uniform shape of the flame in the image. Figure 4.5 illustrates the differences in processing steps between the two configurations.

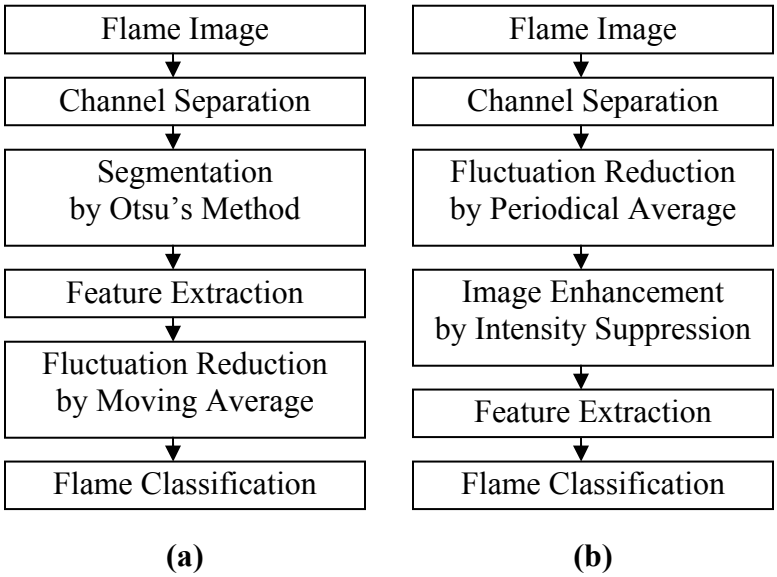

Figure 4.5 Feature Extraction Procedures for (a) Configuration 1 and (b) Configuration 2

Both configurations convert the original flame image into red, green, blue, hue, saturation and value channels. Each of these channels is treated as a separate grayscale image. The main difference between the two configurations is in the preprocessing stage afterwards. For configuration 1, Otsu method's is applied to segment the image and the features are extracted afterwards. In configuration 2 intensity suppression method is applied to the flame profiles and the features are extracted afterwards. Configuration 1 utilizes moving average process while configuration 2 does not.

5. FEATURE SELECTION AND EXPERIMENT ANALYSIS

5.1 Overview

The results based on prior study [25] have already shown that it is feasible to detect the changes in the flame using certain features such as average, variance and kurtosis. These features and the new ones are investigated further in this chapter to develop a procedure on how the classification can be done on individual level of fuel and oxidizer as well.

Additionally, flame profiles that are introduced in chapter 4 are used as a tool for visually confirming the classification feasibility. A feature selection method is then proposed to identify key features and eliminate less sensitive ones, thereby improving the classification performance. The existence of these key features is very crucial since it will allow the possibility for an improved flame analysis system that will be discussed in the later chapter.

The features' sensitivity and potential as key features are investigated by incorporating them in experimental data collected from a pilot scale glass melting furnace. Using a pilot scale furnace is appropriate because it depicts an environment close to a small commercial furnace that is arguably hard to model and simulate otherwise.

The data used in this study were collected on March 16, 2002 with experiments covering various levels of fuel and oxidizer in the pilot-scale furnace.

5.2 Furnace Description

The glass furnace is a pilot-scale furnace which is capable of producing from 45 to 900 kg glass daily and operating at 23 – 146 kW (0.16 Million Btu/hr). It has the flexibility to arrange different burner setups, which allows either air-fuel or oxy-fuel type of combustion. In the experiment for this study, only oxy-fuel configuration is selected with natural gas (CH_4) as fuel and oxygen (O_2) as oxidizer. The flow rate of fuel during the experimental runs varies from 80 to 140 standard cubic feet per hour (scfh) while the oxidizer flow rate varies from 144 to 336 scfh.

LabVIEW [58] hardware and software package are used for control in this particular furnace. Furnace temperature is monitored using three thermocouples installed inside its interior. Also, as well as providing record of periodical log output on the fuel and oxidizer consumption is available.

The furnace has an ideal experimental environment since it provides flexibility in configuring the fuel and oxidizer intakes. The LabVIEW system allows an easy way to adjust both fuel and oxidizer flow level in the furnace, along with their actual flow rate readings on furnace control console. Additionally, the furnace has only a single burner which makes the flame analysis task easier since there is no need to separate several flame regions in the image.

5.2.1 Equipment Setup and Image Acquisition

The video footage of the flame is recorded at 30 frames per second using a CCD camera. The camera used is Panasonic GP KR-222 which is an interlaced color camera with single CCD [32]. The camera is a ½" interline transfer CCD with resolution 768 x 494 pixels.

To protect the camera from the extreme heat of the furnace, it is enclosed in a water-cooled casing or periscope. As shown in Figure 5.1, the tip of the periscope is placed into a port hole on the side wall of the furnace at a position that would be directly pointing at the flame. The periscope has a 90 degree viewing angle lens which allows a complete view of the flame along with some part of furnace interior.

The output from the CCD camera is connected via S-video cable and recorded to MiniDV tape [59] using Sony DV Camcorder [60]. The camcorder is only utilized as a video recorder from the Panasonic CCD camera. The resulting video footages on the tapes are later transferred to the workstation using video editing software.

For this experiment, the video footage from the MiniDV tape is converted into raw 24-bit 720x480 pixels RGB images. The data transfer is done by connecting the camcorder to a workstation using IEEE 1394 cable [61]. The workstation is a PC with Intel 3.0 GHz CPU [62] and 2GB RAM running Windows XP [63] operating system.

The video to image conversion is done using Adobe Premiere v6.0 video editing software [64]. These set of images then become the input images for the flame analysis in this study. Figure 5.2 shows the summary configuration of the image acquisition process.

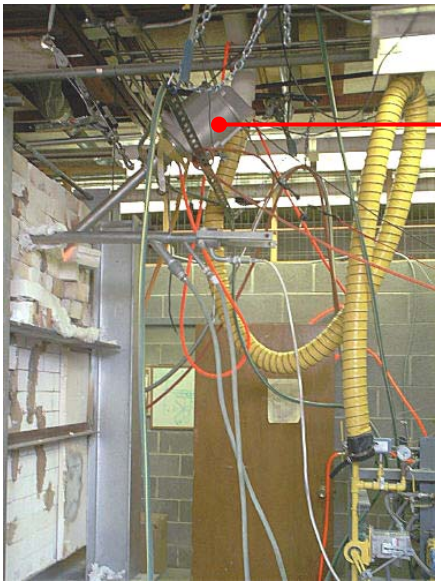

Figure 5.1 Periscope Setup in the Pilot Scale Glass Furnace

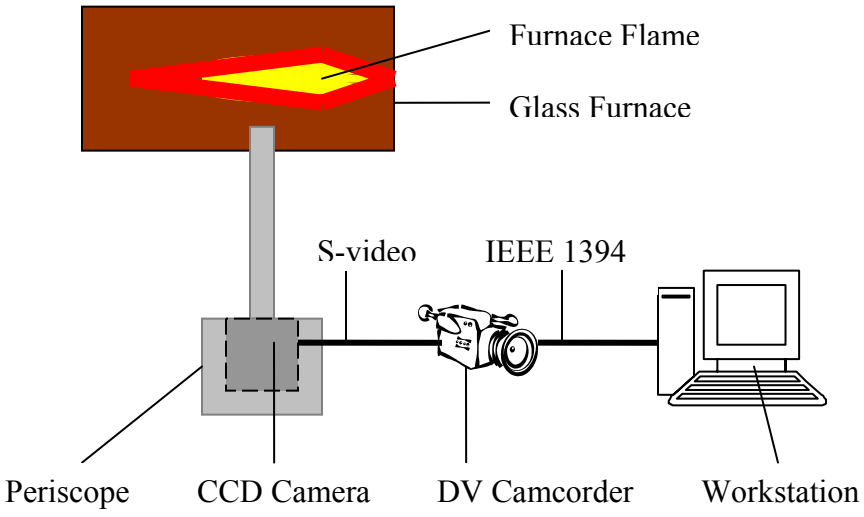

Figure 5.2 Equipment Configuration for Flame Image Acquisition

5.2.2 Experiment Configuration

The experiments conducted at the pilot scale furnace are grouped into several runs with various levels of gas and fuel as summarized in Table 5.1. There are a total of 15 experiment runs, with each run lasting approximately a minute (about 1800 image frames) except for 14th and 15th run which lasts about 3 minutes each. Table 5.1 also shows the furnace temperature measured by furnace thermocouple during each run. Each run is separated from one another approximately by 10 minutes to allow the flame to stabilize as fuel and/or oxidizer change from one experiment to another.

The experiments contain a good number of runs with various flow rates for both fuel and oxidizer. The experiment or run number 1 through 13 shows various experiments with changes in fuel and oxidizer. Run number 14 has a gradual decrease change in fuel flow rate, defined as "ramp down", at the rate of 0.5 scfh/sec. Run number 15 has an abrupt change in fuel flow rate from 128 scfh to 96 scfh, stay at 96 scfh for more than a minute, then another abrupt increase to 128 scfh. Abrupt flow rate change is defined as "step" changes and run number 15 has both step up and step down changes.

Table 5.1 Pilot Scale Furnace Experiment Run Summary

Run #	NG (scfh)	O2 (scfh)	O2/NG ratio	T (°C)	Number of Image Frame
1	110	231	2.1	1185	1791
2	80	144	1.8	1166	1784
3	110	198	1.8	1170	1786
4	140	252	1.8	1184	1788
5	80	168	2.1	1161	1788
6	110	231	2.1	1164	1790
7	140	294	2.1	1180	1786
8	80	192	2.4	1154	1702
9	110	264	2.4	1156	1791
10	140	336	2.4	1174	1780
11	96	231	2.4	1153	1805
12	110	231	2.1	1155	1792
13	128	231	1.8	1167	1768

14	128-96	231	1.8-2.4	1167	5100
15	128-96-128	231	1.8-2.4-1.8	1168-1164	5100

All the runs depicted in Table 5.1 can be grouped into 9 classes, based on its fuel and oxidizer flow rate. Figure 5.3 shows the range of the input dimension depicting the three classes of O/F ratios. The marked 9 yellow points on the figure represent the 9 group of O/F ratios sampled for this experiment.

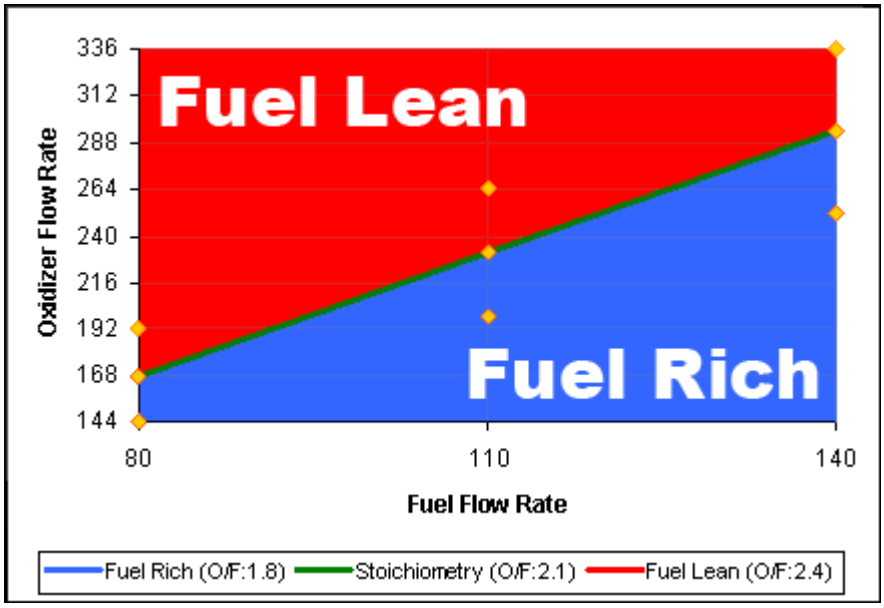

Figure 5.3 Oxidizer to Fuel Relationship Diagram

5.2.3 Sample Feature Output

To provide some idea on how the feature output look like, a sample feature output are provided here. It is Otsu's threshold level from blue channel, extracted from experiment run number 15. The extraction process is based on configuration 1.

Run number 15 is chosen particularly because some of its feature outputs can clearly depicts the changes intuitively. The run lasted for approximately 3 minutes, in which the changes occurred twice with relatively equal amount but at opposite direction. Figure 5.4 shows the feature output extracted from this particular run. A complete

feature output set output for all the features extracted from run number 15 for configuration 1 and 2 is provided in appendix A.

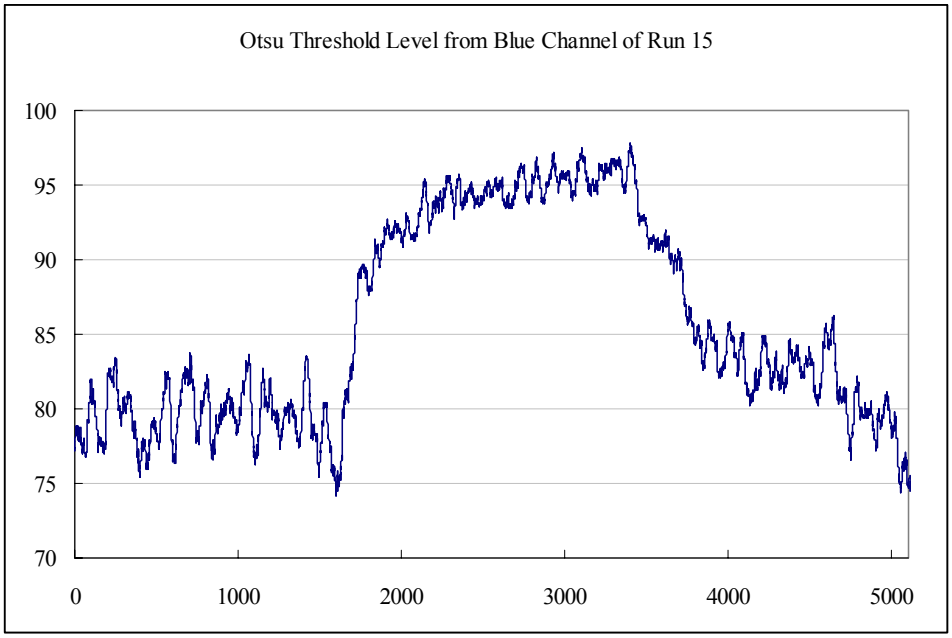

Figure 5.4 Sample of a Feature Output Extracted from Run Number 15

5.3 Building Flame Profiles

Flame profiles are used to investigate whether visible structural patterns can be found from the flames. The profiles discussed here are generated by averaging a minute-worth of flame images for each experimental run.

There are 9 runs selected based on their fuel and oxidizer configuration and arranged to represent changes of natural gas from minimum to maximum (80 to 140 scfh). Also the O/F ratio is arranged from minimum to maximum (1.8 to 2.4) corresponding to each level of natural gas. This arrangement is shown in Table 5.2.

Table 5.2 Experiment Run for Building Flame Profiles

Run #	NG (scfh)	O2 (scfh)	O/F Ratio
2	80	144	1.8
5	80	168	2.1
8	80	192	2.4
3	110	198	1.8
6	110	231	2.1
9	110	264	2.4
4	140	252	1.8
7	140	294	2.1
10	140	336	2.4

For each run, 6 flame profiles will be generated based on the red, green, blue, hue, saturation and value channels. For easier visualization and comparison, the profiles are grouped based on their channel and arranged corresponding to Table 5.3. Table 5.3 is arranged in such a way so that fuel will increases column-wise from 80 to 140 scfh, while the O/F ratio increases row-wise from 1.8 to 2.4.

Table 5.3 Flame Profiles' Runs Arrangement

Run 2 NG: 80 scfh O2: 144 scfh O/F ratio : 1.8	Run 3 NG: 110 scfh O2: 198 scfh O/F ratio: 1.8	Run 4 NG: 140 scfh O2: 252 scfh O/F ratio: 1.8
Run 5 NG: 80 scfh O2: 144 scfh O/F ratio : 2.1	Run 6 NG: 110 scfh O2: 231 scfh O/F ratio: 2.1	Run 7 NG: 140 scfh O2: 294 scfh O/F ratio: 2.1
Run 8 NG: 80 scfh O2: 192 scfh O/F ratio : 2.4	Run 9 NG: 110 scfh O2: 264 scfh O/F ratio: 2.4	Run 10 NG: 140 scfh O2: 336 scfh O/F ratio: 2.4

Figure 5.5 through 5.10 show flame profiles for each channel. Each figure contains 9 profiles, one from each run with their corresponding run number and arrangement as shown in Table 5.3. The red vertical line on each profile is drawn as

visual aid to compare length of the flames within the same fuel level (Such as run 2, 5, and 8).

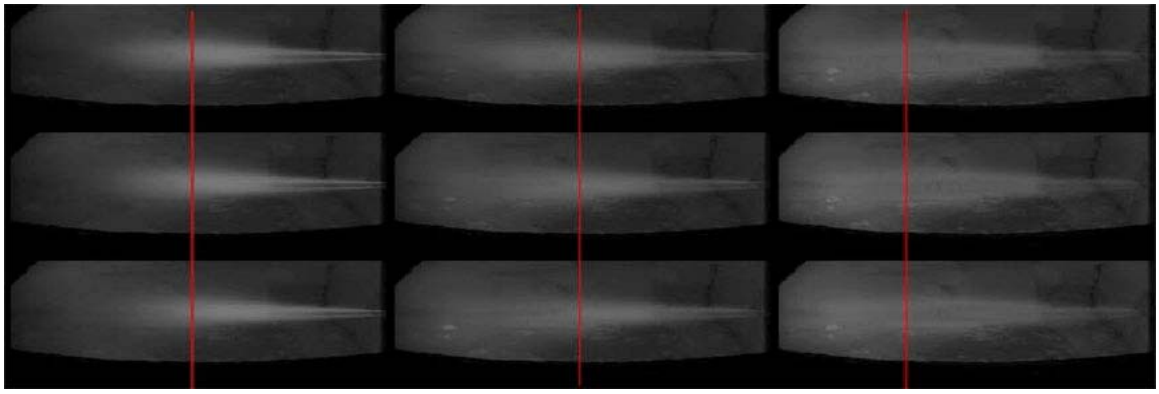

Figure 5.5 Nine Flame Profiles Based on Red Channel

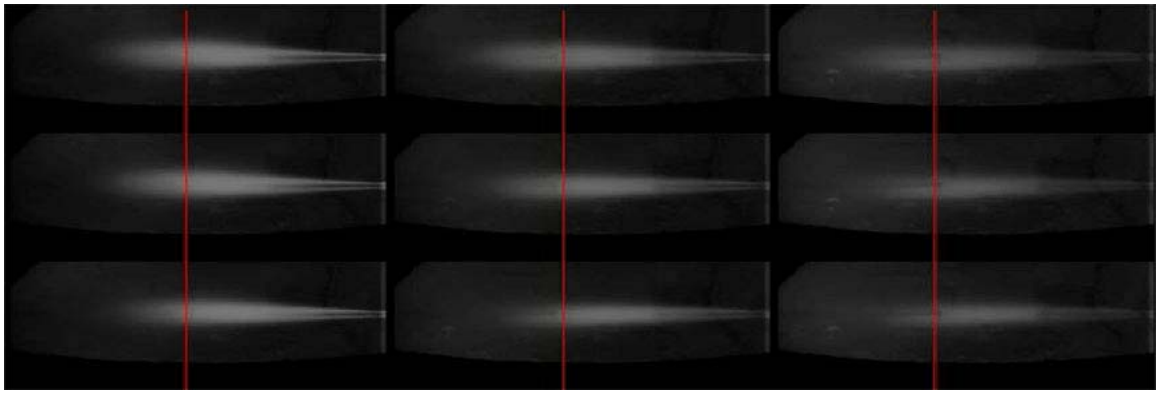

Figure 5.6 Nine Flame Profiles Based on Green Channel

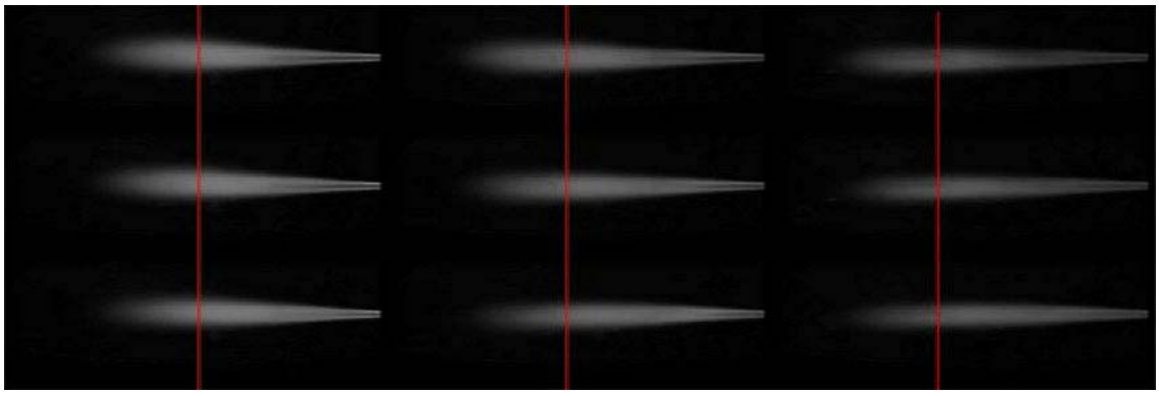

Figure 5.7 Nine Flame Profiles Based on Blue Channel

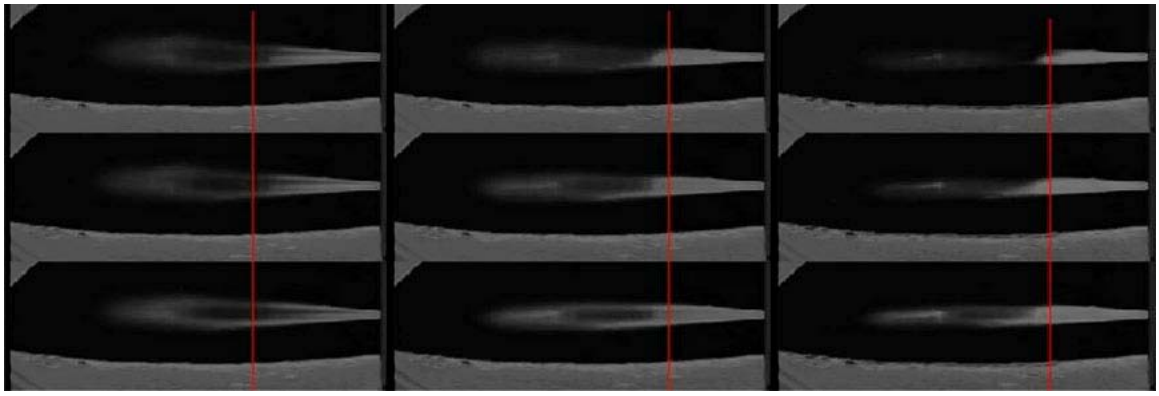

Figure 5.8 Nine Flame Profiles Based on Hue Channel

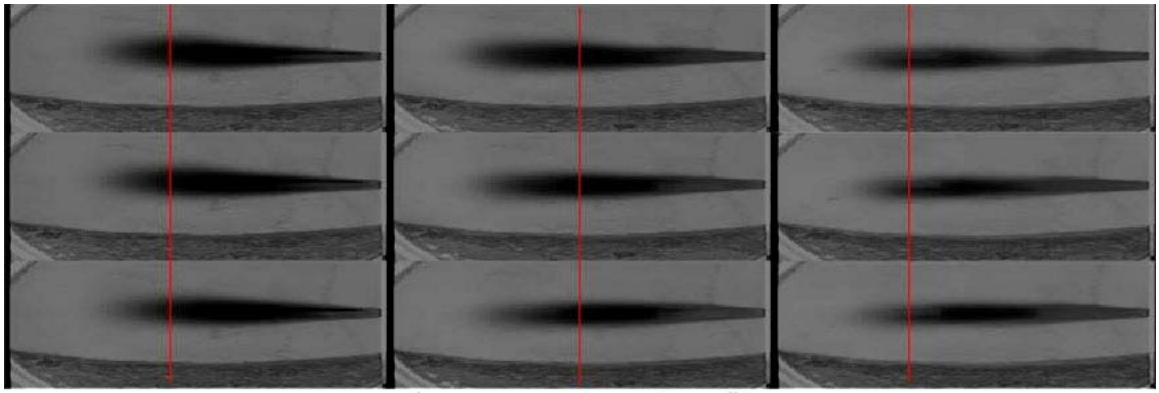

Figure 5.9 Nine Flame Profiles Based on Saturation Channel

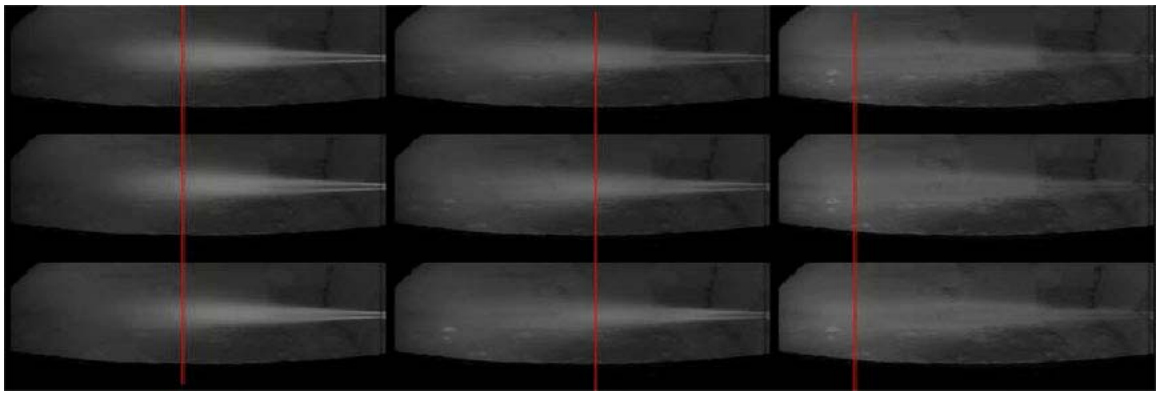

Figure 5.10 Nine Flame Profiles Based on Value Channel

The profiles indeed show some interesting visible patterns. These patterns are more apparent in some channels than others. Blue and saturation channels, as shown in Figure 5.7 and 5.9, particularly depict the best visible patterns that occur in the flame region. This is due to the fact that the flame object has brightest pixel intensity close to

white, while the background in general are less white with color predominantly resulted from combination of red and green channel. Hence, blue pixels are predominantly high in the flame region only. Additionally, only in the flame region that the saturation is close to zero which implies close to white.

Based on the blue and saturation profiles, it appears that changes in fuel level affect the shape of the flame. At the lowest fuel level, shape of the flame is thicker and it becomes thinner as the fuel level increases. Additionally, the overall length of the flame appears to change depending on the oxidizer level. At lower oxidizer level, the flame is actually longer and becomes shorter as the oxidizer level increases.

Flame profiles are proven useful in providing insights on correlation between the shape of the flame and its corresponding fuel and air oxidizer level. These patterns appear to be in a certain order and indicate that the shape of the flame can be correlated with the changes in both level of fuel and oxidizer involved. Additionally, it also confirms the feasibility in using the proposed features in this study for reflecting the flame changes.

It must be mentioned that the profiles are utilized in this study more for human observer's benefit in confirming its feasibility than for the actual machine learning process. Even though the patterns are not as obvious visually in other channels, it does not mean they are less sensitive. As discussed later in this chapter, the features extracted from other channels are able to perform as well if not better in depicting the flame changes compared to those extracted from blue and saturation channel.

5.4 Feature Selection

The main goal in the feature selection process is to identify the key features for classifying both fuel and oxidizer levels. This goal is achieved by analyzing a classifier algorithm performance in classifying the data according to the feature outputs extracted from the experimental runs.

5.4.1 Dataset Preparation

For this experiment, the dataset used as the base for the classification is taken from the 11 experimental runs numbered 1 through 10 and run 12. They are selected since they can be arranged and labeled in an intuitive way according to their fuel and oxidizer flow rates.

The runs are grouped and labeled such that classification can be done based on their label. For fuel changes, the labels are "HIGH", "NORMAL" and "LOW" which correspond to 140, 110 and 80 scfh respectively. 80 scfh is the minimum fuel rate of the furnace and 140 scfh is the maximum. The 110 scfh is the fuel flow rate for normal stoichiometry furnace operation. For oxidizer, the labels are according to the O/F ratio's terms which are "FUEL LEAN" (2.4), "STOICHIOMETRY" (2.1) and "FUEL RICH" (1.8) that correspond to O/F ratios of 2.4, 2.1 and 1.8 respectively. The O/F terms are used rather than the actual oxidizer flow rate since most run has different oxidizer level. Moreover feature selection based on the actual oxidizer flow rate level is proven in this study to be undesirable and impractical as shown later in this chapter.

The 11 runs are then grouped based on the classes as shown in Table 5.3. From each run, 1500 consecutive image frames are used and de-interlaced; hence it doubles the data size.

Table 5.3 Runs Classification

Run #	NG Scfh	O2 scfh	Total Data	Fuel Label	O/F Ratio	Oxidizer Label
2	80	144	9000	LOW	1.8	FUEL RICH
5	80	168			2.1	STOICHIOMETRY
8	80	192			2.4	FUEL LEAN
3	110	198	15000	NORMAL	1.8	FUEL RICH
1	110	231			2.1	STOICHIOMETRY
6	110	231			2.1	STOICHIOMETRY
12	110	231			2.1	STOICHIOMETRY
9	110	264			2.4	FUEL LEAN
4	140	252	9000	HIGH	1.8	FUEL RICH
7	140	294			2.1	STOICHIOMETRY
10	140	336			2.4	FUEL LEAN

Once the classes have been defined, the next step is to select a classifier algorithm that will classify the dataset according to its class label. Decision tree algorithm as described below is used for this task.

5.4.2 Decision Tree as Classifier

Decision tree is a well-known machine learning and data-mining tool used for classifying data and/or predicting outcome. The tree itself is a hierarchical structure comprised of intermediary nodes called “branches” and terminal nodes called “leaves”. Each branch represents conjunction of features that would lead to certain leaves which represent the outcome or class. Given a sample data, it will then traverse through the branches undergoing intermediary decisions made based on its feature values and eventually lead to a leaf which defines its class [65].

The first step in using decision tree for feature selection is to select a particular algorithm for building the tree. There are several types for decision tree algorithm available. For this particular study, a commercial software for decision tree analysis tool named See5 [66] is utilized.

The decision tree performance evaluation is based on confusion matrices produced using by ten-fold cross validation technique. The matrices reflect how good the decision tree is in classifying the datasets. Once a tree with the best matrix is found, one can investigate the features selected by it. This set of selected features become candidate of key features.

5.4.3 Feature Cost Consideration

It is possible to have decision trees that are built with different set of features and complexities but still yield similar performance. The decision tree algorithm however has no ability to differentiate computational cost of the features such as time cost to compute them. Different features require different amount of time to compute depending on their mathematical operation. Moreover, certain features have some of their input parameters depend on the others' output.

To get an idea on computational cost related to time, Table 5.4 shows the average time it takes to compute an image frame for each feature based on configuration 1. Each image frame has 99000 pixels in total and the time measurement is done in milliseconds based on average of 100 frames. The time cost is measured from the moment the extraction process begins to the moment the actual feature output value is obtained. Based on the required time shown in Table 5.4, one can obtain insight on features' computational cost. More complex features require more time to compute such as skew and kurtosis.

Note that features based on HSV channels are consistently more expensive than RGB since the data is originally in RGB format and extra time for conversion of RGB to HSV step is required.

Table 5.4 Feature's Time Cost in Milliseconds for Extracting 1 Frames

Feature Name	R	G	B	H	S	V
Otsu Threshold	66.56	66.72	69.84	75.00	73.91	74.53
Area	76.56	77.19	79.68	89.06	88.60	87.97
Average	76.88	76.72	80.79	89.38	88.28	88.44
Center of Mass about Y axis	77.81	77.19	79.85	89.22	88.91	88.29
Entropy	77.50	77.65	79.84	89.54	88.12	89.22
Average Flame Temperature	79.84	77.97	82.03	90.62	90.47	91.56
Variance	90.16	86.25	90.31	103.28	102.97	105.00
Skew	96.09	90.16	93.60	105.16	106.57	110.16
Kurtosis	95.94	89.84	93.28	105.78	107.03	110.00

Beside time cost consideration, it is also preferable to select features that can be computed with the least dependency on other features. The more dependent a feature is, the longer it takes to compute and the more likely its output is influenced by the features it depends on. Figure 5.11 and 5.12 shows the order of features computed based on their parameter interdependencies for each configuration. Note that for configuration 2, no segmentation threshold is computed, hence, features at its group 1 level can be calculated independently.

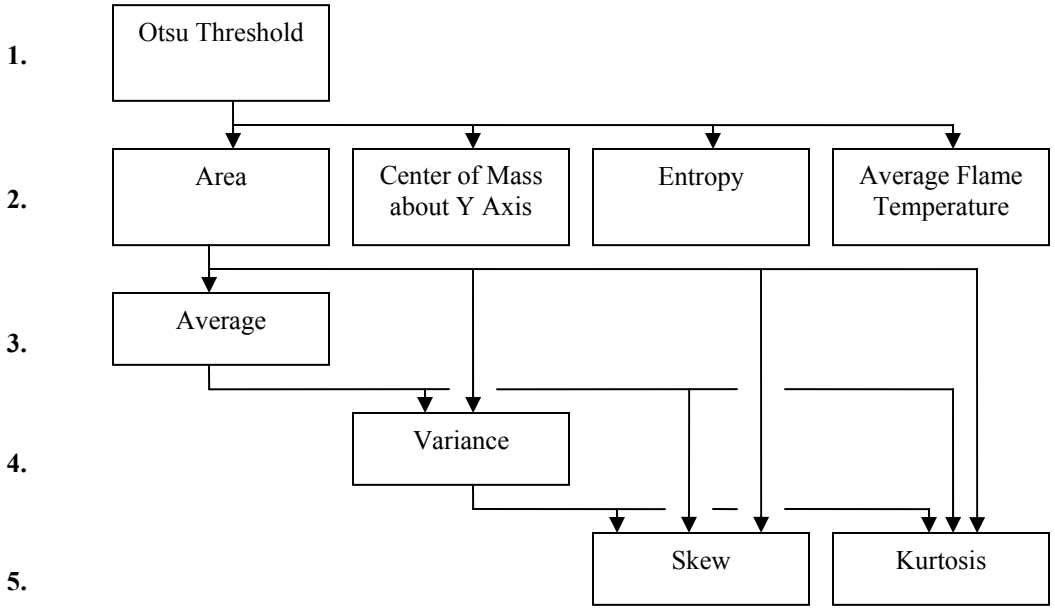

Figure 5.11 Order of Feature Computation for Configuration 1, with Arrows Representing Flows of Dependent Information

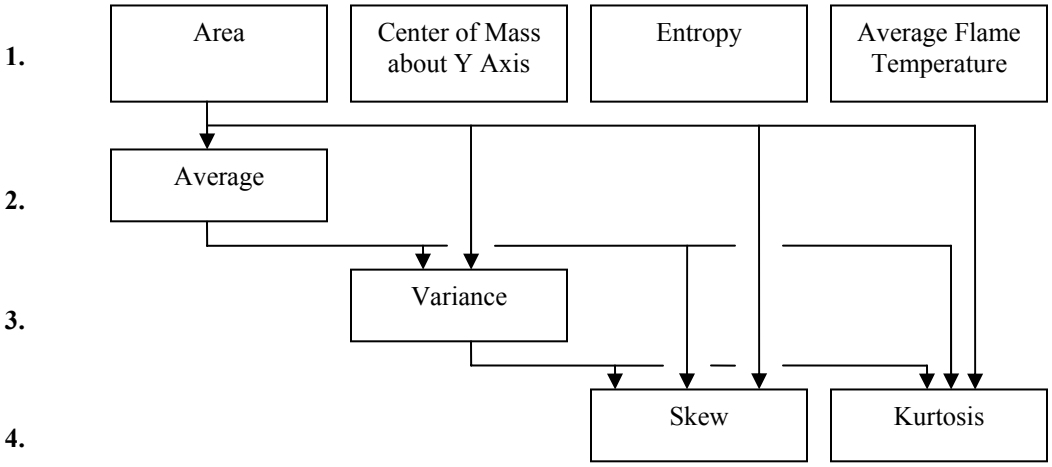

Figure 5.12 Order of Feature Computation for Configuration 2, with Arrows Representing Flows of Dependent Information

To incorporate this idea of feature cost, one can use feature subset selection method. In this particular study, a method for selecting the desired feature subset called wrappers is used. It is a method proposed by Kohavi and John [67] for selecting features and is known for its simplicity and practicality. The method regards the classifier, in this case the decision tree, as a black box into which features are the input and the classification is the output. Features are selected based on using either forward selection or backward elimination method. Both respectively either add or remove certain features from the classifier until desired performance is achieved. Forward selection starts with a defined small set of features and progressively new features are added. Backward elimination works in reverse, starting with all features and progressively removing features from the classifier. Desired performance is measured based on the confusion matrix the decision tree produces and also the size of the tree.

In this study, the features are grouped based on their computational cost and interdependency. Table 5.5 shows the proposed subsets with subset 1 being the least expensive feature. The features are added or removed during the selection process as a group rather than individually. Configuration 1 has 5 groups while configuration 2 has 4. The additional conversion cost from RGB to HSV is not considered as it is small relative to features cost.

Table 5.5 Features' Cost Group

FEATURE GROUP	CONFIGURATION 1	CONFIGURATION 2
1	Otsu's Threshold	n/a
2	Area Center of Mass about Y Axis Entropy Average Flame Temperature	Area Center of Mass About Y Axis Entropy Average Flame Temperature
3	Average	Average
4	Variance	Variance
5	Skew Kurtosis	Skew Kurtosis

Each configuration has its own separate feature selection process. The reason being it is hard to compare inter-configuration complexity since they have different stages during feature extraction process. For example, the speed in configuration 2 is affected by the time interval while in configuration 1 it is not.

5.4.4 Fuel Classification

Once the data is labeled according to their class label and the features are grouped based on their cost, the decision trees can be built using the wrapper method as discussed above. The first feature selection process is for fuel classification.

5.4.4.1 Fuel Classification using Configuration 1

Figure 5.13 show the results based on forward selection, which shows that a single feature is sufficient to provide good fuel classification. Two of such features are

blue channel's otsu threshold level and value channel's entropy level. For backward elimination, similarly a single feature is sufficient, which is red channel's center of mass about Y axis as shown in Figure 5.13. All three features has identical confusion matrix with zero classification error for all three fuel levels.

Confusion matrix however cannot reflect the actual separability between different fuel classes on each feature. The easiest way to investigate this is by observing the actual feature output plots for the three fuel classes using each selected features.

```
a)
    BLU_OTS <= 128.717: high (9000)
    BLU_OTS > 128.717:
    :...BLU_OTS <= 138.133: normal (15000)
        BLU_OTS > 138.133: low (9000)

          (a)   (b)   (c)    <-classified as
         ----  ----  ----
         9000                 (a): class low
               15000          (b): class normal
                     9000     (c): class high

    Error rate: 0%
b)
    VAL_ENT <= -473996: high (9000)
    VAL_ENT > -473996:
    :...VAL_ENT <= -296588: normal (15000)
        VAL_ENT > -296588: low (9000)

              (a)   (b)   (c)    <-classified as
             ----  ----  ----
             9000                 (a): class low
                   15000          (b): class normal
                         9000     (c): class high

    Error rate: 0%
```

Figure 5.13 Decision Trees for Fuel Classification using Forward Selection: (a) Blue Channel's Otsu Threshold Level and (b) Value Channel's Entropy

```
RED_COM <= 254.938: high (9000)
RED_COM > 254.938:
:...RED_COM <= 311.489: normal (15000)
    RED_COM > 311.489: low (9000)

              (a)   (b)   (c)    <-classified as
             ----  ----  ----
             9000                 (a): class low
                  15000           (b): class normal
                         9000     (c): class high

Error rate: 0%
```

Figure 5.14 Decision Tree for Fuel Classification based on Backward Elimination Result

As shown from two-dimensional scatter plots in Figure 5.15 to 5.17, fuel level classification is indeed feasible. Each of the fuel class is completely separable from one another for all the selected features. Each cluster represents one class of natural gas. Center for each of the three clusters are computed as the mean of each features in that class.

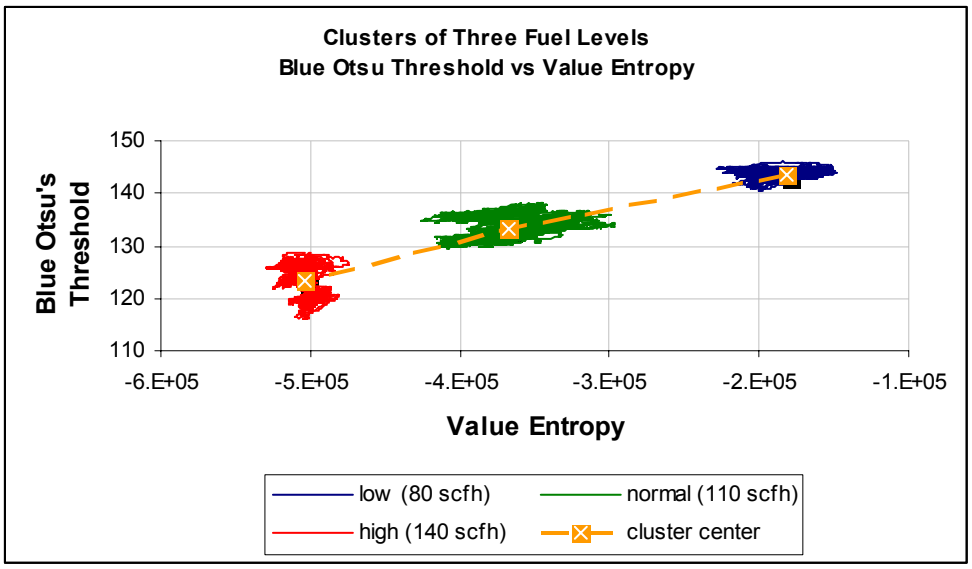

Figure 5.15 Scatter Plot of Blue Channel's Otsu Threshold Level and Value Channel's Entropy

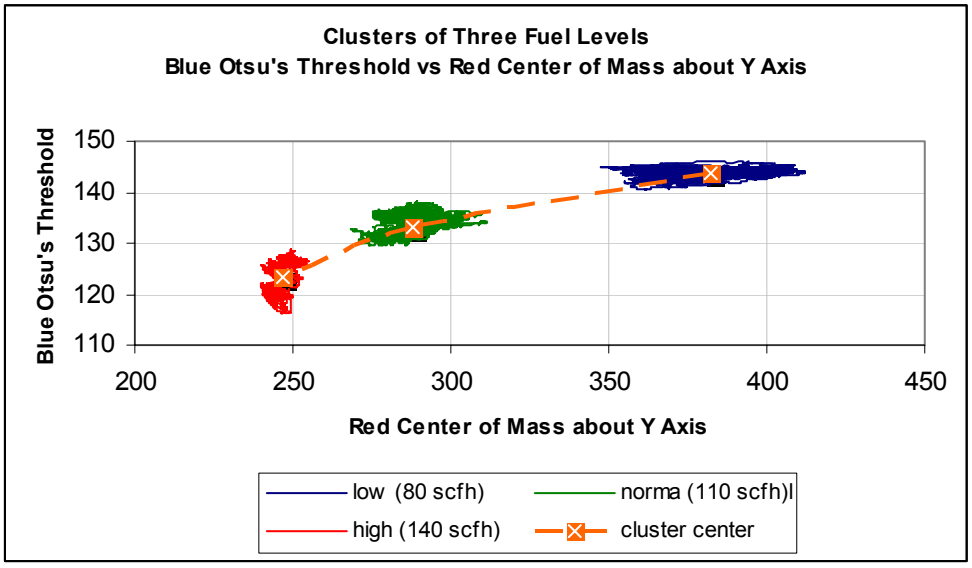

Figure 5.16 Scatter Plot of Blue Channel's Otsu Threshold Level and Red Channel's Center of Mass about Y Axis

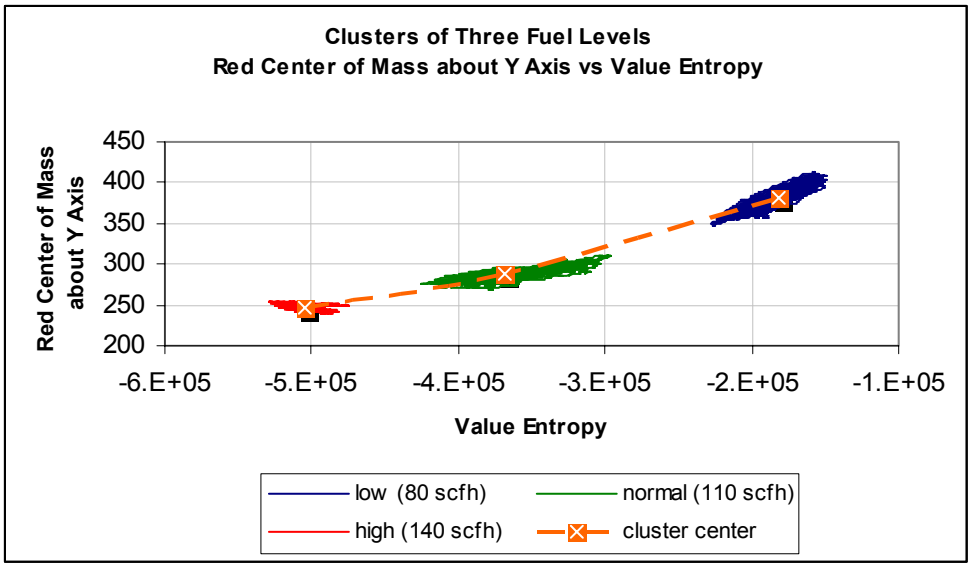

Figure 5.17 Scatter Plot of Red Channel's Center of Mass about Y Axis and Value Channel's Entropy

The correlation between the features' output values and the actual fuel flow rate as read from the furnace control may not have a linear relationship. The flow rate level of natural gas for each class is correspondingly 80, 110 and 140 scfh. Each of this level differs equally by 30 scfh. However, the distance between the classes in the feature outputs as shown in Figure 5.15 to 5.17 do not appear to be the same for different plots. Using blue channel's otsu's threshold and value channel's entropy as shown in Figure 5.15 produces similar distances between the three classes as compared to using the other two as shown in Figure 5.15 and 5.17. This is because feature output values from red channel's center of mass about Y axis have different distance between clusters while it is not the case for the other two features.

Aside from similar distances between classes, Blue channel's Otsu's threshold and value channel's entropy also has relatively linear relationship between classes. The linearity nature of Blue channel's Otsu's threshold and value channel's entropy is desirable. For example, it is possible to have fuel level set between 80 and 110 scfh.

Should this occur, then one would expect that the features' output values would lie between low and normal class. The linearity provides an opportunity to approximate this fuel level.

Note that there exist some variances or fluctuations within each class that differ from one another. Easily noticeable from the scatter plots, each cluster has different shape and size. The correlation between the cluster variance and fuel level might be influenced by the O/F ratio or oxidizer level which will be discussed later.

5.4.4.2 Fuel Classification using Configuration 2

For configuration 2, similar method is used for the feature selection process as mentioned before. The features selected are different, but similarly provides good classifications with zero error as shown in Figure 5.18 and 5.19, one feature from forward selection and two features from backward elimination. Figure 5.20 to 5.22 shows the two-dimensional scatter plots of the three features.

```
VAL_COM <= 321.047: high (150)
VAL_COM > 321.047:
:...VAL_COM <= 347.746: normal (250)
    VAL_COM > 347.746: low (150)

          (a)   (b)   (c)    <-classified as
         ----  ----  ----
         150                 (a): class low
               250           (b): class normal
                     150     (c): class high

Error rate: 0%
```

Figure 5.18 Decision Tree for Fuel Classification based on Forward Selection

a)

```
GRE_VAR <= 5.4e-005: high (150)
GRE_VAR > 5.4e-005:
:...GRE_VAR <= 0.000107444: normal (250)
    GRE_VAR > 0.000107444: low (150)

           (a)   (b)   (c)    <-classified as
          ----  ----  ----
           150                 (a): class low
                 250           (b): class normal
                       150     (c): class high

Error rate: 0%
```

b)

```
VAL_SKW <= 0.522905: high (150)
VAL_SKW > 0.522905:
:...VAL_SKW <= 1.32689: normal (250)
    VAL_SKW > 1.32689: low (150)

           (a)   (b)   (c)    <-classified as
          ----  ----  ----
           150                 (a): class low
                 250           (b): class normal
                       150     (c): class high

Error rate: 0%
```

Figure 5.19 Decision Tree for Fuel Classification based on Backward Elimination: (a) Green Channel's Variance and (b) Value Channel's Skew

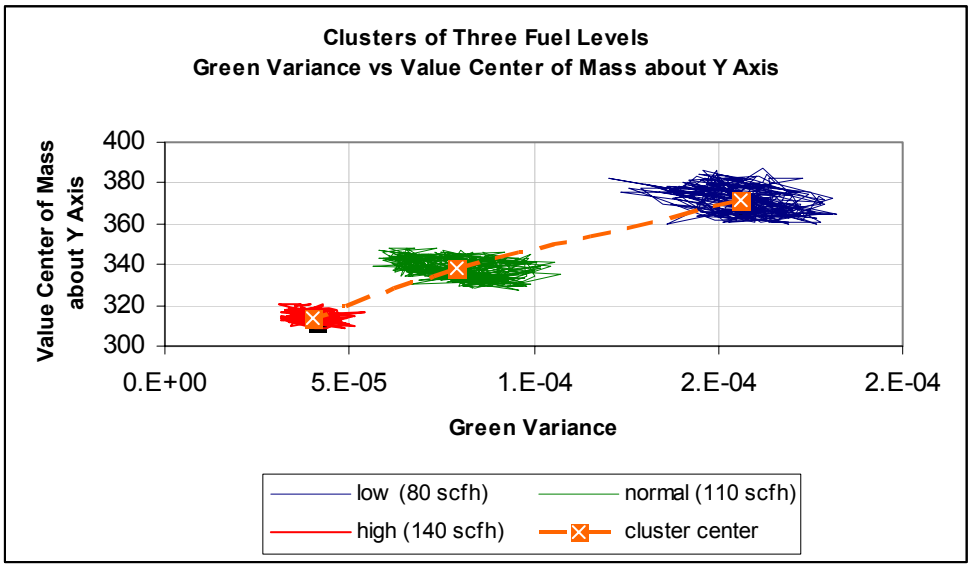

Figure 5.20 Scatter Plot of Value Channel's Center of Mass about Y Axis and Green Channel's Variance

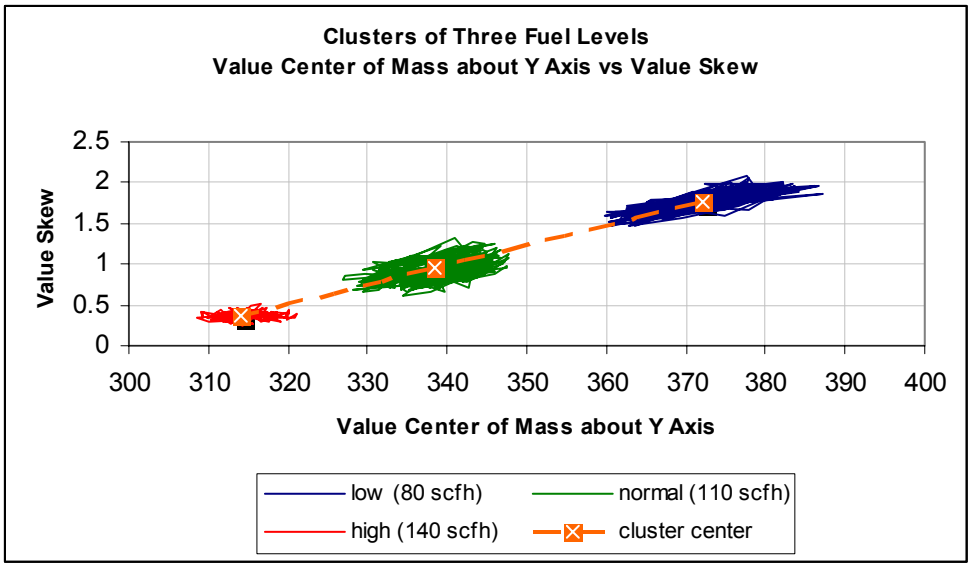

Figure 5.21 Scatter Plot of Value Channel's Center of Mass about Y Axis and Value Channel's Skew

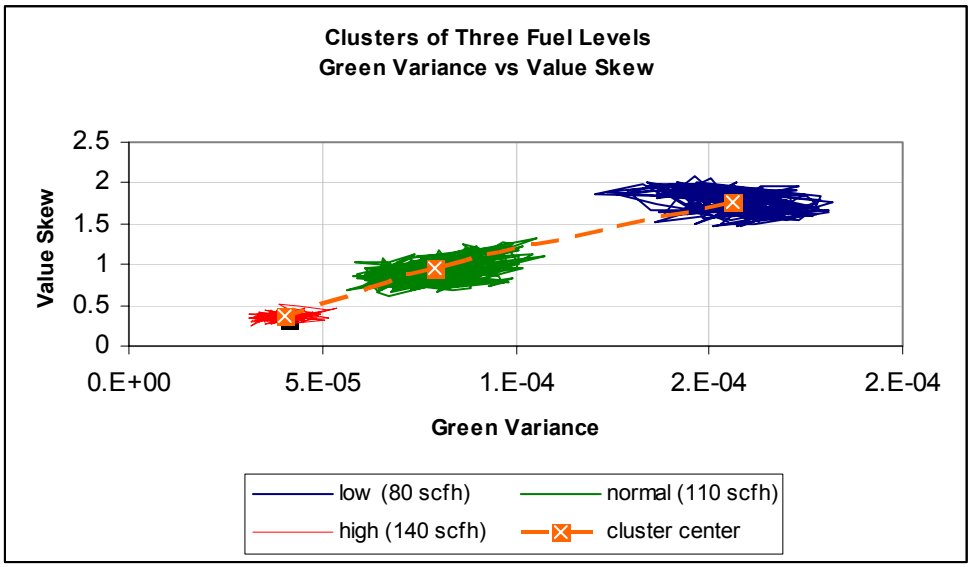

Figure 5.22 Scatter Plot of Green Channel's Variance and Value Channel's Skew

All the three plots show that the three features are able to provide good separability for all the three different classes. Similar to configuration 1, each cluster has different variance and size. However the features have less linearity characteristic.

Table 5.6 summarizes the six features and the absolute distances between classes based on the classes' means using each feature. The ratio of distances also provided to

provide approximation of similarity between class distances with 1 being equal distance between class low to class normal and class normal to class high. In overall, both configurations provide good separation and several key features to select from exist. Configuration 1's blue channel's otsu's threshold and value channel's entropy are selected since not only the features has more linearity characteristic compared to the others, but they require less computational cost as well. Furthermore configuration 1 can produce output faster than configuration 2.

Table 5.6 Six Selected Features and their Distances between Classes

Feature	High to Normal	Normal to Low	(High to Normal) / (Normal to Low)
Blue Otsu Threshold	10.6	11.1	0.96
Value Entropy	18.6E+3	13E+3	1.36
Red Center of Mass about Y Axis	94.5	135.8	0.69
Value Center of Mass about Y Axis	33.7	24.3	1.96
Green Variance	7.7E-05	3.9E-05	1.39
Value Skew	0.82	0.58	1.41

5.4.5 Oxidizer Classification

Oxidizer classification however is not as straight forward as fuel's because of the different level of flow rates in the experimental runs. Several different arrangements of the classes are tested in the feature selection process to investigate the classification feasibility.

5.4.5.1 Different Ways of Arranging Class Label

Table 5.7 shows one possible arrangement that has 7 different classes of oxidizer, however the resulting decision tree is very complex for both configurations using either forward selection or backward elimination as shown in Figure 5.23 to 5.26 respectively. The features involved are also numerous. Additionally, all of them have non-zero classification errors that varies from 0.06% to 1.2% which are relatively small nonetheless.

Table 5.7 Arrangement of Experimental Runs based on Oxidizer Level

Test #	NG Scfh	O2 Scfh	CLASS LABEL
2	80	144	EXTREME LOW
5	80	168	VERY LOW
8	80	192	LOW
3	110	198	LOW
1	110	231	NORMAL
6	110	231	NORMAL
12	110	231	NORMAL
4	140	252	HIGH
9	110	264	HIGH
7	140	294	VERY HIGH
10	140	336	EXTREME HIGH

```
SAT_OTS <= 161.1:
:...RED_OTS <= 187.383:
:   :...HUE_OTS <= 96.55:
:   :   :...BLU_OTS <= 125.6: high (213)
:   :   :   BLU_OTS > 125.6: normal (171)
:   :   HUE_OTS > 96.55:
:   :   :...SAT_OTS <= 161.033: high (5615)
:   :       SAT_OTS > 161.033:
:   :       :...BLU_OTS <= 133.317: normal (6)
:   :           BLU_OTS > 133.317: high (27)
:   RED_OTS > 187.383:
:   :...HUE_OTS <= 91.3833:
:       :...BLU_OTS <= 124.25: very_high (93/1)
:       :   BLU_OTS > 124.25:
:       :   :...VAL_OTS > 189.017: extreme_high (2730)
:       :       VAL_OTS <= 189.017:
:       :       :...BLU_OTS <= 126.2: very_high (3)
:       :           BLU_OTS > 126.2: extreme_high (22)
:       HUE_OTS > 91.3833:
:       :...VAL_OTS > 190.5: extreme_high (173)
:           VAL_OTS <= 190.5:
:           :...BLU_OTS > 126.483:
:               :...SAT_OTS <= 156.15: extreme_high (10)
:               :   SAT_OTS > 156.15: very_high (16)
:               BLU_OTS <= 126.483:
:               :...SAT_ARE <= 19815.7: very_high (2810/1)
:                   SAT_ARE > 19815.7:
:                   :...HUE_ARE <= 10375.7: very_high (21)
:                       HUE_ARE > 10375.7: extreme_high (4)
SAT_OTS > 161.1:
:...SAT_OTS <= 164.267:
    :...GRE_ARE > 19555.8: low (91)
    :   GRE_ARE <= 19555.8:
    :   :...VAL_OTS <= 188.333: normal (8521/6)
    :       VAL_OTS > 188.333:
    :       :...HUE_ARE <= 11602.3: normal (6)
    :           HUE_ARE > 11602.3: high (21)
    SAT_OTS > 164.267:
    :...SAT_OTS <= 170.1:
        :...SAT_OTS > 164.617: low (5396)
        :   SAT_OTS <= 164.617:
        :   :...BLU_OTS <= 133.583: low (395)
        :       BLU_OTS > 133.583: normal (125)
        SAT_OTS > 170.1:
        :...HUE_OTS <= 99.2333:
            :...GRE_ARE > 18081.7: extreme_low (483)
            :   GRE_ARE <= 18081.7:
            :   :...RED_ARE <= 23021.3: extreme_low (43)
            :       RED_ARE > 23021.3: very_low (12)
            HUE_OTS > 99.2333:
            :...SAT_OTS > 172.617:
                :...GRE_OTS > 170.417:
                :   :...RED_OTS > 193.217: extreme_low (40)
                :   :   RED_OTS <= 193.217:
                :   :   :...RED_ARE <= 19025.9: extreme_low (5)
                :   :       RED_ARE > 19025.9: very_low (34)
                :   GRE_OTS <= 170.417:
                :   :...GRE_OTS <= 170.183: extreme_low (601/1)
                :       GRE_OTS > 170.183:
                :       :...GRE_ARE <= 15535.8: very_low (2)
                :           GRE_ARE > 15535.8:
                :           :...VAL_ARE <= 20077.4: extreme_low (52)
                :               VAL_ARE > 20077.4: very_low (3)
                SAT_OTS <= 172.617:
                :...SAT_ARE > 23400.5: extreme_low (164)
                    SAT_ARE <= 23400.5:
                    :...BLU_OTS <= 142.933:
                        :...HUE_ARE > 11956.5:
                        :   :...SAT_OTS <= 172.1: very_low (100/2)
                        :   :   SAT_OTS > 172.1: extreme_low (5)
                        :   HUE_ARE <= 11956.5:
                        :   :...RED_ARE > 23206:
                        :       :...SAT_ARE > 22940.7: extreme_low (41)
                        :       :   SAT_ARE <= 22940.7:
                        :       :   :...HUE_ARE > 11515: very_low (107)
                        :       :       HUE_ARE <= 11515:
                        :       :       :...GRE_ARE <= 17669: very_low (4)
                        :       :           GRE_ARE > 17669:
                        :       :           :...BLU_OTS <= 142.8: extreme_low (31)
                        :       :               BLU_OTS > 142.8: very_low (2)
                        :       RED_ARE <= 23206:
                        :       :...SAT_OTS > 171.567:
                        :           :...BLU_OTS <= 142.767:
                        :           :   :...GRE_ARE > 17066: extreme_low (425/1)
                        :           :   :   GRE_ARE <= 17066:
                        :           :   :   :...HUE_ARE <= 10849: extreme_low (4)
                        :           :   :       HUE_ARE > 10849: very_low (3)
                        :           :   BLU_OTS > 142.767:
                        :           :   :...RED_OTS <= 190.767: very_low (12/1)
                        :           :       RED_OTS > 190.767:
                        :           :       :...RED_ARE <= 22102.9: extreme_low (139/1)
                        :           :           RED_ARE > 22102.9: [S1]
                        :           SAT_OTS <= 171.567:
                        :           :...SAT_OTS <= 171.117: very_low (28)
                        :               SAT_OTS > 171.117:
                        :               :...RED_OTS <= 191.05: very_low (18)
                        :                   RED_OTS > 191.05:
                        :                   :...BLU_OTS <= 142.583: extreme_low (102)
                        :                       BLU_OTS > 142.583: [S2]
                        BLU_OTS > 142.933:
                        :...SAT_OTS <= 172:
                            :...BLU_OTS > 143.5: very_low (877)
                            :   BLU_OTS <= 143.5:
                            :   :...SAT_OTS <= 171.617:
                            :       :...BLU_OTS > 142.967: very_low (481)
                            :       :   BLU_OTS <= 142.967:
                            :       :   :...RED_OTS <= 192.65: very_low (29)
                            :       :       RED_OTS > 192.65: extreme_low (2)
                            :       SAT_OTS > 171.617:
                            :       :...RED_OTS <= 191.517: very_low (113)
                            :           RED_OTS > 191.517:
                            :           :...HUE_ARE > 11480.8:
                            :               :...GRE_ARE <= 18081.7: very_low (75)
                            :               :   GRE_ARE > 18081.7: extreme_low (2)
                            :               HUE_ARE <= 11480.8:
                            :               :...SAT_ARE <= 20396: very_low (36)
                            :                   SAT_ARE > 20396:
                            :                   :...GRE_OTS > 169.85: [S3]
                            :                       GRE_OTS <= 169.85: [S4]
                            SAT_OTS > 172:
                            :...BLU_OTS > 144.133:
                                :...RED_OTS > 193.75:
                                :   :...SAT_OTS <= 172.3: very_low (11)
                                :   :   SAT_OTS > 172.3: extreme_low (15)
                                :   RED_OTS <= 193.75:
                                :   :...GRE_OTS <= 169.633:
                                :       :...VAL_ARE <= 18214: extreme_low (4)
                                :       :   VAL_ARE > 18214: very_low (22/2)
                                :       GRE_OTS > 169.633:
                                :       :...BLU_OTS > 144.167: very_low (517)
                                :           BLU_OTS <= 144.167:
```

```
:          :...SAT_OTS <= 172.4: very_low (14)
:          :   SAT_OTS > 172.4: extreme_low (3)
BLU_OTS <= 144.133:
:...GRE_ARE <= 15778.3:
    :...RED_OTS <= 191.933: very_low (130)
    :   RED_OTS > 191.933:
    :   :...SAT_OTS <= 172.25: very_low (27)
    :       SAT_OTS > 172.25: extreme_low (14)
    GRE_ARE > 15778.3:
    :...HUE_ARE <= 10914.9:
        :...GRE_OTS <= 168.333: very_low (12)
        :   GRE_OTS > 168.333:
        :   :...SAT_OTS > 172.167: extreme_low (384)
        :       SAT_OTS <= 172.167: [S5]
        HUE_ARE > 10914.9:
        :...SAT_OTS > 172.317: extreme_low (49)
            SAT_OTS <= 172.317:
            :...HUE_OTS <= 99.8667: extreme_low (19/1)
                HUE_OTS > 99.8667:
                :...SAT_OTS > 172.267: [S6]
                    SAT_OTS <= 172.267: [S7]

SubTree [S1]

GRE_OTS <= 169.633: very_low (14)
GRE_OTS > 169.633: extreme_low (14)

SubTree [S2]

GRE_OTS > 170.05: extreme_low (37/1)
GRE_OTS <= 170.05:
:...SAT_OTS <= 171.483: very_low (41)
    SAT_OTS > 171.483:
    :...BLU_OTS <= 142.75: extreme_low (11)
        BLU_OTS > 142.75: very_low (3)

SubTree [S3]

BLU_OTS <= 143.333: extreme_low (66)
BLU_OTS > 143.333:
:...SAT_OTS > 171.85: extreme_low (12)
    SAT_OTS <= 171.85:
    :...GRE_OTS <= 170.283: very_low (8)
        GRE_OTS > 170.283: extreme_low (2)

SubTree [S4]

HUE_ARE <= 10445.2: extreme_low (22)
HUE_ARE > 10445.2:
:...GRE_OTS <= 169: extreme_low (7)
    GRE_OTS > 169:
    :...GRE_OTS <= 169.467: very_low (30)
        GRE_OTS > 169.467:
        :...VAL_OTS <= 193.083: extreme_low (7)
            VAL_OTS > 193.083: very_low (8/1)

SubTree [S5]

BLU_OTS > 143.8: very_low (14)
BLU_OTS <= 143.8:
:...GRE_ARE > 16135.6: extreme_low (96/1)
    GRE_ARE <= 16135.6:
    :...BLU_OTS <= 143.467: extreme_low (6)
        BLU_OTS > 143.467: very_low (5)

SubTree [S6]

BLU_OTS <= 143.333: extreme_low (10)
BLU_OTS > 143.333:
:...HUE_OTS <= 100.833: extreme_low (3)
    HUE_OTS > 100.833: very_low (7)

SubTree [S7]

HUE_OTS > 102.267: very_low (100/1)
HUE_OTS <= 102.267:
:...HUE_ARE > 11314.2: very_low (26)
    HUE_ARE <= 11314.2:
    :...BLU_OTS > 143.683: very_low (10)
        BLU_OTS <= 143.683:
        :...RED_OTS <= 191.683: very_low (7)
            RED_OTS > 191.683: extreme_low (20)
```

```
 (a)   (b)   (c)   (d)   (e)   (f)   (g)    <-classified as
----  ----  ----  ----  ----  ----  ----
2993     7                                   (a): class extreme_low
   6  2994                                   (b): class very_low
               5999                         (c): class low
                     9000                   (d): class normal
                        6  5994              (e): class high
                                 3000        (f): class very_high
                                    2  2998  (g): class extreme_high

Error rate: 0.06%
```

Figure 5.23 Decision Tree for Configuration 1 using Forward Selection

```
HUE_TMP <= 1874.16:
:...RED_OTS <= 187.383: high (5882)
:   RED_OTS > 187.383:
:   :...BLU_SKW <= -0.217246: extreme_high (2934/1)
:       BLU_SKW > -0.217246:
:       :...SAT_OTS > 152.8: very_high (2923)
:           SAT_OTS <= 152.8:
:           :...BLU_SKW <= -0.123637: extreme_high (8)
:               BLU_SKW > -0.123637: very_high (17)
HUE_TMP > 1874.16:
:...RED_TMP <= 1820.8: normal (8823)
    RED_TMP > 1820.8:
    :...SAT_SKW > 1.01652: low (5882)
        SAT_SKW <= 1.01652:
        :...SAT_SKW <= 1.01513:
            :...GRE_OTS <= 170.267:
            :   :...BLU_VAR > 0.0145155: extreme_low (1269)
            :   :   BLU_VAR <= 0.0145155:
            :   :   :...SAT_TMP <= 1904.19: very_low (10)
            :   :       SAT_TMP > 1904.19: extreme_low (41)
            :   GRE_OTS > 170.267:
            :   :...SAT_SKW > 1.01487:
            :       :...BLU_SKW <= -0.671247: very_low (104)
            :       :   BLU_SKW > -0.671247: extreme_low (27/1)
            :       SAT_SKW <= 1.01487:
            :       :...BLU_KRT <= -0.435997: extreme_low (174)
            :           BLU_KRT > -0.435997:
            :           :...SAT_VAR <= 55466.2: very_low (9)
            :               SAT_VAR > 55466.2: extreme_low (6)
            SAT_SKW > 1.01513:
            :...BLU_SKW > -0.612152:
                :...HUE_TMP <= 1902.94:
                :   :...GRE_ARE <= 18049: very_low (205/2)
                :   :   GRE_ARE > 18049: extreme_low (58)
                :   HUE_TMP > 1902.94:
                :   :...RED_TMP <= 1889.54:
                :       :...BLU_KRT <= -0.810661: extreme_low (37)
                :       :   BLU_KRT > -0.810661: very_low (64)
                :       RED_TMP > 1889.54:
                :       :...SAT_COM > 358.817:
                :           :...BLU_SKW <= -0.588554: very_low (24)
                :           :   BLU_SKW > -0.588554: extreme_low (18)
                :           SAT_COM <= 358.817:
                :           :...BLU_KRT <= -0.718058: extreme_low (1018)
                :               BLU_KRT > -0.718058:
                :               :...RED_TMP <= 1893.32: very_low (7)
                :                   RED_TMP > 1893.32: extreme_low (25)
                BLU_SKW <= -0.612152:
                :...GRE_COM <= 384.399: extreme_low (35)
                    GRE_COM > 384.399:
                    :...GRE_VAR > 0.010845:
                        :...SAT_KRT <= -1.95974: extreme_low (130/1)
                        :   SAT_KRT > -1.95974: very_low (107)
                        GRE_VAR <= 0.010845:
                        :...HUE_TMP > 1905.69:
                            :...GRE_VAR > 0.010357: extreme_low (35)
                            :   GRE_VAR <= 0.010357:
                            :   :...HUE_VAR <= 72008.7: very_low (52)
                            :       HUE_VAR > 72008.7: extreme_low (3)
                            HUE_TMP <= 1905.69:
                            :...SAT_OTS > 172.633:
                                :...GRE_COM <= 410.617: extreme_low (13)
                                :   GRE_COM > 410.617: very_low (12)
                                SAT_OTS <= 172.633:
                                :...SAT_COM > 334.9: very_low (1650)
                                    SAT_COM <= 334.9:
                                    :...SAT_SKW <= 1.0154:
                                        :...BLU_AVG <= 0.844772: extreme_low (27)
                                        :   BLU_AVG > 0.844772:
                                        :   :...VAL_ENT <= -157502: very_low (116)
                                        :       VAL_ENT > -157502: extreme_low (18/1)
                                        SAT_SKW > 1.0154:
                                        :...BLU_SKW <= -0.617094: very_low (550/1)
                                            BLU_SKW > -0.617094:
                                            :...RED_COM <= 373.125: very_low (29)
                                                RED_COM > 373.125: [S1]

SubTree [S1]

VAL_OTS <= 193.35: extreme_low (7)
VAL_OTS > 193.35: very_low (2)
```

```
 (a)   (b)   (c)   (d)   (e)   (f)   (g)    <-classified as
----  ----  ----  ----  ----  ----  ----
2997     3                                   (a): class extreme_low
   3  2997                                   (b): class very_low
               6000                         (c): class low
                     9000                   (d): class normal
                           6000             (e): class high
                                 2999     1  (f): class very_high
                                       3000  (g): class extreme_high

 Error rate: 0.02%
```

Figure 5.24 Decision Tree for Configuration 1 using Backward Elimination

```
RED_AVG > 0.0202968:
:...GRE_TMP <= 1376.08: extreme_high (49)
:   GRE_TMP > 1376.08: very_high (50/2)
RED_AVG <= 0.0202968:
:...VAL_COM <= 347.746:
    :...GRE_TMP > 1424.86: low (50/1)
    :   GRE_TMP <= 1424.86:
    :   :...VAL_AVG <= 0.018592:
    :       :...GRE_TMP <= 1393.85: high (29)
    :       :   GRE_TMP > 1393.85: normal (187/1)
    :       VAL_AVG > 0.018592:
    :       :...GRE_TMP <= 1413.55: high (70/1)
    :           GRE_TMP > 1413.55: normal (3)
    VAL_COM > 347.746:
    :...HUE_COM <= 550.729:
        :...GRE_TMP <= 1430.48: low (47)
        :   GRE_TMP > 1430.48: very_low (3/1)
        HUE_COM > 550.729:
        :...GRE_TMP <= 1429.83:
            :...VAL_AVG <= 0.0169017: very_low (9)
            :   VAL_AVG > 0.0169017: low (2)
            GRE_TMP > 1429.83:
            :...RED_COM > 375.144: extreme_low (14)
                RED_COM <= 375.144:
                :...SAT_COM > 418.422: very_low (14/1)
                    SAT_COM <= 418.422:
                    :...RED_COM > 370.215: extreme_low (13)
                        RED_COM <= 370.215:
                        :...GRE_TMP <= 1444.65: very_low (15/1)
                            GRE_TMP > 1444.65:
                            :...HUE_AVG > 0.00111426: extreme_low (14)
                                HUE_AVG <= 0.00111426:
                                :...BLU_AVG <= 0.00675775: extreme_low (5)
                                    BLU_AVG > 0.00675775:
                                    :...GRE_TMP > 1451: extreme_low (2/1)
                                        GRE_TMP <= 1451:
                                        :...RED_COM <= 362.503: very_low (8)
                                            RED_COM > 362.503:
                                            :...RED_AVG <= 0.0167444: extreme_low (2)
                                                RED_AVG > 0.0167444: very_low (2)


        (a)   (b)   (c)   (d)   (e)   (f)   (g)    <-classified as
       ----  ----  ----  ----  ----  ----  ----
         49     1                                   (a): class extreme_low
          1    49                                   (b): class very_low
                1    99                            (c): class low
                      1   149                       (d): class normal
                            1    99                 (e): class high
                                 1    49            (f): class very_high
                                      1    49       (g): class extreme_high
        Error rate: 1.5%
```

Figure 5.25 Decision Tree for Configuration 2 using Forward Elimination

```
RED_AVG > 0.0202968:
:...GRE_TMP <= 1376.08: extreme_high (49)
:   GRE_TMP > 1376.08: very_high (50/1)
RED_AVG <= 0.0202968:
:...VAL_COM <= 347.746:
    :...GRE_TMP > 1424.86: low (50/1)
    :   GRE_TMP <= 1424.86:
    :   :...SAT_VAR <= 0.000211992:
    :       :...VAL_VAR <= 7.81e-005: normal (6)
    :       :   VAL_VAR > 7.81e-005: high (82/2)
    :       SAT_VAR > 0.000211992:
    :       :...GRE_TMP > 1398.07: normal (188)
    :           GRE_TMP <= 1398.07:
    :           :...VAL_AVG <= 0.017836: normal (4)
    :               VAL_AVG > 0.017836: high (20)
    VAL_COM > 347.746:
    :...RED_SKW <= -1.00433:
        :...RED_KRT <= -1.9654: very_low (1)
        :   RED_KRT > -1.9654: low (50/1)
        RED_SKW > -1.00433:
        :...RED_SKW > -0.975867: extreme_low (19/1)
            RED_SKW <= -0.975867:
            :...VAL_ENT > -1360000:
                :...GRE_TMP <= 1448.6: very_low (22/1)
                :   GRE_TMP > 1448.6:
                :   :...SAT_SKW <= 1.80662: very_low (2)
                :       SAT_SKW > 1.80662: extreme_low (4/1)
                VAL_ENT <= -1360000:
                :...RED_SKW > -0.991308:
                    :...VAL_ENT <= -1370000: extreme_low (7)
                    :   VAL_ENT > -1370000:
                    :   :...GRE_TMP <= 1436.41: very_low (2/1)
                    :       GRE_TMP > 1436.41: extreme_low (11/1)
                    RED_SKW <= -0.991308:
                    :...GRE_TMP > 1437.85:
                        :...GRE_VAR <= 0.000165712: extreme_low (5)
                        :   GRE_VAR > 0.000165712: very_low (3/1)
                        GRE_TMP <= 1437.85:
                        :...VAL_AVG > 0.0155511: very_low (18)
                            VAL_AVG <= 0.0155511:
                            :...GRE_TMP <= 1429.83: very_low (1)
                                GRE_TMP > 1429.83: extreme_low (3)


 (a)   (b)   (c)   (d)   (e)   (f)   (g)    <-classified as
----  ----  ----  ----  ----  ----  ----
  47     3                                   (a): class extreme_low
   3    47     1                            (b): class very_low
             100                            (c): class low
               1   147     2                (d): class normal
                         100                (e): class high
                           1    49          (f): class very_high
                                 2    48    (g): class extreme_high

Error rate: 2.4%
```

Figure 5.26 Decision Tree for Configuration 2 using Backward Elimination

Although the classification performances are acceptable, the drawback to the arrangement is that it involves various features which can make the fuzzy logic implementation complex. The resulting decision trees are also less intuitive and it is hard to find correlation between the selected features and the oxidizer level. The non-uniform choice of features for branching also makes it challenging to approximate the classification of unknown level of oxidizer changes that is beyond the dataset.

Another possible arrangement is to group the oxidizer level based on the O/F ratio as mentioned earlier in Table 5.3. The arrangement reduces the class from 7 to 3 as shown in Table 5.8. However, it has similar problem on the decision tree as previous arrangement. That is, even though the classification errors are small, the decision trees themselves are complex involving numerous features. The decision tree results are shown in Figure 5.27 to 5.30 for both configurations using forward selection and backward elimination respectively. Note that even though configuration 2's decision trees has higher classification error rate, the complexity of the tree is much less than configuration 1's.

Table 5.8 Arrangement of Experimental Runs based on O/F Ratio

Run #	NG Scfh	O2 Scfh	O/F Ratio	Oxidizer Label
2	80	144	1.8	FUEL RICH
3	110	198	1.8	FUEL RICH
4	140	252	1.8	FUEL RICH
5	80	168	2.1	STOICHIOMETRY
1	110	231	2.1	STOICHIOMETRY
6	110	231	2.1	STOICHIOMETRY
12	110	231	2.1	STOICHIOMETRY
7	140	294	2.1	STOICHIOMETRY
8	80	192	2.4	FUEL LEAN
9	110	264	2.4	FUEL LEAN
10	140	336	2.4	FUEL LEAN

```
BLU_OTS <= 121.75:
:...RED_OTS <= 187.233: fuel_rich (2871)
:   RED_OTS > 187.233: stoichiometry (25/1)
BLU_OTS > 121.75:
:...VAL_OTS <= 184.35:
    :...HUE_ARE <= 12216.9: fuel_rich (2304)
    :   HUE_ARE > 12216.9: stoichiometry (141)
    VAL_OTS > 184.35:
    :...SAT_OTS <= 170.917:
        :...VAL_OTS > 189.983:
        :   :...HUE_ARE <= 9568.65: stoichiometry (156)
        :   :   HUE_ARE > 9568.65:
        :   :   :...SAT_OTS <= 170.1: fuel_lean (5395)
        :   :       SAT_OTS > 170.1: stoichiometry (25)
        :   VAL_OTS <= 189.983:
        :   :...GRE_ARE <= 15848.5:
        :       :...SAT_OTS <= 161.567: fuel_lean (2754)
        :       :   SAT_OTS > 161.567: stoichiometry (220)
        :       GRE_ARE > 15848.5:
        :       :...SAT_OTS > 164.617: fuel_rich (637)
        :           SAT_OTS <= 164.617:
        :           :...HUE_OTS <= 90.9833:
        :           :   :...BLU_OTS <= 124.75: stoichiometry (26)
        :           :   :   BLU_OTS > 124.75: fuel_lean (452)
        :           :   HUE_OTS > 90.9833:
        :           :   :...HUE_ARE <= 7298.35: fuel_rich (69)
        :           :       HUE_ARE > 7298.35:
        :           :       :...HUE_ARE > 13216.9:
        :           :           :...VAL_OTS <= 186.417: stoichiometry (401)
        :           :           :   VAL_OTS > 186.417: fuel_lean (148)
        :           :           HUE_ARE <= 13216.9:
        :           :           :...HUE_OTS <= 91.5667:
        :           :               :...BLU_OTS <= 125.55: stoichiometry (132)
        :           :               :   BLU_OTS > 125.55: fuel_lean (34)
        :           :               HUE_OTS > 91.5667:
        :           :               :...GRE_ARE > 15949.5: stoichiometry (10480/3)
        :           :                   GRE_ARE <= 15949.5:
        :           :                   :...SAT_OTS <= 161.133: fuel_lean (37)
        :           :                       SAT_OTS > 161.133: stoichiometry (187)
        :           :
        :       SAT_OTS > 170.917:
        :       :...HUE_OTS <= 99.2333:
        :           :...GRE_ARE > 18081.7: fuel_rich (483)
        :           :   GRE_ARE <= 18081.7:
        :           :   :...RED_ARE <= 23021.3: fuel_rich (43)
        :           :       RED_ARE > 23021.3: stoichiometry (12)
        :           HUE_OTS > 99.2333:
        :           :...SAT_OTS > 172.617:
        :               :...GRE_OTS > 170.417:
        :               :   :...RED_OTS > 193.217: fuel_rich (40)
        :               :   :   RED_OTS <= 193.217:
        :               :   :   :...RED_ARE <= 19025.9: fuel_rich (5)
        :               :   :       RED_ARE > 19025.9: stoichiometry (34)
        :               :   GRE_OTS <= 170.417:
        :               :   :...GRE_OTS <= 170.183: fuel_rich (601/1)
        :               :       GRE_OTS > 170.183:
        :               :       :...GRE_ARE <= 15535.8: stoichiometry (2)
        :               :           GRE_ARE > 15535.8:
        :               :           :...VAL_ARE <= 20077.4: fuel_rich (52)
        :               :               VAL_ARE > 20077.4: stoichiometry (3)
        :               SAT_OTS <= 172.617:
        :               :...SAT_ARE > 23400.5: fuel_rich (164)
        :                   SAT_ARE <= 23400.5:
        :                   :...BLU_OTS <= 142.933:
        :                   :   :...HUE_ARE > 11956.5:
        :                   :   :   :...SAT_OTS > 172.1: fuel_rich (5)
        :                   :   :   :   SAT_OTS <= 172.1:
        :                   :   :   :   :...SAT_ARE <= 23137.5: stoichiometry (96)
        :                   :   :   :       SAT_ARE > 23137.5:
        :                   :   :   :       :...RED_ARE <= 22491: stoichiometry (2)
        :                   :   :   :           RED_ARE > 22491: fuel_rich (2)
        :                   :   :   HUE_ARE <= 11956.5:
        :                   :   :   :...SAT_OTS > 171.733:
        :                   :   :       :...BLU_OTS <= 142.8: fuel_rich (352)
        :                   :   :       :   BLU_OTS > 142.8:
        :                   :   :       :   :...RED_ARE <= 22102.9: fuel_rich (112)
        :                   :   :       :       RED_ARE > 22102.9:
        :                   :   :       :       :...GRE_OTS <= 169.65: stoichiometry (17)
        :                   :   :       :           GRE_OTS > 169.65: fuel_rich (6)
        :                   :   :       SAT_OTS <= 171.733:
        :                   :   :       :...RED_OTS <= 191.05:
        :                   :   :           :...BLU_OTS <= 141.95: fuel_rich (6)
        :                   :   :           :   BLU_OTS > 141.95: stoichiometry (75)
        :                   :   :           RED_OTS > 191.05:
        :                   :   :           :...SAT_OTS <= 171.117: stoichiometry (45/1)
        :                   :   :               SAT_OTS > 171.117:
        :                   :   :               :...BLU_OTS <= 142.567: fuel_rich (207/1)
        :                   :   :                   BLU_OTS > 142.567: [S1]
        :                   :   BLU_OTS > 142.933:
        :                   :   :...SAT_OTS <= 172:
        :                   :       :...BLU_OTS > 143.5: stoichiometry (877)
        :                   :       :   BLU_OTS <= 143.5:
        :                   :       :   :...SAT_OTS <= 171.617:
        :                   :       :       :...BLU_OTS > 142.967: stoichiometry (481)
        :                   :       :       :   BLU_OTS <= 142.967:
        :                   :       :       :   :...RED_OTS <= 192.65: stoichiometry (29)
        :                   :       :       :       RED_OTS > 192.65: fuel_rich (2)
        :                   :       :       SAT_OTS > 171.617:
        :                   :       :       :...RED_OTS <= 191.517: stoichiometry (113)
        :                   :       :           RED_OTS > 191.517:
        :                   :       :           :...HUE_ARE > 11480.8: stoichiometry (77/2)
        :                   :       :               HUE_ARE <= 11480.8: [S2]
        :                   :       SAT_OTS > 172:
        :                   :       :...BLU_OTS > 144.133:
        :                   :           :...RED_OTS > 193.75:
        :                   :           :   :...SAT_OTS <= 172.3: stoichiometry (11)
        :                   :           :   :   SAT_OTS > 172.3: fuel_rich (15)
        :                   :           :   RED_OTS <= 193.75:
        :                   :           :   :...GRE_OTS <= 169.633:
        :                   :           :       :...VAL_ARE <= 18214: fuel_rich (4)
        :                   :           :       :   VAL_ARE > 18214: stoichiometry (22/2)
        :                   :           :       GRE_OTS > 169.633:
        :                   :           :       :...BLU_OTS > 144.183: stoichiometry (513)
        :                   :           :           BLU_OTS <= 144.183: [S3]
        :                   :           BLU_OTS <= 144.133:
        :                   :           :...GRE_ARE <= 15778.3:
```

```
:...RED_OTS <= 191.933: stoichiometry (130)
:   RED_OTS > 191.933:
:   :...SAT_OTS <= 172.25: stoichiometry (27)
:       SAT_OTS > 172.25: fuel_rich (14)
GRE_ARE > 15778.3:
:...HUE_ARE <= 10914.9:
    :...GRE_OTS <= 168.417: [S4]
    :   GRE_OTS > 168.417:
    :   :...SAT_OTS > 172.167: fuel_rich (373)
    :       SAT_OTS <= 172.167: [S5]
    HUE_ARE > 10914.9:
    :...SAT_OTS > 172.317: fuel_rich (49)
        SAT_OTS <= 172.317:
        :...HUE_OTS <= 99.8667: fuel_rich (19/1)
            HUE_OTS > 99.8667:
            :...SAT_OTS > 172.267: [S6]
                SAT_OTS <= 172.267: [S7]


SubTree [S1]

RED_OTS <= 191.617: stoichiometry (26)
RED_OTS > 191.617:
:...SAT_OTS > 171.5: fuel_rich (93/1)
    SAT_OTS <= 171.5:
    :...GRE_OTS <= 170.083: stoichiometry (45/1)
        GRE_OTS > 170.083: fuel_rich (27/1)

SubTree [S2]

SAT_ARE <= 20396: stoichiometry (36)
SAT_ARE > 20396:
:...GRE_OTS > 169.85:
    :...BLU_OTS <= 143.333: fuel_rich (66)
    :   BLU_OTS > 143.333:
    :   :...SAT_OTS > 171.85: fuel_rich (12)
    :       SAT_OTS <= 171.85:
    :       :...GRE_OTS <= 170.283: stoichiometry (8)
    :           GRE_OTS > 170.283: fuel_rich (2)
    GRE_OTS <= 169.85:
    :...HUE_ARE <= 10445.2: fuel_rich (22)
        HUE_ARE > 10445.2:
        :...GRE_OTS <= 169: fuel_rich (7)
            GRE_OTS > 169:
            :...GRE_OTS <= 169.467: stoichiometry (30)
                GRE_OTS > 169.467:
                :...VAL_OTS <= 193.083: fuel_rich (7)
                    VAL_OTS > 193.083: stoichiometry (8/1)

SubTree [S3]

SAT_OTS <= 172.467: stoichiometry (18)
SAT_OTS > 172.467: fuel_rich (3)

SubTree [S4]

SAT_OTS <= 172.333: stoichiometry (12)
SAT_OTS > 172.333: fuel_rich (11)

SubTree [S5]

BLU_OTS > 143.8: stoichiometry (14)
BLU_OTS <= 143.8:
:...GRE_ARE > 16135.6: fuel_rich (96/1)
    GRE_ARE <= 16135.6:
    :...BLU_OTS <= 143.467: fuel_rich (6)
        BLU_OTS > 143.467: stoichiometry (5)

SubTree [S6]

BLU_OTS <= 143.333: fuel_rich (10)
BLU_OTS > 143.333:
:...HUE_OTS <= 100.833: fuel_rich (3)
    HUE_OTS > 100.833: stoichiometry (7)

SubTree [S7]

HUE_OTS > 102.267: stoichiometry (100/1)
HUE_OTS <= 102.267:
:...HUE_ARE > 11314.2: stoichiometry (26)
    HUE_ARE <= 11314.2:
    :...BLU_OTS > 143.683: stoichiometry (10)
        BLU_OTS <= 143.683:
        :...RED_OTS <= 191.683: stoichiometry (7)
            RED_OTS > 191.683: fuel_rich (20)


            (a)   (b)   (c)    <-classified as
           ----  ----  ----
           8991     9          (a): class fuel_rich
              6 14994          (b): class stoichiometry
                    3  8997    (c): class fuel_lean

           Error rate: 0.1%
```

Figure 5.27 Decision Tree for Configuration 1 using Forward Selection

```
RED_TMP <= 1777.18:
:...BLU_SKW <= -0.148437: fuel_lean (2776)
:   BLU_SKW > -0.148437: stoichiometry (48)
RED_TMP > 1777.18:
:...GRE_ARE <= 15850.2:
    :...SAT_SKW > 1.01652:
    :   :...VAL_OTS <= 186: stoichiometry (138)
    :   :   VAL_OTS > 186:
    :   :...BLU_OTS <= 133.917: stoichiometry (69)
    :       BLU_OTS > 133.917:
    :       :...GRE_ARE <= 15814.4: fuel_lean (4951)
    :           GRE_ARE > 15814.4:
    :           :...RED_SKW <= 0.588576: fuel_lean (84)
    :               RED_SKW > 0.588576: stoichiometry (16)
    :   SAT_SKW <= 1.01652:
    :   :...SAT_SKW <= 1.01504: fuel_rich (101/2)
    :       SAT_SKW > 1.01504:
    :       :...SAT_COM > 334.9: stoichiometry (642)
    :           SAT_COM <= 334.9:
    :           :...HUE_TMP > 1904.59:
    :               :...VAL_ENT <= -161980: stoichiometry (2)
    :               :   VAL_ENT > -161980: fuel_rich (12)
    :               HUE_TMP <= 1904.59:
    :               :...GRE_VAR <= 0.0107398: stoichiometry (140)
    :                   GRE_VAR > 0.0107398:
    :                   :...BLU_COM <= 314.55: fuel_rich (13)
    :                       BLU_COM > 314.55: stoichiometry (17)
    :
    GRE_ARE > 15850.2:
    :...GRE_OTS > 171.133:
        :...SAT_SKW <= 1.01652: stoichiometry (169)
        :   SAT_SKW > 1.01652: fuel_lean (518)
        GRE_OTS <= 171.133:
        :...BLU_SKW > -0.0223269: fuel_rich (2941)
            BLU_SKW <= -0.0223269:
            :...RED_TMP <= 1820.8:
                :...VAL_OTS > 190.5: fuel_lean (165)
                :   VAL_OTS <= 190.5:
                :   :...HUE_ARE > 13216.9:
                :       :...SAT_SKW <= 1.02594: stoichiometry (459)
                :       :   SAT_SKW > 1.02594: fuel_lean (148)
                :       HUE_ARE <= 13216.9:
                :       :...GRE_ARE > 15949.5: stoichiometry (10851/2)
                :           GRE_ARE <= 15949.5:
                :           :...SAT_SKW <= 1.02567: stoichiometry (185)
                :               SAT_SKW > 1.02567: fuel_lean (35)
                RED_TMP > 1820.8:
                :...BLU_OTS <= 142.117:
                    :...BLU_KRT <= -0.737893: fuel_rich (3460)
                    :   BLU_KRT > -0.737893:
                    :   :...BLU_COM <= 304.1: fuel_rich (21)
                    :       BLU_COM > 304.1: stoichiometry (4)
                    BLU_OTS > 142.117:
                    :...SAT_KRT <= -1.96082:
                        :...BLU_VAR <= 0.0144449:
                        :   :...SAT_SKW <= 1.0147: fuel_rich (63)
                        :   :   SAT_SKW > 1.0147: stoichiometry (70)
                        :   BLU_VAR > 0.0144449:
                        :   :...RED_TMP <= 1896.07:
                        :       :...BLU_VAR > 0.0153348: fuel_rich (150)
                        :       :   BLU_VAR <= 0.0153348:
                        :       :   :...BLU_COM <= 283.683: fuel_rich (3)
                        :       :       BLU_COM > 283.683: stoichiometry (57)
                        :       RED_TMP > 1896.07:
                        :       :...SAT_SKW <= 1.01513: fuel_rich (1209/1)
                        :           SAT_SKW > 1.01513:
                        :           :...GRE_KRT <= -1.00545: fuel_rich (51)
                        :               GRE_KRT > -1.00545: stoichiometry (4)
                        :   SAT_KRT > -1.96082:
                        :   :...BLU_SKW > -0.612152:
                        :       :...SAT_SKW > 1.01588: stoichiometry (194/2)
                        :       :   SAT_SKW <= 1.01588:
                        :       :   :...RED_KRT > -1.11143: stoichiometry (30/1)
                        :       :       RED_KRT <= -1.11143:
                        :       :       :...HUE_TMP <= 1903.84:
                        :       :           :...RED_TMP <= 1892.78: stoichiometry (62)
                        :       :           :   RED_TMP > 1892.78: [S1]
                        :       :           HUE_TMP > 1903.84:
                        :       :           :...VAL_ENT > -204263: fuel_rich (523/1)
                        :       :               VAL_ENT <= -204263: [S2]
                        :       BLU_SKW <= -0.612152:
                        :       :...GRE_COM <= 384.399: fuel_rich (25)
                        :           GRE_COM > 384.399:
                        :           :...GRE_VAR > 0.0108621:
                        :           :   :...SAT_SKW <= 1.01557: fuel_rich (99)
                        :           :   :   SAT_SKW > 1.01557: stoichiometry (44)
                        :           :   GRE_VAR <= 0.0108621:
                        :           :   :...SAT_OTS > 172.55:
                        :           :       :...GRE_OTS <= 170: fuel_rich (13)
                        :           :       :   GRE_OTS > 170: stoichiometry (15)
                        :           :       SAT_OTS <= 172.55:
                        :           :       :...HUE_AVG > 0.732535: [S3]
                        :           :           HUE_AVG <= 0.732535:
                        :           :           :...SAT_COM > 329.5: [S4]
                        :           :               SAT_COM <= 329.5: [S5]

SubTree [S1]

HUE_VAR <= 73229: stoichiometry (3)
HUE_VAR > 73229: fuel_rich (68)

SubTree [S2]

SAT_COM <= 320.133: fuel_rich (15)
SAT_COM > 320.133: stoichiometry (4)

SubTree [S3]

HUE_TMP <= 1897.62: fuel_lean (144)
HUE_TMP > 1897.62: stoichiometry (21)

SubTree [S4]

HUE_SKW <= 1.11039: stoichiometry (1099)
HUE_SKW > 1.11039:
:...HUE_TMP <= 1906.13: stoichiometry (22)
```

```
    HUE_TMP > 1906.13: fuel_rich (3)

SubTree [S5]

BLU_VAR > 0.0156205: fuel_rich (16)
BLU_VAR <= 0.0156205:
:...SAT_SKW <= 1.01532:
    :...BLU_OTS <= 143.85: fuel_rich (26)
    :   BLU_OTS > 143.85: stoichiometry (15)
    SAT_SKW > 1.01532:
    :...BLU_SKW <= -0.62248: stoichiometry (289/1)
        BLU_SKW > -0.62248:
        :...RED_COM <= 373.125: stoichiometry (34)
            RED_COM > 373.125:
            :...RED_TMP <= 1892.35: stoichiometry (4)
                RED_TMP > 1892.35: fuel_rich (11)


            (a)   (b)   (c)    <-classified as
           ----  ----  ----
           8994     4          (a): class fuel_rich
              4 14996          (b): class stoichiometry
                    2  8998    (c): class fuel_lean

           Error rate: 0.06%
```

Figure 5.28 Decision Tree for Configuration 1 using Backward Elimination

```
SAT_COM <= 404.595:
:...HUE_COM > 568.8994: fuel_rich (91/2)
:   HUE_COM <= 568.8994:
:   :...GRE_AVG <= 0.007720813: fuel_rich (7/1)
:       GRE_AVG > 0.007720813: fuel_lean (2)
SAT_COM > 404.595:
:...SAT_AVG > 0.01074972:
    :...RED_AVG > 0.01633964: stoichiometry (11)
    :   RED_AVG <= 0.01633964:
    :   :...BLU_COM <= 422.6686: fuel_rich (40)
    :       BLU_COM > 422.6686:
    :       :...RED_COM <= 370.9891: stoichiometry (12)
    :           RED_COM > 370.9891: fuel_rich (7)
    SAT_AVG <= 0.01074972:
    :...HUE_COM <= 538.399:
        :...VAL_AVG > 0.01817645: fuel_lean (72)
        :   VAL_AVG <= 0.01817645:
        :   :...RED_COM <= 341.1211: stoichiometry (15)
        :       RED_COM > 341.1211: fuel_lean (47/2)
        HUE_COM > 538.399:
        :...VAL_AVG > 0.02138686:
            :...GRE_COM <= 330.9509: stoichiometry (4)
            :   GRE_COM > 330.9509: fuel_lean (26)
            VAL_AVG <= 0.02138686:
            :...GRE_COM <= 393.8683: stoichiometry (207/9)
                GRE_COM > 393.8683:
                :...RED_COM > 372.7943: fuel_rich (3)
                    RED_COM <= 372.7943:
                    :...VAL_AVG <= 0.01716943: stoichiometry (4)
                        VAL_AVG > 0.01716943: fuel_lean (2)


           (a)   (b)   (c)    <-classified as
          ----  ----  ----
           145     5          (a): class fuel_rich
                 248     2    (b): class stoichiometry
             3     4   153    (c): class fuel_lean

           Error rate: 2.5%
```

Figure 5.29 Decision Tree for Configuration 2 using Forward Selection

```
RED_TMP <= 1192.47:
:...RED_SKW <= -0.9702253: fuel_lean (134/5)
:   RED_SKW > -0.9702253: stoichiometry (5)
RED_TMP > 1192.47:
:...SAT_COM <= 404.595:
    :...VAL_VAR <= 9.24e-005: fuel_rich (68)
    :   VAL_VAR > 9.24e-005:
    :   :...HUE_COM <= 569.0953: fuel_lean (2)
    :       HUE_COM > 569.0953: fuel_rich (30/2)
    SAT_COM > 404.595:
    :...GRE_TMP > 1442.045: fuel_rich (48/1)
        GRE_TMP <= 1442.045:
        :...RED_SKW <= -1.009382: fuel_lean (14)
            RED_SKW > -1.009382:
            :...BLU_COM > 429.3526:
                :...RED_KRT <= -1.96472: fuel_rich (2)
                :   RED_KRT > -1.96472: stoichiometry (7/1)
                BLU_COM <= 429.3526:
                :...BLU_ENT > -994246:
                    :...HUE_SKW <= 4.393744: stoichiometry (7)
                    :   HUE_SKW > 4.393744: fuel_lean (2)
                    BLU_ENT <= -994246:
                    :...SAT_COM > 407.1514: stoichiometry (224/2)
                        SAT_COM <= 407.1514:
                        :...HUE_KRT > 19.42931: fuel_rich (1/1)
                            HUE_KRT <= 19.42931:
                            :...GRE_AVG <= 0.007144373: fuel_rich (1)
                                GRE_AVG > 0.007144373: stoichiometry (6)


 (a)   (b)   (c)    <-classified as
----  ----  ----
 148     2          (a): class fuel_rich
   1   244     5    (b): class stoichiometry
   3     1   146    (c): class fuel_lean

Error rate: 2.1%
```

Figure 5.30 Decision Tree for Configuration 2 using Backward Elimination

The final arrangement follows the grouping as defined previously in Table 5.3. It is an attempt to see if there is any correlation between changes in fuel with the oxidizer classification. The flame profiles discussed before supports this idea as well.

One discovery made in this study is that the previously complex decision tree classifications of oxidizer can indeed be simplified provided the fuel level is known beforehand. This particular arrangement groups the original 11 runs in two levels, first by the fuel level then for each fuel level by the O/F ratio. The total number of class for oxidizer level is still three according to the O/F ratio.

5.4.5.2 Oxidizer Classification using Configuration 1

The arrangement based on Table 5.3 improves the simplicity of the decision tree for certain fuel level thus substantially reduces the number of features selected to classify oxidizer level. The classification error rates are also improved. However, the selected features are not the same for each class of fuel as shown in Figure 5.31 to 5.36. It still does not solve the complex classification process involving many features. Fortunately configuration 2 is able to provide a much better solution.

```
SAT_OTS <= 170.1: fuel_lean (2941)
SAT_OTS > 170.1:
:...HUE_OTS <= 99.2333:
    :...BLU_OTS <= 142.683: fuel_rich (410)
    :   BLU_OTS > 142.683:
    :   :...SAT_OTS > 171.533: fuel_rich (104)
    :       SAT_OTS <= 171.533:
    :       :...HUE_OTS <= 98.9833: fuel_rich (9)
    :           HUE_OTS > 98.9833:
    :           :...BLU_OTS > 142.817: stoichiometry (9)
    :               BLU_OTS <= 142.817:
    :               :...RED_OTS <= 192.25: stoichiometry (3)
    :                   RED_OTS > 192.25: fuel_rich (3)
    HUE_OTS > 99.2333:
    :...SAT_OTS > 172.617:
        :...GRE_OTS > 170.417:
        :   :...RED_OTS > 193.217: fuel_rich (40)
        :   :   RED_OTS <= 193.217:
        :   :   :...BLU_OTS <= 144.617: fuel_rich (5)
        :   :       BLU_OTS > 144.617: stoichiometry (34)
        :   GRE_OTS <= 170.417:
        :   :...GRE_OTS <= 170.183: fuel_rich (601/1)
        :       GRE_OTS > 170.183:
        :       :...HUE_OTS > 104.45: stoichiometry (2)
        :           HUE_OTS <= 104.45:
        :           :...RED_OTS > 192.55: fuel_rich (46)
        :               RED_OTS <= 192.55:
        :               :...BLU_OTS <= 144.467: fuel_rich (6)
        :                   BLU_OTS > 144.467: stoichiometry (3)
        SAT_OTS <= 172.617:
        :...BLU_OTS <= 142.9:
            :...SAT_OTS <= 171.1: stoichiometry (58)
            :   SAT_OTS > 171.1:
            :   :...RED_OTS <= 191.1:
            :       :...GRE_OTS <= 168.183: fuel_rich (151/1)
            :       :   GRE_OTS > 168.183:
            :       :   :...SAT_OTS > 172.1: fuel_rich (11)
            :       :       SAT_OTS <= 172.1:
            :       :       :...RED_OTS > 191.017:
            :       :           :...BLU_OTS <= 142.25: fuel_rich (7)
            :       :           :   BLU_OTS > 142.25: stoichiometry (10/1)
            :       :           RED_OTS <= 191.017:
            :       :           :...BLU_OTS > 142.067: stoichiometry (131)
            :       :               BLU_OTS <= 142.067:
            :       :               :...RED_OTS <= 190.583: stoichiometry (3)
            :       :                   RED_OTS > 190.583: fuel_rich (3)
            :       RED_OTS > 191.1:
            :       :...BLU_OTS <= 142.567:
            :           :...GRE_OTS > 168.283: fuel_rich (407)
            :           :   GRE_OTS <= 168.283:
            :           :   :...HUE_OTS <= 100.233: stoichiometry (8/1)
            :           :       HUE_OTS > 100.233: fuel_rich (13)
            :           BLU_OTS > 142.567:
            :           :...SAT_OTS <= 171.5:
            :               :...GRE_OTS > 170.067: fuel_rich (24)
            :               :   GRE_OTS <= 170.067:
            :               :   :...VAL_OTS > 193.517: fuel_rich (9/1)
            :               :       VAL_OTS <= 193.517:
            :               :       :...SAT_OTS <= 171.483: stoichiometry (64)
            :               :           SAT_OTS > 171.483:
            :               :           :...BLU_OTS <= 142.7: fuel_rich (2)
            :               :               BLU_OTS > 142.7: stoichiometry (2)
            :               SAT_OTS > 171.5:
            :               :...RED_OTS > 191.8: fuel_rich (194)
            :                   RED_OTS <= 191.8:
            :                   :...HUE_OTS <= 100.033:
            :                   :   :...BLU_OTS <= 142.617: fuel_rich (3)
            :                   :   :   BLU_OTS > 142.617: stoichiometry (16/1)
            :                   :   HUE_OTS > 100.033:
            :                   :   :...SAT_OTS > 171.917: fuel_rich (96)
            :                   :       SAT_OTS <= 171.917:
            :                   :       :...RED_OTS <= 191.5: stoichiometry (10/1)
            :                   :           RED_OTS > 191.5: fuel_rich (21)
            BLU_OTS > 142.9:
            :...SAT_OTS > 172:
                :...BLU_OTS > 144.133:
                :   :...RED_OTS > 193.75:
                :   :   :...SAT_OTS <= 172.3: stoichiometry (11)
```

```
|   |   |   SAT_OTS > 172.3: fuel_rich (15)
|   |   RED_OTS <= 193.75:
|   |   :...GRE_OTS <= 169.633:
|   |       :...SAT_OTS <= 172.483: stoichiometry (17)
|   |       |   SAT_OTS > 172.483:
|   |       |   :...GRE_OTS <= 169.2: stoichiometry (3)
|   |       |       GRE_OTS > 169.2: fuel_rich (6)
|   |       GRE_OTS > 169.633:
|   |       :...BLU_OTS > 144.183: stoichiometry (513)
|   |           BLU_OTS <= 144.183:
|   |           :...SAT_OTS <= 172.467: stoichiometry (18)
|   |               SAT_OTS > 172.467: fuel_rich (3)
|   BLU_OTS <= 144.133:
|   :...HUE_OTS > 104.5:
|       :...RED_OTS > 192.35: fuel_rich (9)
|       |   RED_OTS <= 192.35:
|       |   :...HUE_OTS > 104.65: stoichiometry (137)
|       |       HUE_OTS <= 104.65:
|       |       :...SAT_OTS <= 172.333: stoichiometry (23)
|       |           SAT_OTS > 172.333: fuel_rich (8)
|       HUE_OTS <= 104.5:
|       :...SAT_OTS > 172.317: fuel_rich (337)
|           SAT_OTS <= 172.317:
|           :...BLU_OTS > 143.933: stoichiometry (33)
|               BLU_OTS <= 143.933:
|               :...RED_OTS <= 191.75:
|                   :...SAT_OTS > 172.233: fuel_rich (13/1)
|                   |   SAT_OTS <= 172.233:
|                   |   :...BLU_OTS > 143.183: stoichiometry (76)
|                   |       BLU_OTS <= 143.183: [S1]
|                   RED_OTS > 191.75:
|                   :...BLU_OTS > 143.7:
|                       |   :...RED_OTS <= 192.383: stoichiometry (29)
|                       |       RED_OTS > 192.383: [S2]
|                       BLU_OTS <= 143.7:
|                       :...RED_OTS > 192.017: fuel_rich (164)
|                           RED_OTS <= 192.017: [S3]
|
SAT_OTS <= 172:
:...BLU_OTS > 143.5: stoichiometry (877)
    BLU_OTS <= 143.5:
    :...SAT_OTS <= 171.617:
        |   :...BLU_OTS > 142.967: stoichiometry (481)
        |   BLU_OTS <= 142.967:
        |   :...RED_OTS <= 192.683: stoichiometry (53/2)
        |       RED_OTS > 192.683: fuel_rich (6)
        SAT_OTS > 171.617:
        :...RED_OTS <= 191.517: stoichiometry (119)
            RED_OTS > 191.517:
            :...GRE_OTS > 170.283: fuel_rich (25)
                GRE_OTS <= 170.283:
                :...SAT_OTS > 171.9:
                    |   :...BLU_OTS <= 143.3:
                    |   |   :...RED_OTS > 191.75: fuel_rich (43)
                    |   |       RED_OTS <= 191.75: [S4]
                    |   BLU_OTS > 143.3:
                    |   :...GRE_OTS <= 169.7: stoichiometry (18)
                    |       GRE_OTS > 169.7: [S5]
                    SAT_OTS <= 171.9:
                    :...BLU_OTS > 143.183: stoichiometry (71)
                        BLU_OTS <= 143.183:
                        :...VAL_OTS > 193.4: fuel_rich (27)
                            VAL_OTS <= 193.4:
                            :...GRE_OTS > 169.95: [S6]
                                GRE_OTS <= 169.95: [S7]
```

```
SubTree [S1]

GRE_OTS <= 169.133: stoichiometry (9/1)
GRE_OTS > 169.133: fuel_rich (3)

SubTree [S2]

VAL_OTS <= 194: fuel_rich (31)
VAL_OTS > 194: stoichiometry (5)

SubTree [S3]

HUE_OTS <= 101.733: stoichiometry (17)
HUE_OTS > 101.733:
:...BLU_OTS <= 143.367: fuel_rich (43)
    BLU_OTS > 143.367:
    :...RED_OTS <= 191.9: stoichiometry (12)
        RED_OTS > 191.9: fuel_rich (6)

SubTree [S4]

GRE_OTS <= 169.317: stoichiometry (6)
GRE_OTS > 169.317: fuel_rich (9)

SubTree [S5]

VAL_OTS <= 193.683: fuel_rich (9)
VAL_OTS > 193.683: stoichiometry (2)

SubTree [S6]

SAT_OTS <= 171.7: stoichiometry (3)
SAT_OTS > 171.7: fuel_rich (12)

SubTree [S7]

GRE_OTS <= 169.5: stoichiometry (41)
GRE_OTS > 169.5:
:...HUE_OTS <= 101.033: stoichiometry (15)
    HUE_OTS > 101.033:
    :...VAL_OTS <= 193.217: fuel_rich (4)
        VAL_OTS > 193.217: stoichiometry (2)
```

```
 (a)   (b)   (c)    <-classified as
----  ----  ----
2993     7          (a): class fuel_rich
   4  2996          (b): class stoichiometry
             3000   (c): class fuel_lean

Error rate: 0.1%
```

Figure 5.31 Decision Trees for Configuration 1 using Forward Selection for Low Fuel Level

```
SAT_SKW > 1.01652: fuel_lean (2941)
SAT_SKW <= 1.01652:
:...SAT_SKW <= 1.01513:
    :...GRE_OTS <= 170.267:
    :   :...BLU_VAR > 0.0145154: fuel_rich (1269)
    :   :   BLU_VAR <= 0.0145154:
    :   :   :...SAT_TMP <= 1904.19: stoichiometry (10)
    :   :       SAT_TMP > 1904.19: fuel_rich (41)
    :   GRE_OTS > 170.267:
    :   :...SAT_SKW > 1.01487:
    :       :...BLU_SKW <= -0.671247: stoichiometry (104)
    :       :   BLU_SKW > -0.671247: fuel_rich (27/1)
    :       SAT_SKW <= 1.01487:
    :       :...BLU_KRT <= -0.435997: fuel_rich (174)
    :           BLU_KRT > -0.435997:
    :           :...SAT_VAR <= 55466.2: stoichiometry (9)
    :               SAT_VAR > 55466.2: fuel_rich (6)
    SAT_SKW > 1.01513:
    :...BLU_SKW > -0.612152:
        :...HUE_TMP <= 1902.94:
        :   :...GRE_ARE > 18047.5: fuel_rich (58)
        :   :   GRE_ARE <= 18047.5:
        :   :   :...RED_SKW > 0.190039: stoichiometry (198)
        :   :       RED_SKW <= 0.190039:
        :   :       :...BLU_SKW <= -0.575634: stoichiometry (5)
        :   :           BLU_SKW > -0.575634: fuel_rich (2)
        :   HUE_TMP > 1902.94:
        :   :...RED_TMP <= 1889.54:
        :       :...BLU_KRT <= -0.810661: fuel_rich (37)
        :       :   BLU_KRT > -0.810661: stoichiometry (64)
        :       RED_TMP > 1889.54:
        :       :...SAT_COM > 358.817:
        :           :...BLU_SKW <= -0.588554: stoichiometry (24)
        :           :   BLU_SKW > -0.588554: fuel_rich (18)
        :           SAT_COM <= 358.817:
        :           :...BLU_KRT <= -0.718058: fuel_rich (1018)
        :               BLU_KRT > -0.718058:
        :               :...RED_TMP <= 1893.32: stoichiometry (7)
        :                   RED_TMP > 1893.32: fuel_rich (25)
        BLU_SKW <= -0.612152:
        :...GRE_COM <= 384.386: fuel_rich (35)
            GRE_COM > 384.386:
            :...GRE_VAR > 0.010845:
            :   :...SAT_KRT <= -1.95974: fuel_rich (130/1)
            :   :   SAT_KRT > -1.95974: stoichiometry (107)
            :   GRE_VAR <= 0.010845:
            :   :...HUE_TMP > 1905.69:
            :       :...GRE_VAR > 0.0103569: fuel_rich (35)
            :       :   GRE_VAR <= 0.0103569:
            :       :   :...HUE_VAR <= 72008.7: stoichiometry (52)
            :       :       HUE_VAR > 72008.7: fuel_rich (3)
            :       HUE_TMP <= 1905.69:
            :       :...SAT_OTS > 172.633:
            :           :...GRE_COM <= 410.617: fuel_rich (13)
            :           :   GRE_COM > 410.617: stoichiometry (12)
            :           SAT_OTS <= 172.633:
            :           :...SAT_COM > 334.9: stoichiometry (1650)
            :               SAT_COM <= 334.9:
            :               :...SAT_SKW <= 1.0154:
            :                   :...BLU_AVG <= 0.844772: fuel_rich (27)
            :                   :   BLU_AVG > 0.844772:
            :                   :   :...VAL_ENT <= -157502: stoichiometry (116)
            :                   :       VAL_ENT > -157502: fuel_rich (18/1)
            :                   SAT_SKW > 1.0154:
            :                   :...BLU_SKW <= -0.617094: stoichiometry (550/1)
            :                       BLU_SKW > -0.617094:
            :                       :...RED_COM <= 373.125: stoichiometry (29)
            :                           RED_COM > 373.125:
            :                           :...VAL_OTS <= 193.35: fuel_rich (7)
            :                               VAL_OTS > 193.35: stoichiometry (2)
```

```
 (a)   (b)   (c)    <-classified as
----  ----  ----
2999     1          (a): class fuel_rich
   3  2997          (b): class stoichiometry
             3000   (c): class fuel_lean

Error rate: 0.04%
```

Figure 5.32 Decision Trees for Configuration 1 using Backward Elimination for Low Fuel Level

```
SAT_OTS <= 161.1:
:...BLU_OTS <= 132.667: stoichiometry (177)
:   BLU_OTS > 132.667: fuel_lean (2914)
SAT_OTS > 161.1:
:...SAT_OTS > 164.25:
    :...BLU_OTS <= 135.05: fuel_rich (2810)
    :   BLU_OTS > 135.05:
    :   :...SAT_OTS <= 165.25: stoichiometry (136)
    :       SAT_OTS > 165.25: fuel_rich (52)
    SAT_OTS <= 164.25:
    :...VAL_OTS <= 183.95: fuel_rich (79)
        VAL_OTS > 183.95:
        :...VAL_OTS <= 188.333: stoichiometry (8510/6)
            VAL_OTS > 188.333:
            :...BLU_OTS <= 134.033: stoichiometry (6)
                BLU_OTS > 134.033: fuel_lean (21)


            (a)   (b)   (c)    <-classified as
           ----  ----  ----
           3000                (a): class fuel_rich
                 9000          (b): class stoichiometry
                    6  2994    (c): class fuel_lean

           Error rate: 0.04%
```

Figure 5.33 Decision Trees for Configuration 1 using Forward Selection for Normal Fuel Level

```
SAT_SKW > 1.02543: fuel_lean (3000)
SAT_SKW <= 1.02543:
:...RED_TMP <= 1820.8: stoichiometry (9000)
    RED_TMP > 1820.8: fuel_rich (3000)


            (a)   (b)   (c)    <-classified as
           ----  ----  ----
           3000                (a): class fuel_rich
                 9000          (b): class stoichiometry
                       3000    (c): class fuel_lean

           Error rate: 0%
```

Figure 5.34 Decision Trees for Configuration 1 using Backward Elimination for Normal Fuel Level

```
RED_OTS <= 187.267: fuel_rich (3000)
RED_OTS > 187.267:
:...HUE_OTS <= 91.3833:
    :...BLU_OTS <= 124.25: stoichiometry (93/1)
    :   BLU_OTS > 124.25:
    :   :...VAL_OTS > 189.017: fuel_lean (2730)
    :       VAL_OTS <= 189.017:
    :       :...BLU_OTS <= 126.2: stoichiometry (3)
    :           BLU_OTS > 126.2: fuel_lean (22)
    HUE_OTS > 91.3833:
    :...VAL_OTS > 190.5: fuel_lean (173)
        VAL_OTS <= 190.5:
        :...BLU_OTS > 126.483:
            :...SAT_OTS <= 156.15: fuel_lean (10)
            :   SAT_OTS > 156.15: stoichiometry (16)
            BLU_OTS <= 126.483:
            :...SAT_OTS > 153.417: stoichiometry (2753)
                SAT_OTS <= 153.417:
                :...BLU_OTS <= 123.867: stoichiometry (77)
                    BLU_OTS > 123.867: fuel_lean (5)


            (a)   (b)   (c)    <-classified as
           ----  ----  ----
           3000                (a): class fuel_rich
                 3000          (b): class stoichiometry
                    1  2999    (c): class fuel_lean

           Error rate: 0.01%
```

Figure 5.35 Decision Trees for Configuration 1 using Forward Selection for High Fuel Level

```
BLU_SKW > -0.0223269: fuel_rich (3000)
BLU_SKW <= -0.0223269:
:...BLU_SKW <= -0.217246: fuel_lean (2992/1)
    BLU_SKW > -0.217246:
    :...SAT_OTS > 152.8: stoichiometry (2982)
        SAT_OTS <= 152.8:
        :...BLU_SKW <= -0.123637: fuel_lean (8)
            BLU_SKW > -0.123637: stoichiometry (17)

           (a)   (b)   (c)    <-classified as
          ----  ----  ----
          3000                (a): class fuel_rich
                2999     1    (b): class stoichiometry
                      3000    (c): class fuel_lean

          Error rate: 0.01%
```

Figure 5.36 Decision Trees for Configuration 1 using Backward Elimination for High Fuel Level

5.4.5.3 Oxidizer Classification using Configuration 2

The flame profiles indicate that differences in various level of oxidizer are visible even for human observer. Configuration 2 uses flame profiles in its extraction process and given the similar class arrangement as before, it turns out to provide a solution to the classification. Figure 5.37 to 5.42 shows the decision tree built based on using configuration 2 using both forward selection and backward elimination.

```
GRE_TMP <= 1489.161: fuel_lean (50)
GRE_TMP > 1489.161:
:...GRE_TMP <= 1517.491: stoichiometry (50)
    GRE_TMP > 1517.491: fuel_rich (50)

       (a)   (b)   (c)    <-classified as
      ----  ----  ----
        50                 (a): class fuel_rich
              50           (b): class stoichiometry
                    50     (c): class fuel_lean

      Error rate: 0%
```

Figure 5.37 Decision Trees for Configuration 2 using Forward Selection for Low Fuel Level

```
HUE_COM <= 544.1109: fuel_lean (50)
HUE_COM > 544.1109:
:...RED_SKW <= -1.017371: stoichiometry (50)
    RED_SKW > -1.017371: fuel_rich (50)

       (a)   (b)   (c)    <-classified as
      ----  ----  ----
        50                 (a): class fuel_rich
              50           (b): class stoichiometry
                    50     (c): class fuel_lean

      Error rate: 0%
```

Figure 5.38 Decision Trees for Configuration 2 using Backward Elimination for Low Fuel Level

```
BLU_COM <= 398.1476: fuel_rich (50)
BLU_COM > 398.1476:
:...GRE_TMP <= 1446.385: fuel_lean (50)
    GRE_TMP > 1446.385: stoichiometry (150)

       (a)   (b)   (c)    <-classified as
      ----  ----  ----
        50                 (a): class fuel_rich
              150          (b): class stoichiometry
                    50     (c): class fuel_lean

      Error rate: 0%
```

Figure 5.39 Decision Trees for Configuration 2 using Forward Selection for Normal Fuel Level

```
SAT_SKW <= 1.132026: fuel_rich (50)
SAT_SKW > 1.132026:
:...GRE_TMP <= 1446.385: fuel_lean (50)
    GRE_TMP > 1446.385: stoichiometry (150)

       (a)   (b)   (c)    <-classified as
      ----  ----  ----
        50                 (a): class fuel_rich
              150          (b): class stoichiometry
                    50     (c): class fuel_lean

      Error rate: 0%
```

Figure 5.40 Decision Trees for Configuration 2 using Backward Elimination for Normal Fuel Level

```
BLU_COM <= 375.9651: fuel_rich (50)
BLU_COM > 375.9651:
:...GRE_COM <= 362.9271: stoichiometry (50)
    GRE_COM > 362.9271: fuel_lean (50)

       (a)   (b)   (c)    <-classified as
      ----  ----  ----
        50                 (a): class fuel_rich
               50          (b): class stoichiometry
                    50     (c): class fuel_lean

      Error rate: 0%
```

Figure 5.41 Decision Trees for Configuration 2 using Forward Selection for High Fuel Level

```
BLU_COM <= 375.9651: fuel_rich (50)
BLU_COM > 375.9651:
:...GRE_COM <= 362.9271: stoichiometry (50)
    GRE_COM > 362.9271: fuel_lean (50)

       (a)   (b)   (c)    <-classified as
      ----  ----  ----
        50                 (a): class fuel_rich
               50          (b): class stoichiometry
                    50     (c): class fuel_lean

      Error rate: 0%
```

Figure 5.42 Decision Trees for Configuration 2 using Backward Elimination for High Fuel Level

The decision trees are much simpler than configuration 1's and the numbers of features selected are much less. The error rates are also superior with zero percent for all classes. It shows that proper arrangement and the usage of flame profiles are important for a good oxidizer level classification.

One particular observation on the results is how green channel's average temperature and blue channel's center of mass about Y axis occurs frequently in most trees. Figure 5.43 and 5.44 show the result of decision tree classifications using only each individual feature.

a)

```
GRE_TMP <= 1489.161: fuel_lean (50)
GRE_TMP > 1489.161:
:...GRE_TMP <= 1517.491: stoichiometry (50)
    GRE_TMP > 1517.491: fuel_rich (50)

 (a)   (b)   (c)    <-classified as
----  ----  ----
  50                 (a): class fuel_rich
        50           (b): class stoichiometry
              50     (c): class fuel_lean

Error rate: 0%
```

b)

```
GRE_TMP <= 1446.385: fuel_lean (50)
GRE_TMP > 1446.385:
:...GRE_TMP <= 1478.176: stoichiometry (150)
    GRE_TMP > 1478.176: fuel_rich (50)

 (a)   (b)   (c)    <-classified as
----  ----  ----
  50                 (a): class fuel_rich
       150           (b): class stoichiometry
              50     (c): class fuel_lean

Error rate: 0%
```

c)

```
GRE_TMP <= 1413.665: fuel_lean (50)
GRE_TMP > 1413.665:
:...GRE_TMP <= 1428.14: stoichiometry (50)
    GRE_TMP > 1428.14: fuel_rich (50)

 (a)   (b)   (c)    <-classified as
----  ----  ----
  50                 (a): class fuel_rich
        50           (b): class stoichiometry
              50     (c): class fuel_lean

Error rate: 0%
```

Figure 5.43 Decision Trees using Green Channel's Average Temperature for (a) Low, (b) Normal, and (c) High Fuel Level

a)

```
BLU_COM > 431.6786: fuel_lean (50)
BLU_COM <= 431.6786:
:...BLU_COM <= 425.9099: fuel_rich (49)
    BLU_COM > 425.9099: stoichiometry (51/1)

 (a)   (b)   (c)    <-classified as
----  ----  ----
  49     1          (a): class fuel_rich
         50          (b): class stoichiometry
               50    (c): class fuel_lean

Error rate: 0.7%
```

b)

```
BLU_COM <= 398.1476: fuel_rich (50)
BLU_COM > 398.1476:
:...BLU_COM <= 429.214: stoichiometry (150)
    BLU_COM > 429.214: fuel_lean (50)

 (a)   (b)   (c)    <-classified as
----  ----  ----
  50                (a): class fuel_rich
        150         (b): class stoichiometry
               50    (c): class fuel_lean

Error rate: 0%
```

c)

```
BLU_COM <= 375.9651: fuel_rich (50)
BLU_COM > 375.9651:
:...BLU_COM <= 402.9732: stoichiometry (50)
    BLU_COM > 402.9732: fuel_lean (50)

 (a)   (b)   (c)    <-classified as
----  ----  ----
  50                (a): class fuel_rich
         50         (b): class stoichiometry
               50    (c): class fuel_lean

Error rate: 0%
```

Figure 5.44 Decision Trees using Blue Channel's Center of Mass about Y Axis for (a) Low, (b) Normal, and (c) High Fuel Level

The single feature classification provides similar result with mostly zero percent of classification error except for one class as shown in Figure 5.44a. However the error is also very small. The two features and their arrangements are attractive because simpler feature implies simpler classification process and makes it feasible to approximate classification for oxidizer levels beyond current dataset.

Similar to fuel classification analysis, scatter plot visualization is used to investigate the feature output. The intention is to confirm the decision trees' results and to insure the feasibility for the oxygen classification as a whole using only these features.

Figure 5.45 to 5.47 depicts the actual feature output using both features. The three figures represent the three different fuel levels and each figure contains the output for the three different O/F ratios.

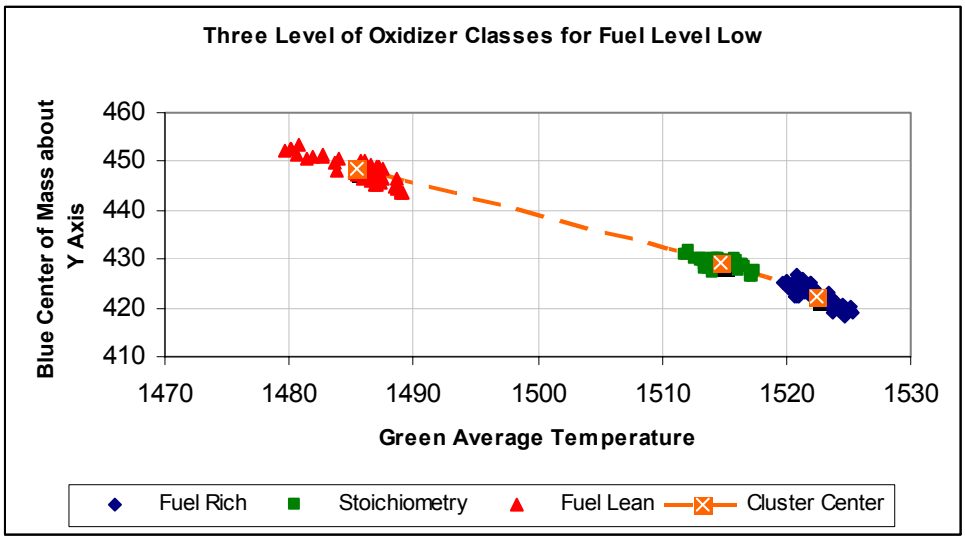

Figure 5.45 Feature Output for Oxidizer Level Classification Fuel Level Low

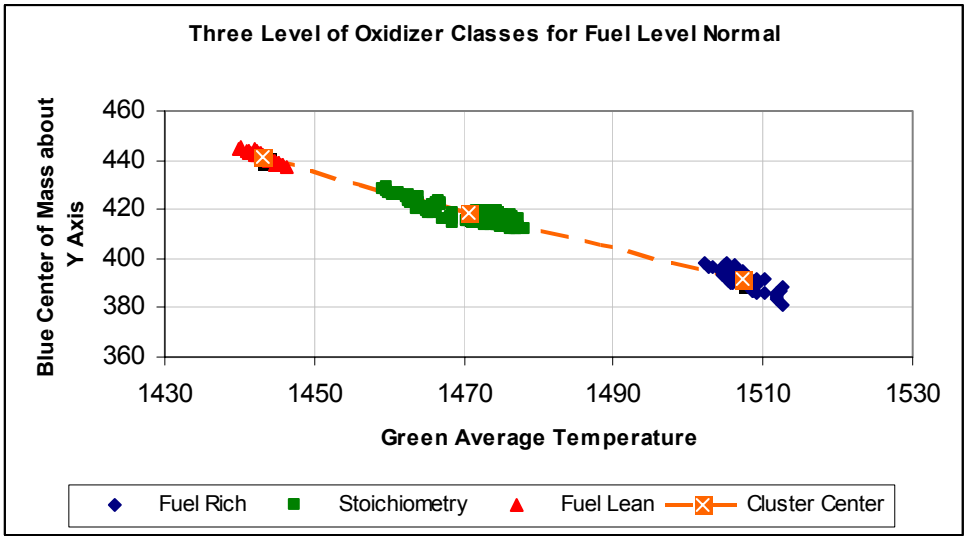

Figure 5.46 Feature Output for Oxidizer Level Classification for Fuel Level Normal

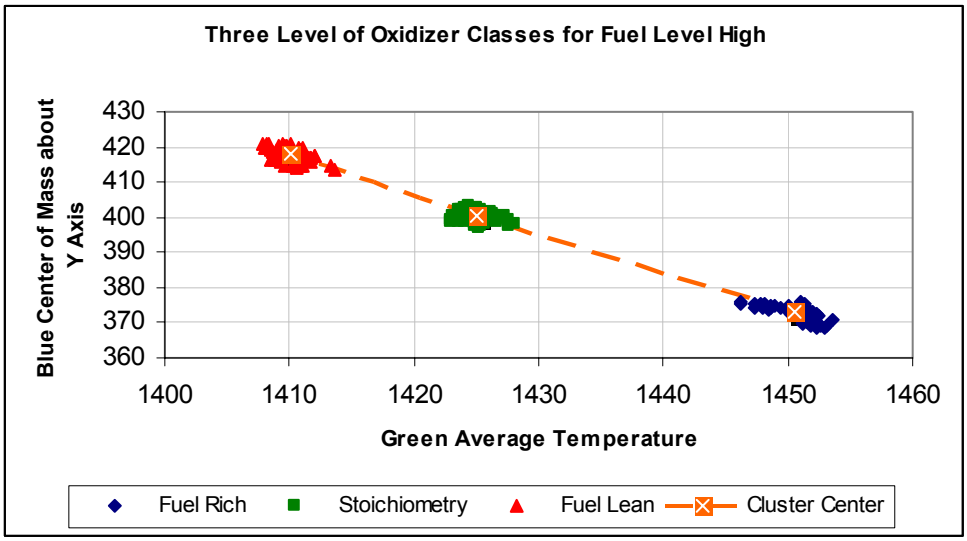

Figure 5.47 Feature Output for Oxidizer Level Classification for Fuel Level High

First immediate impression on the visualizations is there are visible clusters for each oxidizer level thus the classification is feasible. It also explains why previous arrangements failed. Without grouping in fuel level, many runs with different oxidizer level actually have similar output values thereby their clusters overlap and require complex decision trees for proper classification.

Nonetheless, compared to fuel level classification, oxidizer's classification is not as trivial. For example, as shown in Table 5.9 and 5.10, the distances between cluster centers are not uniform for all the fuel classes as in the case for fuel level classification. For high and normal fuel level, the distance between the cluster centers are relatively similar and almost linear. However for low fuel level, the distance between cluster centers are very different from one to another.

Additionally, the proposed arrangement implies that the approximation would require a proper classification of the fuel level beforehand. Thus one's classification on the oxidizer level is affected by the fuel level classification.

Table 5.9 Distances between Cluster Centers for Oxidizer Classes using Green Channel's Average Temperature

Fuel Class	Fuel Rich to Stoichiometry	Stoichiometry to Fuel Lean	(Fuel Rich to Stoichiometry) / (Stoichiometry to Fuel Lean)
Low	7.8	29.2	0.2
Normal	36.7	27.4	1.3
High	25.4	14.9	1.7

Table 5.10 Distances between Cluster Centers for Oxidizer Classes using Blue Channel's Center of Mass about Y Axis

Fuel Class	Fuel Rich to Stoichiometry	Stoichiometry to Fuel Lean	(Fuel Rich to Stoichiometry) / (Stoichiometry to Fuel Lean)
Low	6.7	19.2	0.4
Normal	26.7	22.9	1.2
High	27.4	17.6	1.5

The implication based on the findings, aside for the challenges, is that there is still a good possibility that one can model a system to approximate oxidizer level based on using green channel's average temperature and blue channel's center of mass about Y axis. For classifying the three oxidizer classes, it will be guaranteed feasible.

The two selected features will be the key features for classifying the oxidizer level based on its O/F ratio. They have a relatively low computational costs thus a real-time performance is possible. Moreover their simplicity makes the approximation model possible as it will be investigated further in the next chapter. Note that no key features from configuration 1 are selected.

5.5 Experimental Conclusion

The results of the analysis in this chapter show the feasibility of distinguishing various fuel flow rates and O/F ratios apart based on information extraction from flame images. The last step in this study is in the actual prediction and approximation of the classes. This is achieved through the use of fuzzy logic which is discussed and elaborated in the next chapter.

6. MODELLING APPROXIMATION

6.1 Overview

Fuzzy system is a common strategy adopted for many applications in engineering including control and classification [68, 69] pioneered by Zadeh in 1965 [70] . It is a system that utilizes fuzzy sets instead of crisp sets to accommodate the existence of uncertainty or inherent inaccuracy within the task at hand. This chapter describes how fuzzy system can be adopted and utilized to provide a comprehensive flame status.

The key features selected in the previous chapter can successfully classify the flame according to the three different fuel levels and their corresponding O/F ratio class. However this is not sufficient to provide the flexibility in classifying other possible situation beyond the test data condition. As mentioned in the previous chapter, in reality both fuel and oxidizer flow rate can bet at any levels between their minimum and maximum range.

A method for classifying other possible levels is proposed as a form of approximation based on the key features information as obtained and discussed previously. The approximation model chosen is based on fuzzy system approach.

The fuzzy system built in this study is designed as a promising basis for an expert system to provide similar approximation to a domain expert, using the prior test data and selected key features as the knowledge base.

6.2 Fuzzy Set for Approximating Uncertainty

Fuzzy set theory can be defined as an extension of classical set theory, also known as crisp set. In crisp set, an element has to belong to a set or otherwise. In fuzzy set however, an element can have a certain degree of belonging to one or more sets. This degree is measured using membership functions with degree of membership measured between zero (not a member) to one (complete member) [70]. Figure 6.1 illustrates an example of membership function on a fuzzy set with element values range from 0 to 10.

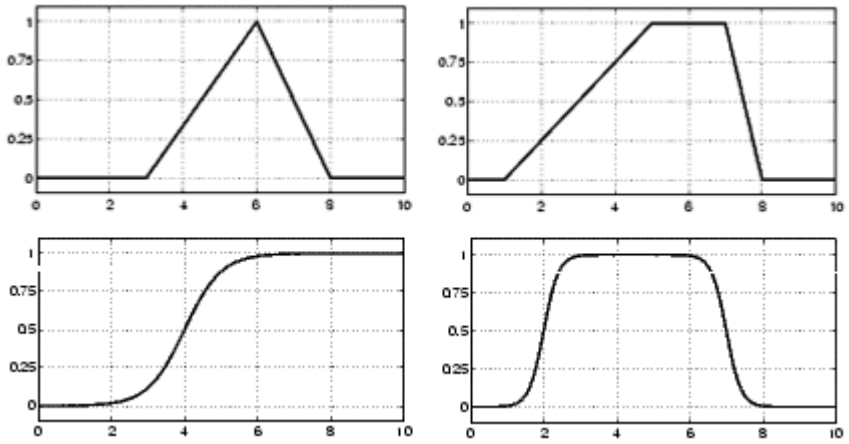

Figure 6.1 Membership Function Examples

Fuzzy set is particularly useful for describing measurement on things that are expected to contain certain degree of inaccuracy or uncertainty. It mimics the way humans, including domain experts, in quantifying measurements. For example, in the domain of measuring furnace flame quality, an experienced furnace operator might measure the quality of the flame based on his/her visual judgment which translates to fuzzy measurement such as “too low”, “too high” or “just right”.

Consequently the main challenge in this study would be how one can model a fuzzy system that will provide a reliable approximation on the furnace flame condition

based on the prior known knowledge. This leads to the task of building the fuzzy sets themselves as membership functions for the approximation.

6.3 Building Membership Functions

Membership functions can be designed in different ways and approaches, depending on many factors. The shape and characteristic of the functions will be crucial in the overall fuzzy system's characteristic. Two particular aspects need to be addressed as well in choosing the right functions: how it represents the task itself and the choice of functions to model them.

In this particular study, the task is to approximate the status of the fuel flow rate and the O/F ratio. Together it provides the current status of the flame, along with capability of providing suggestion of what need to be adjusted when the condition is not at stoichiometry. For this reason, the membership functions are applied at the key feature output space. The approximation is then derived from their outputs.

The shape and position of the membership function can be determined in many ways. In this study, the strategy is for the functions to be built based upon the shape of the feature output distribution of the experiments in the previous chapter. This approach is both intuitive and appropriate since there exist a form of order and consistency from low to high and lean to rich in the feature output space.

Generalized bell function is used to model the membership functions [71]. Its formula is shown in EQ (6.1). Their implementation and parameter setup for fuel and O/F ratio approximation will be discussed below.

$$\mu(x) = \frac{1}{1 + \left| \frac{x - c}{a} \right|^{2b}} \qquad \text{EQ (6.1)}$$

where, μ(x) = degree of membership for output value x
a = curvature parameter, affecting width
b = curvature parameter, affecting steepness
c = center position of the curve

6.4 Fuel Level Approximation

As stated previously, the approximation for fuel level is based on using membership functions that are derived from the key feature outputs. The two previously selected key features, blue channel's Otsu threshold level and value channel's entropy will be the basis for the approximation. Figure 6.2 and 6.3 show the normalized distributions for the three different class labels of the fuel flow rate, which is high, normal and low for both features.

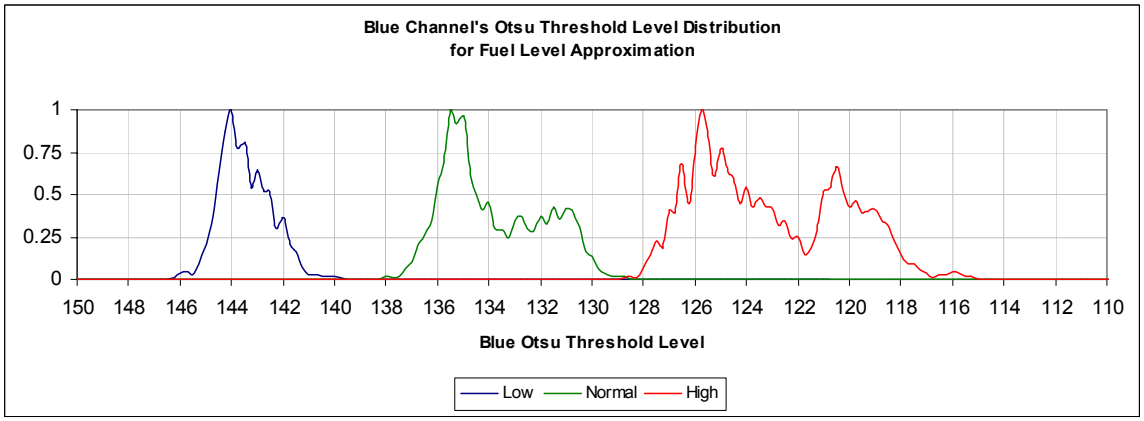

Figure 6.2 Feature Output Distribution based on Blue Channel's Otsu Threshold

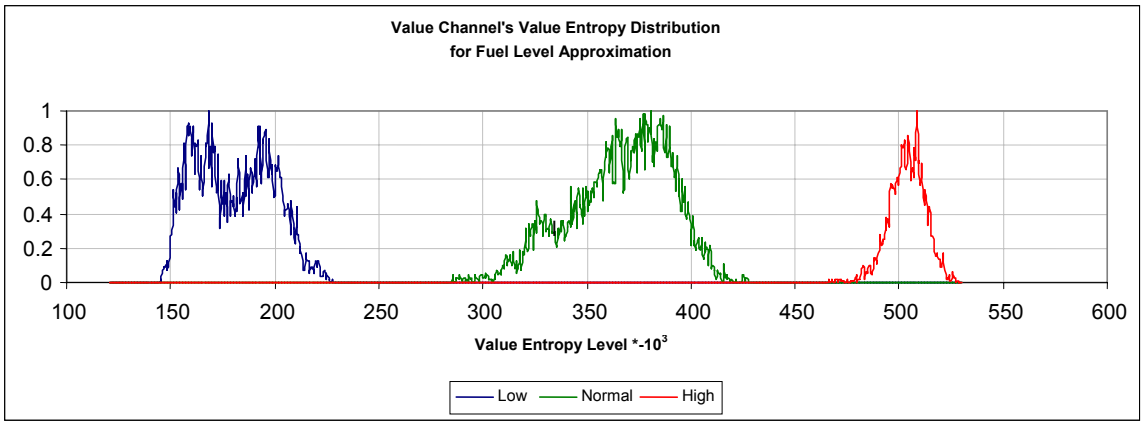

Figure 6.3 Feature Output Distribution based on Value Channel's Entropy

Both features have been proven before to be able to provide good classification as shown by the separability of the output distributions of each class. The distribution shape will then be used as the guideline on creating the membership functions. There are many ways however, with no particular constraint, in modeling the membership function that best describe the nature of relationship between a class and its distribution [72]. The interpretation of boundaries, regions and where a particular class begins and ends are up to the observers. In this particular study, due to their various and non-modal distribution shapes, the generalized bell function is proposed as the membership function. The assumption is that the class begins and ends within the distribution boundary.

Generalized bell requires three parameters to model the membership function as previously shown in EQ (6.1). Parameters a and b, which determine the width and curvature of the function, are derived by using least squares curve fitting method [73] such that it produces a membership function that best model the class distribution. EQ (6.2) shows the function to be minimized to obtain parameter a and b. Parameter c, which defines the center of the curve, is set as the center of mass of the class distribution. Center of mass is used rather than mean since the distribution shape is non-modal. The

center of mass equation used to calculate parameter c is shown in EQ (6.3). The resulting three parameters for each class on both key features are shown in Table 6.1.

$$S_M = \sum_{x=0}^{255} \left(P_M(x) - \frac{1}{1 + \left| \frac{x-c}{a} \right|^{2b}} \right)^2 \qquad \text{EQ (6.2)}$$

where S_M = sum of the squares of residual for class M
$P_M(x)$ = number of feature output values with output x for class M
a = membership function parameter, affecting width
b = membership function parameter, affecting steepness
c = center position of the curve

$$C_M = \frac{\sum_{x=0}^{255} xP(x)}{\sum_{x=0}^{255} P(x)} \qquad \text{EQ (6.3)}$$

where C_M = center of mass for class M
x = feature output value
P(x) = number of feature output with value x

Table 6.1 Generalized Bell Curve Parameter

	Blue Channel's Otsu Threshold			**Value Channel's Entropy**		
	Low	**Normal**	**High**	**Low**	**Normal**	**High**
a	1.45	2.9	3.8	23.2	22.9	11
b	3	3.2	3.5	1.94	1.21	1.54
c	143.5	133.9	123.1	$180.3x\text{-}10^3$	$366.2\ x\text{-}10^3$	$503.8\ x\text{-}10^3$

The resulting membership function is shown in Figure 6.4 and 6.5, along with the actual feature output distribution for comparison. The average differences between the

actual feature output distributions and the modeled curves is about 0.025 unit of measure for both key features. The differences is largely occurs at the middle section of the distribution of class normal and high where the related feature output values do have fluctuations. For the purpose of approximation by membership function, this is still acceptable since the particular region is comprised of data that represent its class.

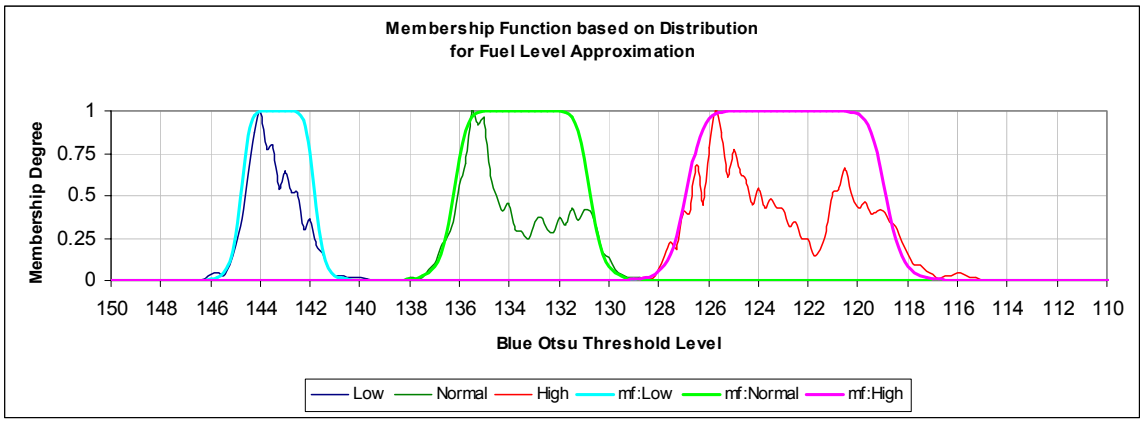

Figure 6.4 Membership Function for Fuel Approximation based on Blue Otsu Threshold Level

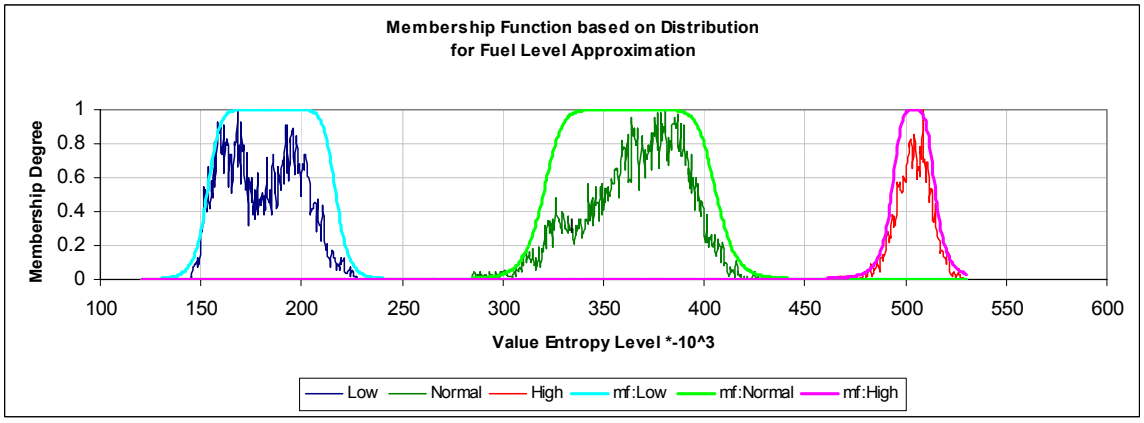

Figure 6.5 Membership Function for Fuel Approximation based on Value Entropy

The three memberships function become the base for modeling additional membership functions to approximate fuel level beyond the known data. Four different such regions exist as shown in Figure 6.6, which are the left side of class low, between low and normal, between normal and high, and the right side of high. However, the

regions one and four of figure 6.x are not of interest here as they are beyond the operating region of fuel rate and hence O/F ratio.

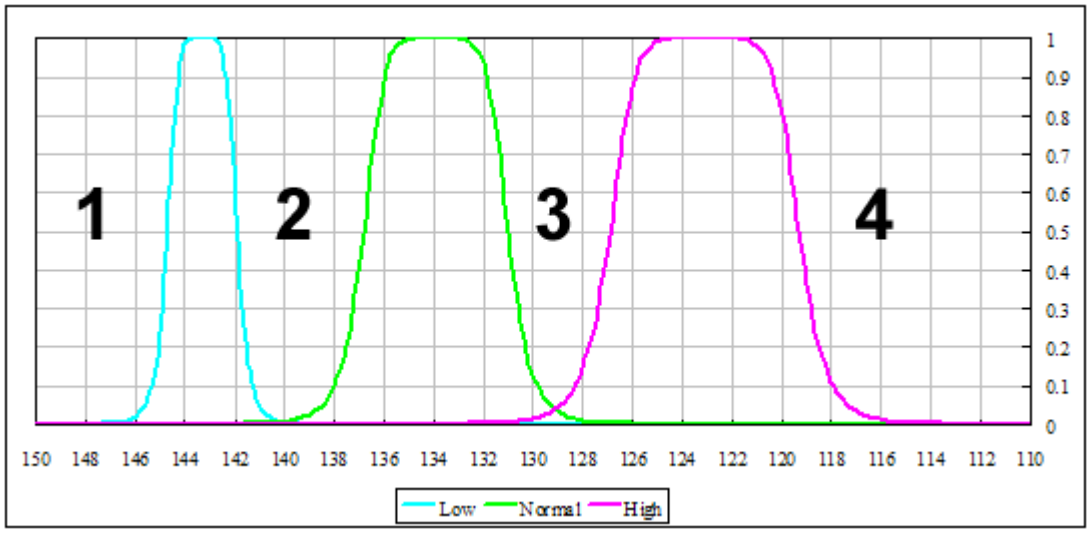

Figure 6.6 Four Regions between the Known Data

The particular interest would be in finding strategy for a good approximation of the two regions between low and normal, and normal and high. To define them, one would need to know the boundaries between classes. One particular challenge is that the boundary between the known classes themselves contains uncertainty since they are derived based on what is reflected by the distribution. Since some classes have the shape of their distribution as non-modal, it is also uncertain whether the test data do represent comprehensive ranges for each class.

Amidst the shortcomings, there are still several aspects that are clear from the membership functions. For example, the position of each class is within the order of the class, such that normal is between high and low. Especially for blue channel's otsu threshold, there is a linear trend of increasing variance with the class distribution from class low to class high as reflected by the width of the membership function. Furthermore, the obtained membership functions' parameters also display an almost

linear trend from one class to another. These characteristics are absent from the value channel's entropy feature. The existence of the trend in blue channel's Otsu threshold feature is the basis for creating the in-between membership functions. In this study, these functions are built by applying linear interpolation of the parameters from the existing membership functions of this particular feature.

. Figure 6.7 to 6.9 shows the trend for each of the three parameters for the membership functions of the three known classes based on the blue channel's otsu threshold feature output. The parameters a, b and c for the in-between functions are then selected using the equation of the linear interpolation as the mid points between the known parameters. Table 6.2 shows the three parameters obtained using linear interpolation for the in-between membership functions.

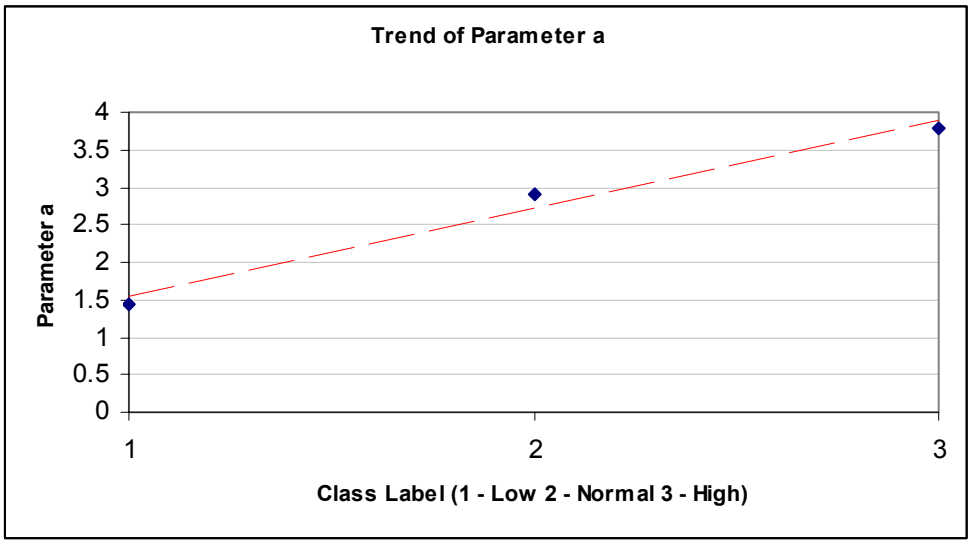

Figure 6.7 Plot of Trend for Membership Functions' for Parameter a

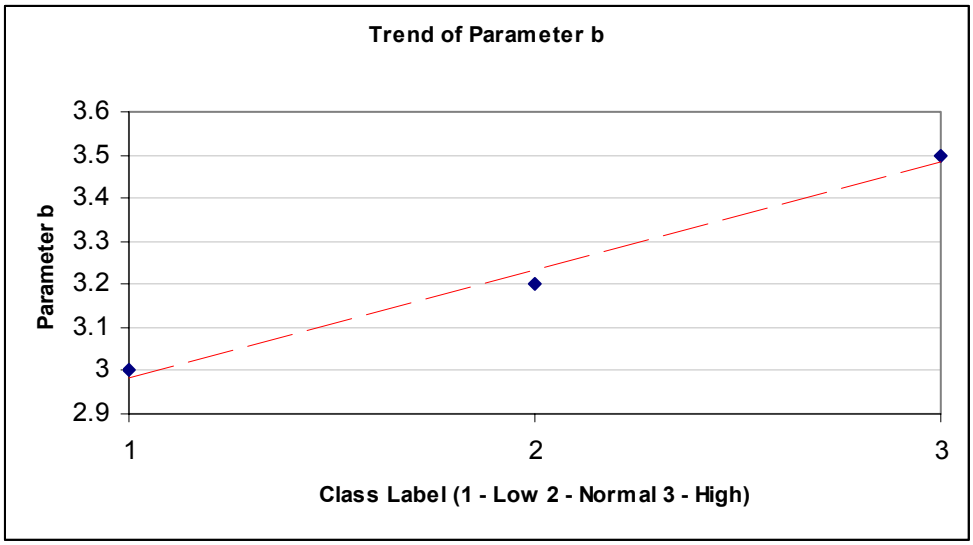

Figure 6.8 Plot of Trend for Membership Functions' for Parameter b

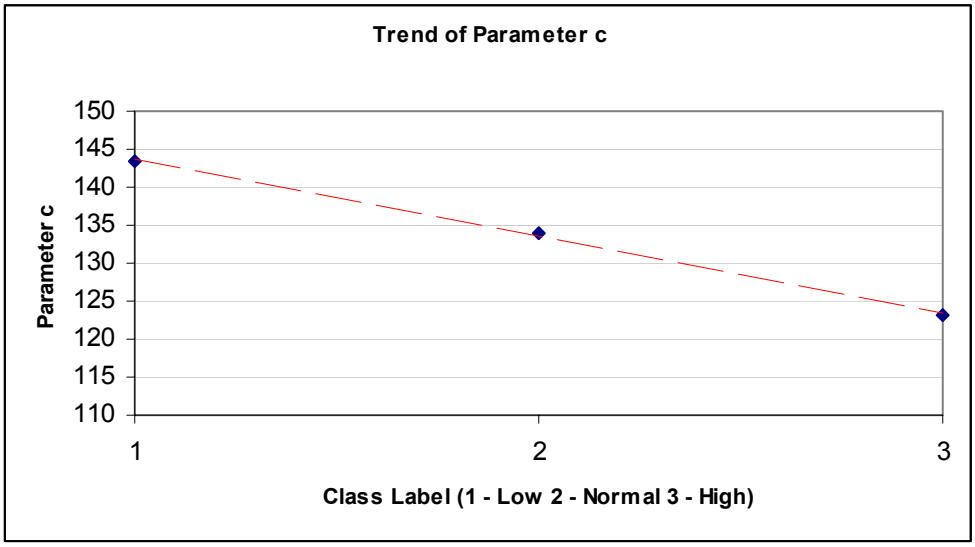

Figure 6.9 Plot of Trend for Membership Functions' for Parameter c

Table 6.2 Membership Functions' Parameters for the In-between Classes

Parameter	Low to Normal	Normal to High
a	2.15	3.35
b	3.1	3.35
c	139	128.5

Figure 6.10 shows the two approximated membership functions along with the original three. The estimated membership functions cover the in-between regions very well as expected and will be used for the approximation of the in-between flow rate level.

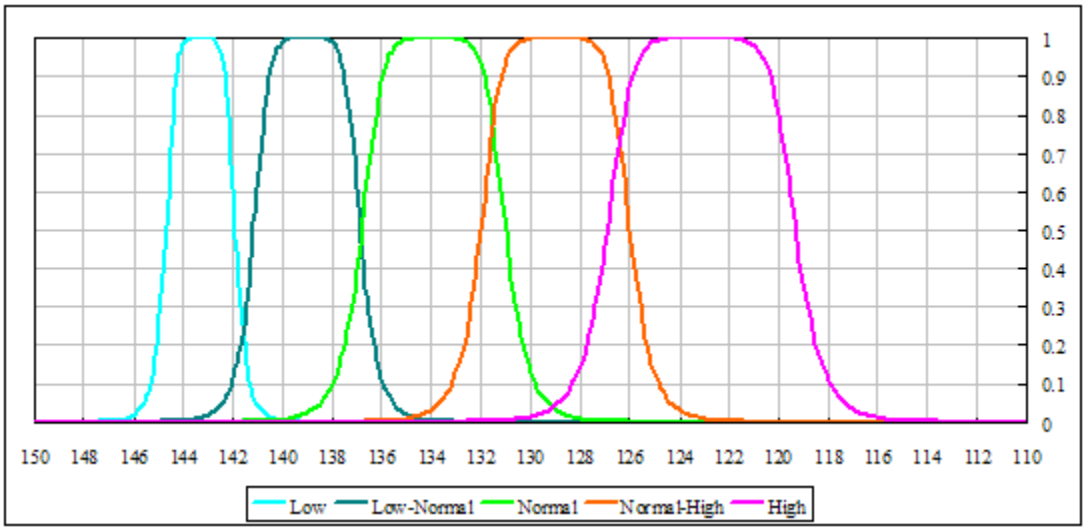

Figure 6.10 Membership Functions using Linear Interpolation

In the case of the left side of "low" and right side of "high", since these are beyond what considered being boundary condition of the fuel flow rate itself, both sides are labeled as "unknown" region. Possible cause of having the feature output at such condition is due many things such as flame shut off, camera disabled or device malfunction. Regardless of the cause, no flame analysis can be or should be done at such condition thus at the unknown region, the "unknown" outcomes implies no further analysis is required. The boundaries of the "unknown" region are assumed to be similar to the feature output distribution boundaries. Hence for using blue otsu threshold, the boundaries are set to be below 112 and above 148. The boundaries are denoted by the membership function for the "unknown" class as shown in EQ (6.4).

$$\mu_{unknown}(x) = \begin{cases} 0 & if \quad 112 \le x \le 148 \\ 1 & if \quad x < 112 \\ 1 & if \quad x > 148 \end{cases} \qquad \text{EQ (6.4)}$$

where, $\mu_{unknown}(x)$ = membership degree for the "unknown" class
x = feature output value

At this point there are a total of six membership functions created. The flow rate approximation then can be obtained based on processing the membership degree outputs from all of them given an output value from the blue channel's otsu threshold. There are many methods that one can use to interpret or process the membership degree outputs. In this study, the approach is to assign the feature output value to the class with the highest membership degree as shown in EQ (6.5). For clarity purpose, each class is assigned a numerical label as well as shown in the equation accordingly. Note that there exist the possibility where there is more than one membership function has the highest degree. This implies a situation where the output value may belong to either class. For simplicity, in this study such output value will be classified to the left-most membership functions or the smaller numerical label. For example, if the membership degree is equal for class "Low" and class "Low to Normal", thus it will be classified as "Low".

$$Class(x) = Max\{\mu_0(x), \mu_1(x), \mu_2(x), \mu_3(x), \mu_4(x), \mu_5(x)\} \qquad \text{EQ (6.5)}$$

where Class(x) = class of output value x
x = feature output value
$\mu_0(x)$ = membership degree for the class unknown
$\mu_1(x)$ = membership degree for the class low
$\mu_2(x)$ = membership degree for the class low-to-normal
$\mu_3(x)$ = membership degree for the class normal
$\mu_4(x)$ = membership degree for the class normal-to-high
$\mu_5(x)$ = membership degree for the class high

To assess the fuel flow rate approximation, experiment run 15 is used. Data for this run is acquired at the same time and camera location as the ones used in feature selection process discussed in the previous chapter. Run 15 data is not used in the feature selection process due to its differences both in fuel level and length of the run. Instead of a consistent one fuel level within a minute like the others, run 15 has its fuel level changes from 128 to 96 and back to 128 scfh within approximately 3 minutes. It is considered to be a good test on the approximation since it starts and ends at 128 scfh which is between 110 and 140 scfh (i.e., above stoichiometry); and it reaches 96 scfh during its run which is between 80 and 110 scfh (i.e., below stoichiometry). Thus it perfectly simulates a condition where the flow rate changes beyond the known three classes of fuel level and a form of approximation will be required.

The first flow rate changes occur approximately within a minute into the run and the second time within a minute later. The changes can be visually confirmed from the feature output as shown in Figure 6.11. The output values are extracted from a total of 5100 flame images or about 2 minutes and 50 seconds worth of flame video footage with 30 frames per second of flame images. Figure 6.12 shows a simulated model of ideal changes in the fuel flow rate during the run. Note that mechanical errors do exist in the actual physical flow itself so its depiction here is only for comparison purpose where one can visually observe and correlate it with the feature output as shown in Figure 6.11.

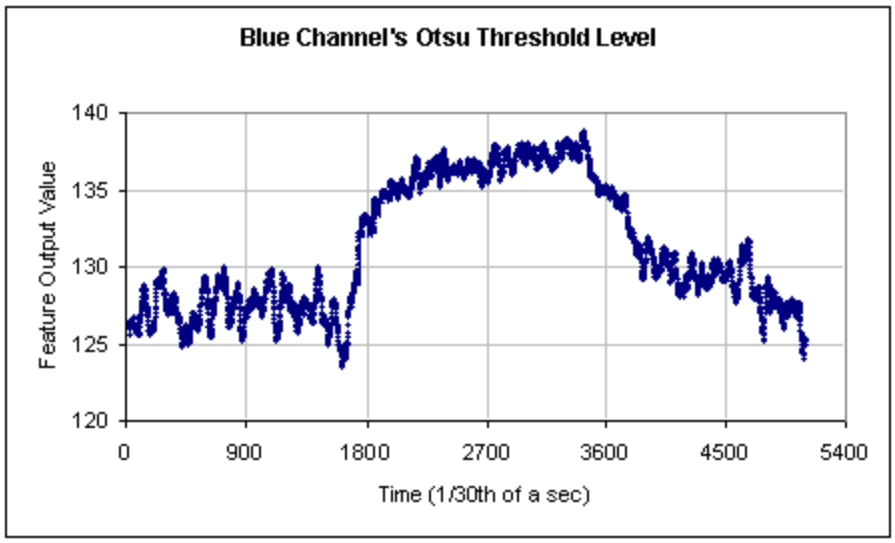

Figure 6.11 Feature Output for Experimental Run 15 based on Blue Channel's Otsu Threshold Level

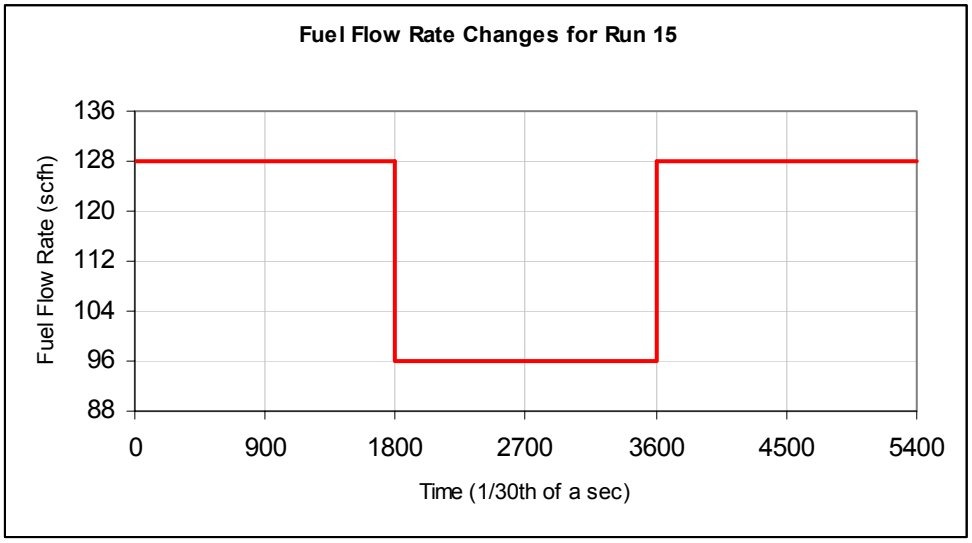

Figure 6.12 Fuel Flow Rate Changes for Run 15

The fuel approximation output is shown in Figure 6.13 which is computed using EQ (6.5) applied on the feature output shown in Figure 6.11. A simulated "ideal" classification output is created shown as red line in Figure 6.13. It acts as a reference so that the classification accuracy can be assessed quantitatively.

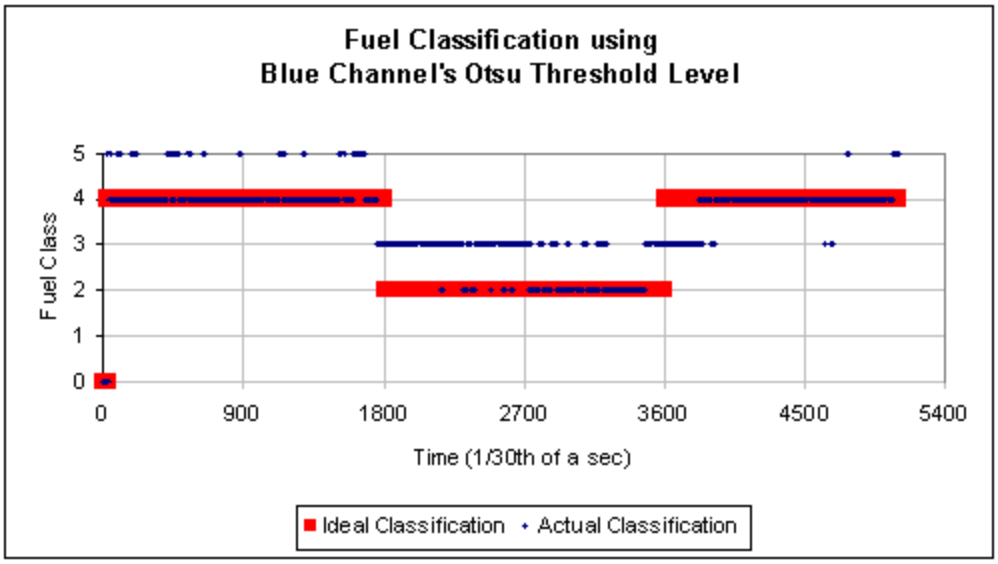

Figure 6.13 Output for Experimental Run 15

As depicted in Figure 6.13, the actual fuel classification do follow the ideal case, which classify the fuel level from "Normal to High" to "Low to Normal" and back to "Normal to High". There are 3570 flame images for class "Normal to High" and 1800 for class "Low to Normal". Note that in the very beginning there is a one second period or 30 flame images with fuel level of class "Unknown", which is needed to represent the delay due to aggregation process during feature extraction.

Assessment of the classification is measured based on the rate of misclassification. The assumption is that a classification error is defined by a classification output that differs from the ideal case counterpart. Table 6.3 summarizes the classification assessment.

Table 6.3 Fuel Approximation Error Assessment

Fuel Class	Total Data (n)	Total Incorrect Classification (x)	Error Rate (x / n) * 100%
Unknown	30	0	0
Normal to High	3570	354	9.9
Low to Normal	1800	1138	63.3

The quality of the classification does not perfectly follow the ideal case. Error rate is particularly very high when the fuel level is expected to be classified as "Low to Normal". Upon observation on the actual feature output, this seems to be caused by the existence of transition periods during the change from one fuel level class to another which is longer than ideally expected. This transition period exist every time the fuel changes and due to the design of the ideal case, it affects the assessment for class "Low to Normal" substantially. During this transition time, it seems that some oscillation behaviors might occur as well between two adjacent classes. The class oscillation indicates that the feature values are close to where the relevant membership function intersects. In this particular test, the feature values seem to be close where the membership function for class "Normal" and "Low" intersect during the transition period. The overall trend of the approximation itself is still correct.

As described in the previous chapter, the fuel classification affects the O/F classification process. It is designed as one output per second whereas fuel classification is at 30 outputs per second. Therefore, for every single feature value for O/F classification there is a set of 30 fuel class labels that needs to be considered. One

possible strategy is to aggregate every 30 class labels from the fuel classification into one. This aggregated class then represents the fuel class label for the O/F classification.

The class label is represented as numerical values as described earlier in EQ (6.5), hence its aggregation can be expressed numerically as well. In this study the aggregation is based on the majority class label as shown in EQ (6.6) which implies at any given time, the aggregate class label is the median of the most recent 30 class labels.

$$C'(t) = Median\{C(t-n-1), C(t-n-2), C(t-n-3)...C(t)\} \qquad \text{EQ (6.6)}$$

where C'(x) = aggregate class label at time x
C(x) = class label at time x
n = number of aggregated class labels, set at 30

The aggregated class output is as shown in Figure 6.14 below. Note that the aggregation also improves the overall trend and error rate of the classification as shown in the assessment results in Table 6.4. At this point, it is then ready to be used for O/F classification which is the next focus in this chapter.

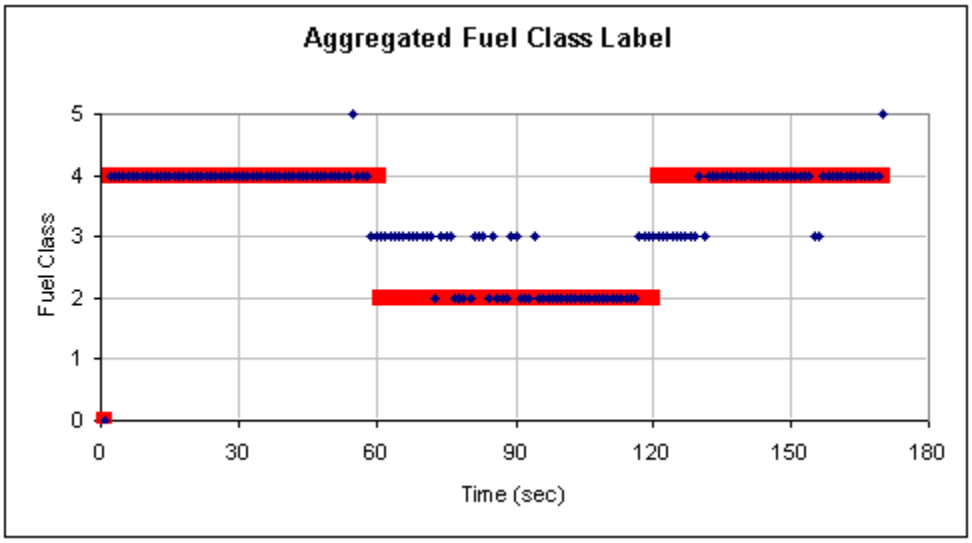

Figure 6.14 Approximation Output for Experimental Run 15

Table 6.4 Fuel Approximation Error Assessment

Fuel Class	Total Data (n)	Total Incorrect Classification (x)	Error Rate (x / n) * 100%
Unknown	1	0	0
Normal to High	119	2	1.7
Low to Normal	60	26	43.3

6.5 O/F Ratio Approximation

Once the fuel flow rate is approximated, the final step would be approximating the O/F ratio. The approach is similar to fuel approximation but with additional complexity. As indicated in the previous chapter, the O/F classification depends on the fuel level. This implies the need to choose different sets of membership functions for each different level of fuel flow rate.

The first step in the approximation is similar as before, that is building membership functions based on the known feature output values. The features used are based on the previously selected key features which are blue channel's center of mass about Y axis and green channel's average temperature. Similar as before, generalized bell function is used to model the membership functions and the parameters are obtained through curve fitting. For each class of fuel flow rate, there are three classes of O/F ratios which is fuel rich (1.8), stoichiometry (2.1)[1] and fuel lean (2.4). Thus for each feature, there are nine membership functions built accordingly based on the three original fuel class of low, normal and high. Note that for modeling the membership functions for the in-between fuel classes, it will be handled separately afterwards. Figure 6.15 to 6.20

[1] In combustion theory, actual stoichiometry ratio is defined at 2.0. Due to oxidizer impurity in this particular furnace, the ratio is compensated to 2.1.

shows the feature output distribution along with the modeled membership function for the three original fuel classes. Table 6.5 to 6.6 shows the parameters of the membership functions accordingly.

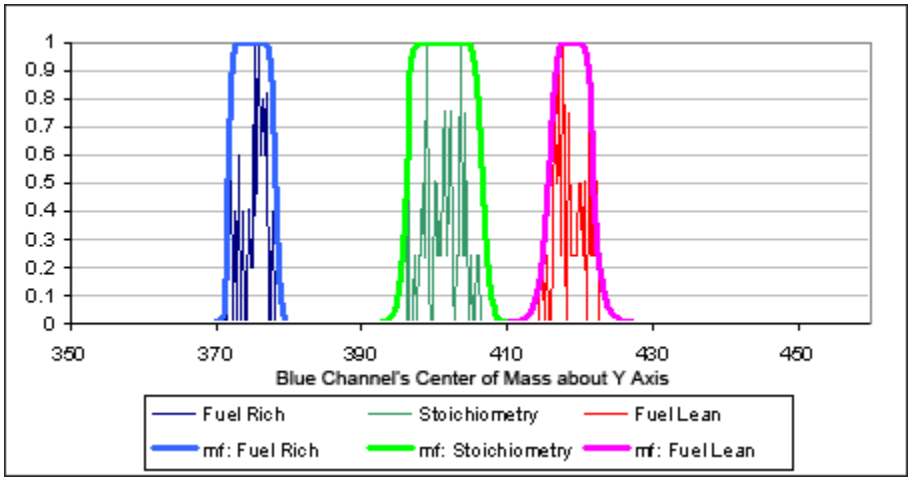

Figure 6.15 Membership Function for O/F Level with Fuel Level at High based on Blue Channel's Center of Mass around Y Axis

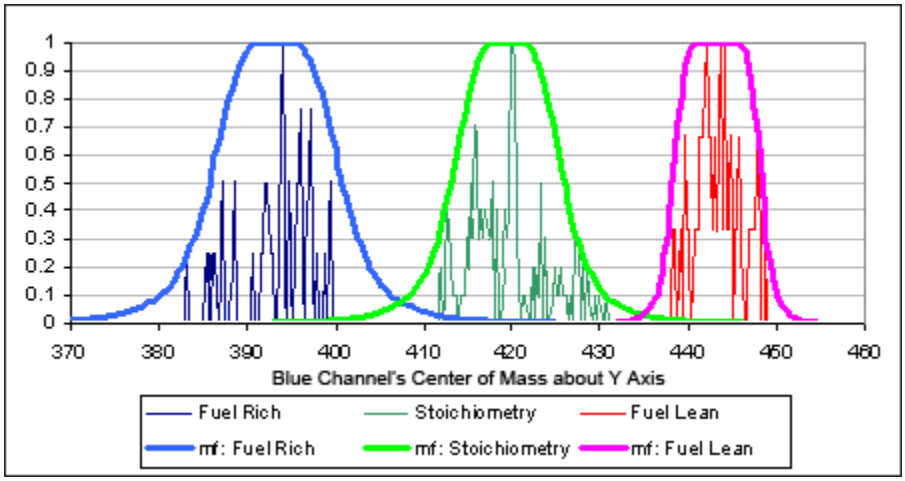

Figure 6.16 Membership Function for O/F Level with Fuel Level at Normal based on Blue Channel's Center of Mass around Y Axis

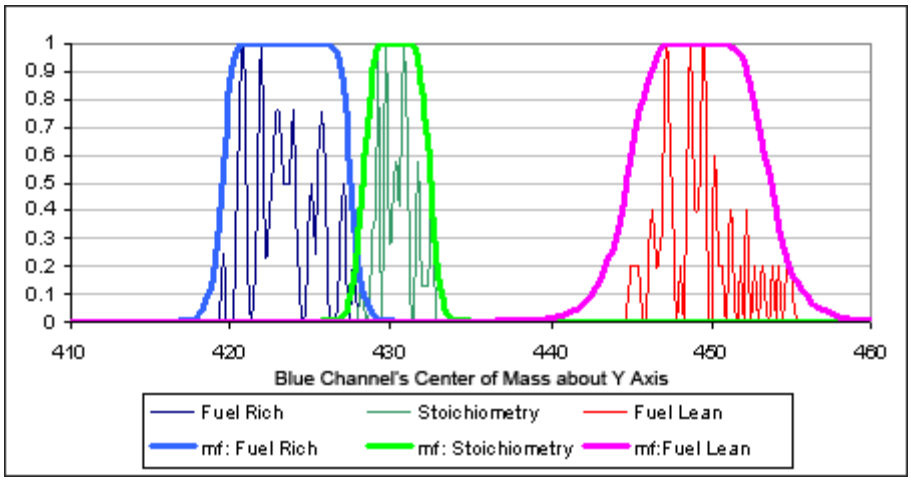

Figure 6.17 Membership Function for O/F Level with Fuel Level at Low based on Blue Channel's Center of Mass around Y Axis

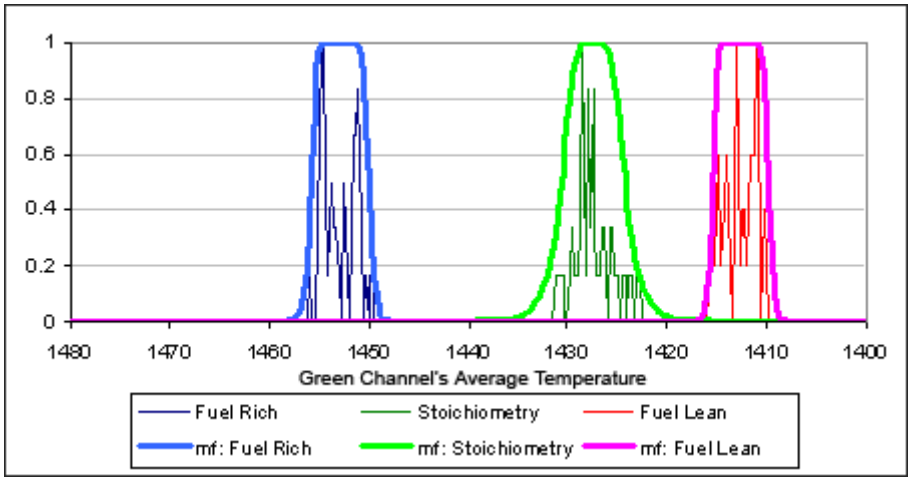

Figure 6.18 Membership Function for O/F Level with Fuel Level at High based on Green Channel's Average Temperature

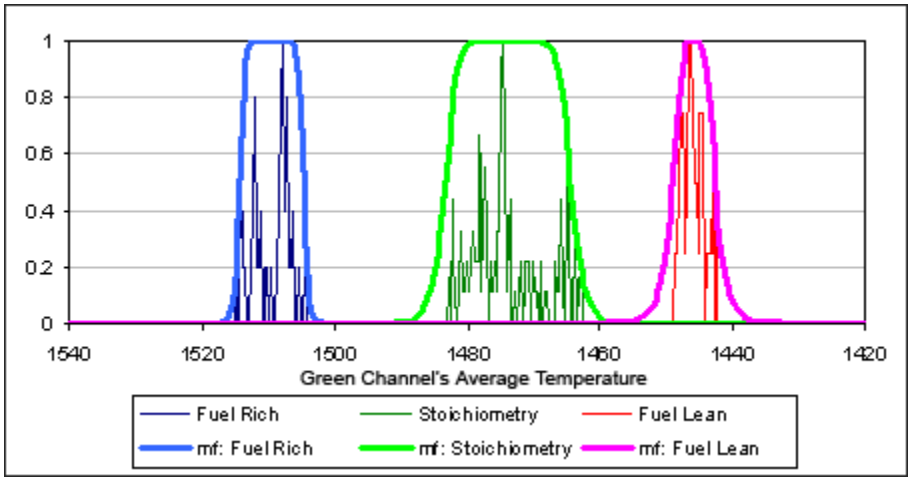

Figure 6.19 Membership Function for O/F Level with Fuel Level at Normal based on Green Channel's Average Temperature

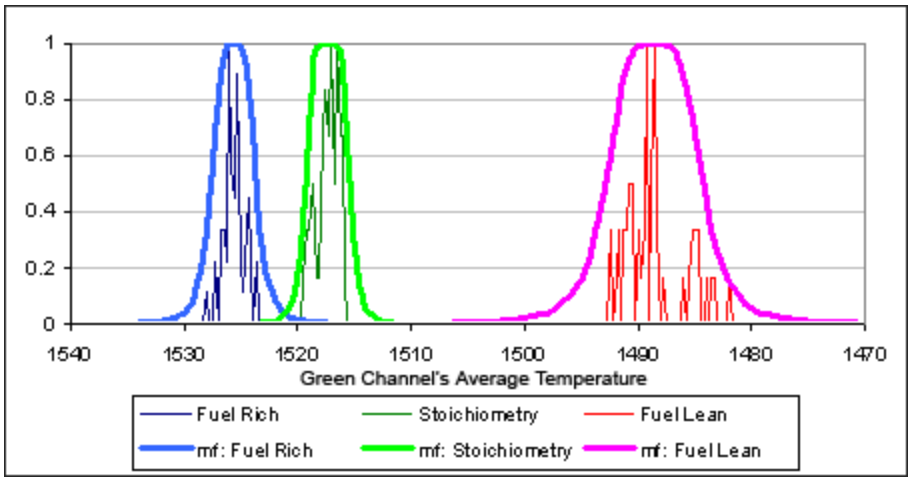

Figure 6.20 Membership Function for O/F Level with Fuel Level at Low based on Green Channel's Average Temperature

Table 6.5 Membership Function Parameters for O/F Level based on Blue Channel's Center of Mass around Y Axis

Fuel Class	Membership Function Parameters	O/F Class		
		Fuel Rich	Stoichiometry	Fuel Lean
High	a	3.12	5.37	3.16
	b	5.59	5.98	2.87
	c	375.02	401.42	418.87
Normal	a	7.54	6.39	5.02
	b	2.0	2.0	3.5
	c	393.3	419.5	443.18
Low	a	4.05	2.06	4.47
	b	5.97	3.67	2.77
	c	423.5	430.35	449.2

Table 6.6 Membership Function Parameters for O/F Level based on Green Channel's Average Temperature

Fuel Class	Membership Function Parameters	O/F Class		
		Fuel Rich	Stoichiometry	Fuel Lean
High	a	2.9	3.2	2.8
	b	5.0	2.2	5.7
	c	1452.9	1427.4	1412.6
Normal	a	4.8	9.5	3.2
	b	5.9	4.8	2.0
	c	1509.6	1473.9	1445.9
Low	a	2.0	2.0	4.3
	b	2.0	2.7	2.0
	c	1525.6	1517.3	1488.6

As shown in Figure 6.15 to 6.20 above, there exist gaps between the membership functions similar to the case of fuel flow rate approximation. This indicates the need to model the in-between classes for the O/F ratio approximation in order to provide a more comprehensive classification.

The parameters that model the current membership functions are similarly used to model the membership functions and become the guideline for the interpolation. However, unlike fuel approximation, the task is less trivial since the trend of changes for the parameters are not linear. Since neither key feature depicts any clear indication of being simpler than the other, both will be investigated simultaneously.

Note that exception case exists where fuel class is low. Between class stoichiometry and class fuel rich, there is no gap for blue channel's center of mass about

Y axis and relatively small for green channel's average temperature. The proposed interpolation process however will still provide an in-between membership functions for this particular class. Although this implies a possible misclassification as will be discussed later, in practicality the consequent is minor since the class fuel low depicts a combustion condition at the mechanical limit that one would naturally avoid during an actual production process.

There are two main tasks related to the building of membership functions for O/F approximation. First is to build two O/F membership functions, positioned at the in-between regions where the known three do not have significant membership degree for each fuel flow rate class of low, normal and high. These regions are labeled as "Rich to Stoichiometry" and "Stoichiometry to Lean" accordingly. Afterward, new sets of O/F membership functions will need to be created for the in-between class of fuel level "normal to high" and "low to normal" as well. In the end, each feature will have a total of 25 membership functions for O/F approximation across different fuel classes.

Interpolation is once again incorporated to approximate the parameters. Due to the non-linearity nature and limited number of known parameters, instead of using linear interpolation as in the case of fuel approximation, O/F approximation is done by using natural cubic spline interpolation which based on experiments yield a relatively good result [74].

In natural cubic spline interpolation, given a data set $\{x_i\}$ of n+1 points and $0 < i < n$, one can assemble a cubic spline S based on n piecewise cubic polynomials between the data as shown in EQ (6.7). Note that the coefficients in EQ (6.7) are determined by solving EQ (6.8).

$$S(x) = \begin{cases} S_0(x), & x \in [x_0, x_1] \\ S_1(x), & x \in [x_1, x_2] \\ \vdots & \vdots \\ S_{n-1}(x) & x \in [x_{n-1}, x_n] \end{cases} \qquad \text{EQ (6.7)}$$

where

$$S_i(x) = \frac{z_{i+1}(x - x_i)^3 + z_i(x_{i+1} - x)^3}{6h_i} + \left(\frac{y_{i+1}}{h_i} - \frac{h_i}{6} z_{i+1} \right)(x - x_i) + \left(\frac{y_i}{h_i} - \frac{h_i}{6} z_i \right)(x_{i+1} - x)$$

$$h_i = x_{i+1} - x_i$$

$$h_{i-1} z_{i-1} + 2(h_{i-1} + h_i) z_i + h_i z_{i+1} = 6\left(\frac{y_{i+1} - y_i}{h_i} - \frac{y_i - y_{i-1}}{h_{i-1}} \right) \qquad \text{EQ (6.8)}$$

where $z_0 = 0$
$z_n = 0$

For each fuel level, three values for each membership function parameter are known based on the O/F class. For the in-between membership functions, the parameter a, b and c are derived based on the mid-point from the spline interpolation between its adjacent membership functions. That is, as shown in EQ (6.7), given the known S(1), S(2) and S(3) for each membership parameter, thus the interpolation will compute S(1.5) and S(2.5) for the in-between membership functions. The results from the interpolation are shown in Table 6.7 and 6.8 below.

Table 6.7 Membership Function Parameters for O/F Level based on Blue Channel's Center of Mass About Y Axis

Fuel Class	Membership Function Parameters	O/F Class	
		Fuel Rich to Stoichiometry	Stoichiometry to Fuel Lean
High	a	4.75	4.99
	b	6.22	4.86
	c	389.34	411.26
Normal	a	6.99	5.73
	b	1.81	2.56
	c	406.72	431.66
Low	a	2.51	2.72
	b	4.65	3.05
	c	425.43	438.27

Table 6.8 Membership Function Parameters for O/F Level based on Green Channel's Average Temperature

Fuel Class	Membership Function Parameters	O/F Class	
		Fuel Rich to Stoichiometry	Stoichiometry to Fuel Lean
High	a	3.1	3.1
	b	2.8	3.2
	c	1438.8	1418.7
Normal	a	8.5	7.7
	b	5.6	3.6
	c	1490.8	1458.9
Low	a	1.7	2.9
	b	2.5	2.5
	c	1524.0	1505.5

Once the parameters for the in-between O/F class are obtained, the next step is to build membership functions for the fuel class “Low to Normal” and “Normal to High”. The difficulty here is that there is no prior test data used as guidelines to model the membership functions as in the case of fuel class “Low”, “Normal” and “High”. There is no data that represent the three O/F classes of “Fuel Rich”, “Stoichiometry” and “Fuel Lean” for fuel class “Low to Normal” and “Normal to High” since the fuel class themselves are results of interpolations.

There are many possible approaches to resolve this condition. In this study, the strategy is to derive the membership function parameters for these classes based on the O/F membership function parameters from fuel class “Low”, “Normal” and “High”. The membership function parameters of a particular fuel and O/F class are obtained using interpolation on the same O/F class of the adjacent fuel class. For fuel class “Low to Normal”, its adjacent fuel class is “Low” and “Normal” while for fuel class “Normal to High” it is “Normal” and “High” respectively. For example, the membership parameter for O/F class “Stoichiometry” with fuel class “Normal to High” would be derived using interpolation on O/F class “Stoichiometry” from fuel class “Normal” and “High”. The interpolation used is also cubic spline due to the non-linearity in the membership parameters. The complete parameters for all fuel and O/F classes are shown in Table 6.9 and 6.10.

Table 6.9 Membership Function Parameters for O/F Level Approximation based on Blue Channel's Center of Mass around Y Axis

Fuel Class	M. F. Parameters	O/F Class				
		1.8	**1.8 - 2.1**	**2.1**	**2.1 – 2.4**	**2.4**
High	**a**	3.12	4.75	5.37	4.99	3.16
	b	5.59	6.22	5.98	4.86	2.87
	c	375.02	389.34	401.42	411.26	418.87
Normal to High	**a**	6.32	6.71	6.55	5.83	4.56
	b	2.85	3.11	3.28	3.36	3.36
	c	382.67	397.87	411.37	423.19	433.31
Normal	**a**	7.54	6.99	6.39	5.73	5.02
	b	2.0	1.81	2.0	2.56	3.5
	c	393.3	406.72	419.5	431.66	443.18
Low to Normal	**a**	6.78	5.59	4.89	4.69	4.99
	b	3.04	2.32	2.13	2.46	3.31
	c	406.91	415.91	425.84	436.69	448.48
Low	**a**	4.05	2.51	2.06	2.72	4.47
	b	5.97	4.65	3.67	3.05	2.77
	c	423.5	425.43	430.35	438.27	449.2

Table 6.10 Membership Function Parameters for O/F Level Approximation based on Green Channel's Average Temperature

Fuel Class	M. F. Parameters	O/F Class				
		1.8	**1.8 - 2.1**	**2.1**	**2.1 – 2.4**	**2.4**
High	**a**	2.9	3.1	3.2	3.1	2.8
	b	5.0	2.8	2.2	3.2	5.7
	c	1452.9	1438.8	1427.4	1418.7	1412.6
Normal to High	**a**	4.5	7.4	8.1	6.6	2.9
	b	6.1	5.0	4.1	3.6	3.4
	c	1486.3	1467.1	1451.0	1438.0	1428.1
Normal	**a**	4.8	8.5	9.5	7.7	3.2
	b	6.0	5.6	4.8	3.6	2.0
	c	1509.6	1490.8	1473.9	1458.9	1445.9
Low to Normal	**a**	4.0	6.7	7.5	6.5	3.6
	b	4.6	4.8	4.3	3.3	1.5
	c	1522.7	1509.7	1496.0	1481.4	1466.1
Low	**a**	2.0	1.7	2.0	2.9	4.3
	b	2.0	2.5	2.7	2.5	2.0
	c	1525.6	1524.0	1517.3	1505.5	1488.6

Figure 6.21 to 6.30 shows the complete membership functions for O/F class approximation for both key features for each fuel class. Note that only O/F class "Unknown" is not shown due to its trivial nature.

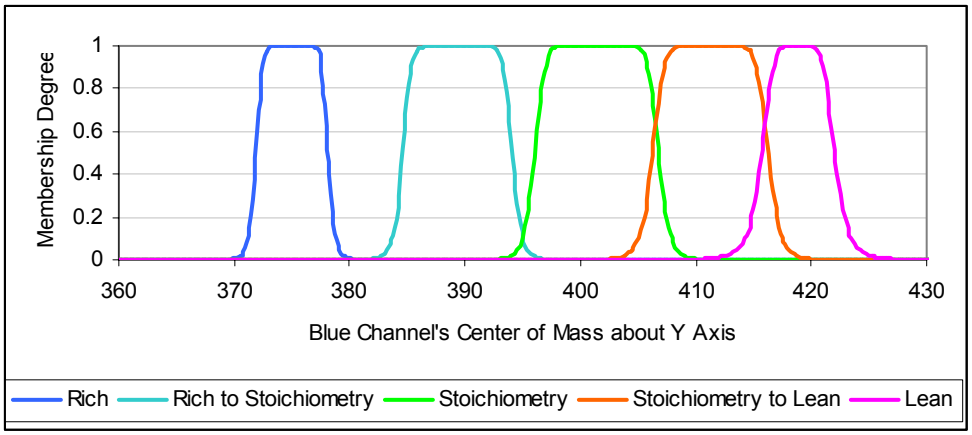

Figure 6.21 Membership Function for O/F Level Approximation with Fuel Level at High based on Blue Channel's Center of Mass around Y Axis

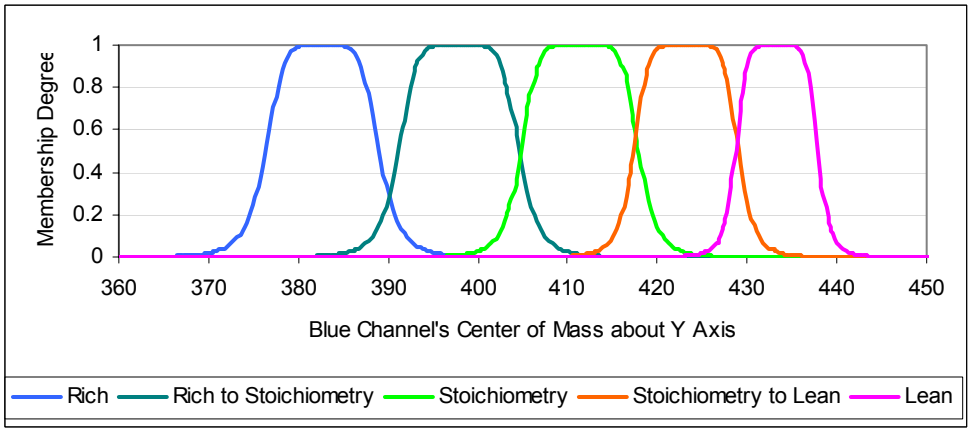

Figure 6.22 Membership Function for O/F Level with Fuel Level at Normal to High based on Blue Channel's Center of Mass around Y Axis

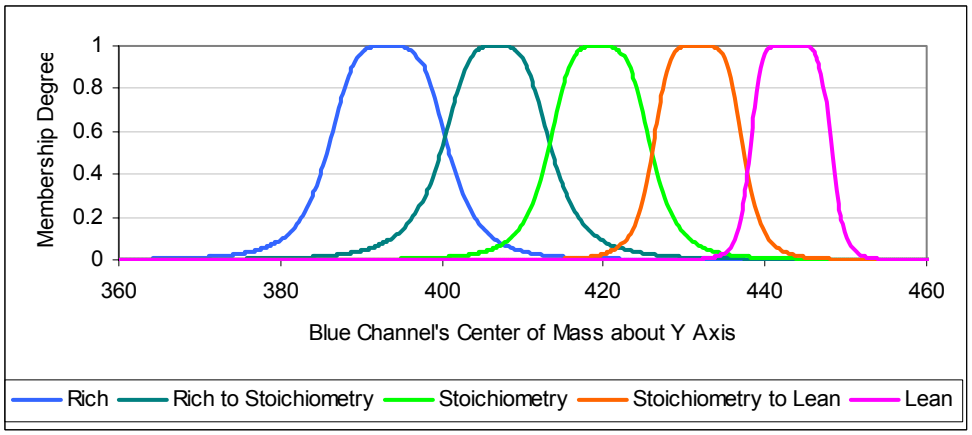

Figure 6.23 Membership Function for O/F Level with Fuel Level at Normal based on Blue Channel's Center of Mass around Y Axis

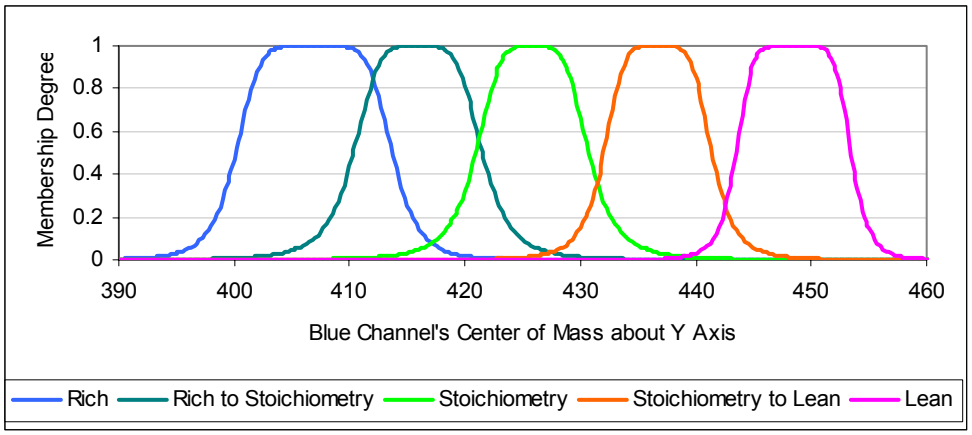

Figure 6.24 Membership Function for O/F Level with Fuel Level at Low to Normal based on Blue Channel's Center of Mass around Y Axis

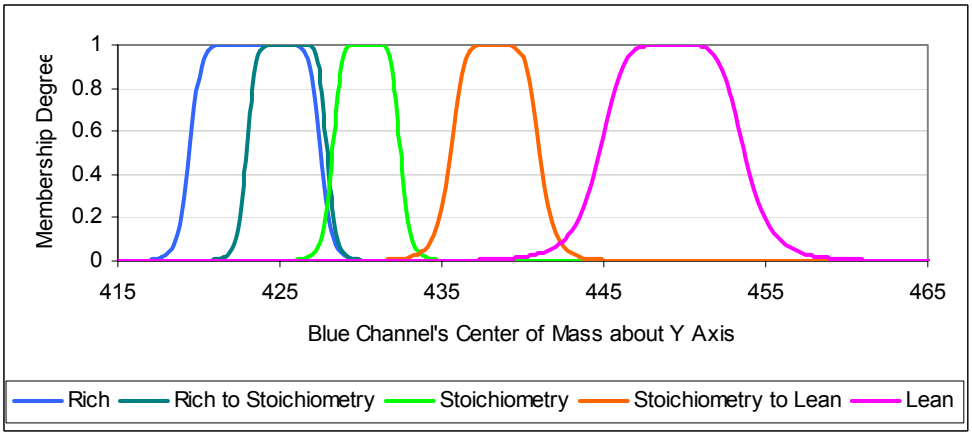

Figure 6.25 Membership Function for O/F Level with Fuel Level at Low based on Blue Channel's Center of Mass around Y Axis

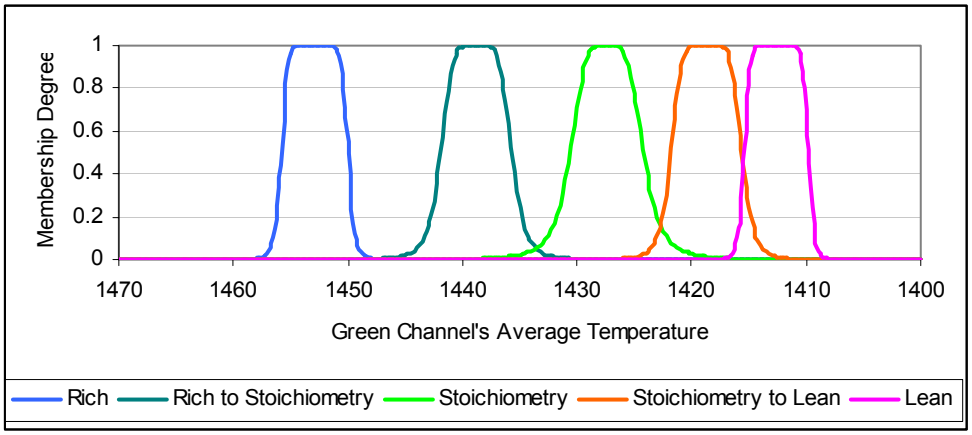

Figure 6.26 Membership Function for O/F Level with Fuel Level at High based on Green Channel's Average Temperature

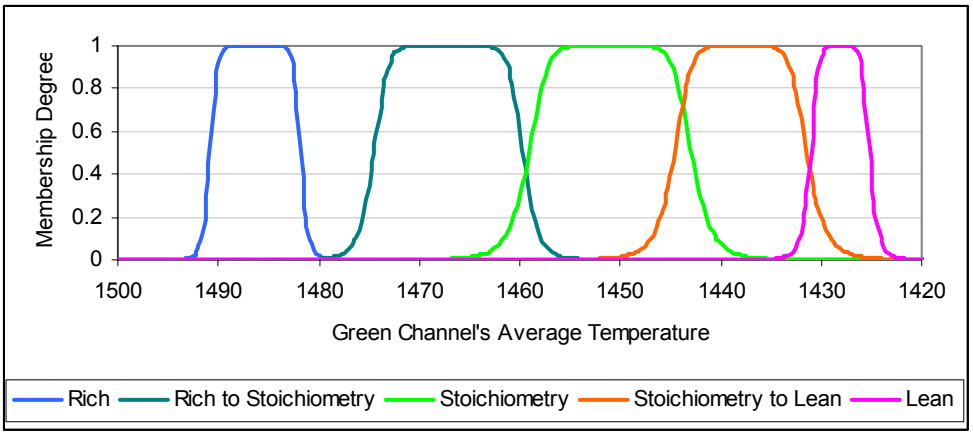

Figure 6.27 Membership Function for O/F Level with Fuel Level at Normal to High based on Green Channel's Average Temperature

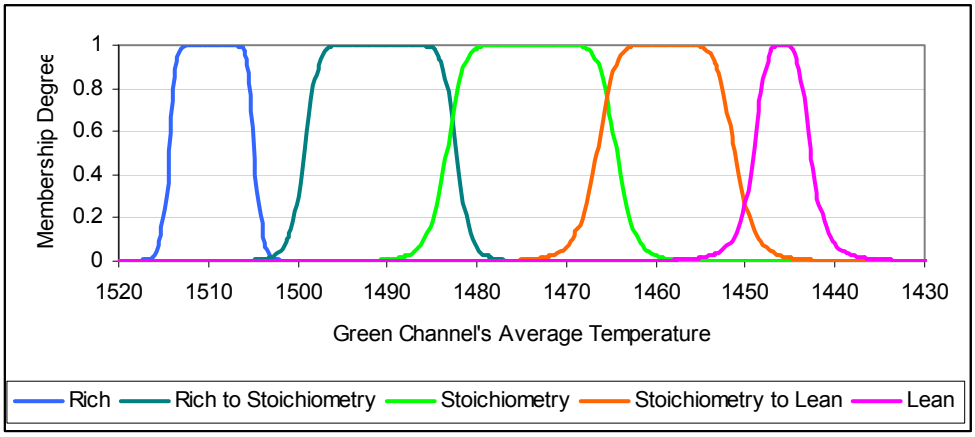

Figure 6.28 Membership Function for O/F Level with Fuel Level at Normal based on Green Channel's Average Temperature

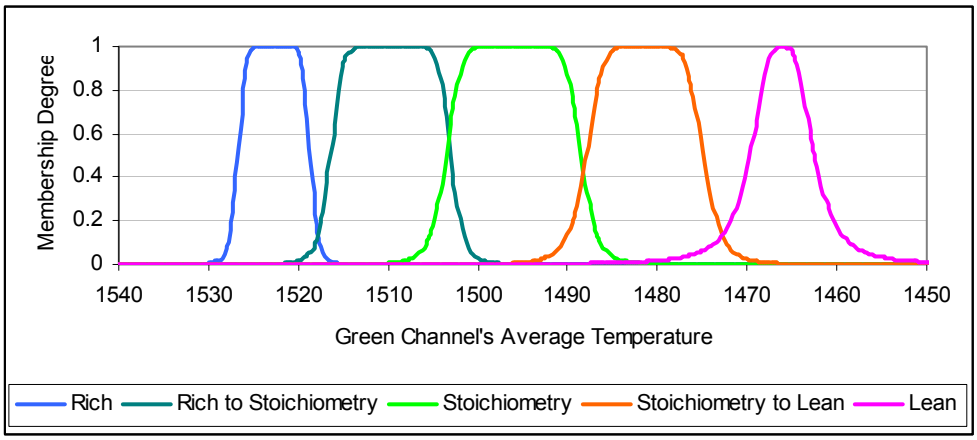

Figure 6.29 Membership Function for O/F Level with Fuel Level at Low to Normal based on Green Channel's Average Temperature

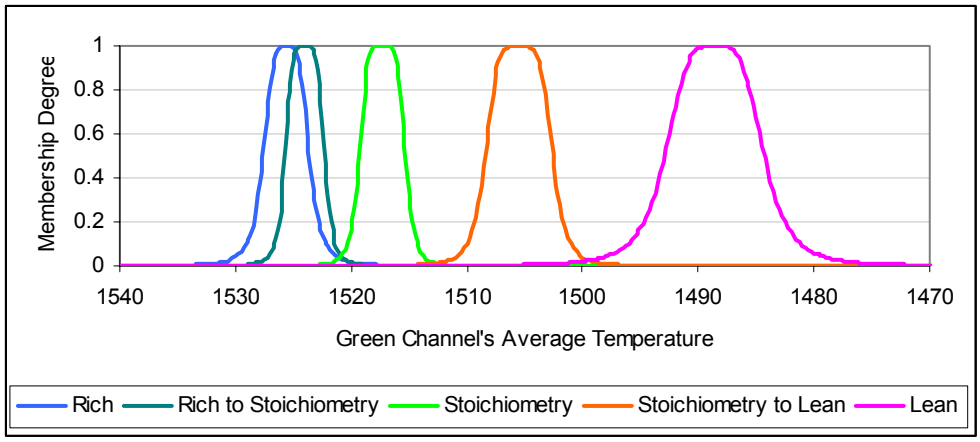

Figure 6.30 Membership Function for O/F Level with Fuel Level at Low based on Green Channel's Average Temperature

From observing the created membership functions, the set from Green Channel's Average Temperature indicates higher possibility of inaccurate approximation since it has more gaps between its membership functions. Fortunately Blue Channel's Center of Mass about Y Axis depicts less gaps problem and seems to be more applicable in overall for the O/F approximation task. However it also has inaccurate membership functions for fuel class "High" and "Low". Particularly at fuel class "Low", the O/F class "Lean" and "Stoichiometry to Lean" is almost completely overlap one another. This is considered to be the current limitation to the approach and strategy. Fortunately in a real practical situation, one never operate the furnace at either extreme of 80 or 140 scfh flow rate thus keeping the approximation at the more manageable in-between ranges.

Finally, similar to fuel approximation, minimum and maximum threshold need to be specified as well for regions that fall outside the range of known O/F class. The selection of these thresholds is done manually for each fuel class by observing the feature output range of the membership functions. The assumption is that even though it is possible for the feature output values to fall on these ranges, but it is highly improbable based on the a priori knowledge from the test data. EQ(6.9) shows the threshold formula

used to classify "Unknown" class for different fuel classes. Table 6.11 and 6.12 shows the minimum and maximum thresholds set for each fuel class. Any output that is less than minimum and bigger than maximum will be assigned with O/F class "Unknown".

$$\mu^{m}{}_{unknown}(x) = \begin{cases} 0 & if \quad Min \le x \le Max \\ 1 & if \quad x < Min \\ 1 & if \quad x > Max \end{cases} \qquad \text{EQ (6.9)}$$

where $\mu^{m}{}_{unknown}(x)$ = membership degree for the class unknown for fuel class m
x = feature output value

Table 6.11 Threshold for O/F Class "Unknown" based on Blue Channel's Center of Mass around Y Axis

Fuel Class	Thresholds	
	Min	**Max**
High	365	430
Normal to High	365	450
Normal	356	450
Low to Normal	390	450
Low	415	460

Table 6.12 Threshold for O/F Class "Unknown" based on Green Channel's Average Temperature

Fuel Class	Thresholds	
	Min	**Max**
High	1400	1460
Normal to High	1420	1500
Normal	1430	1520
Low to Normal	1450	1540
Low	1470	1540

The process of determining the O/F class is done in two steps. First the proper fuel class needs to be selected. This information is obtained using method previously discussed. The fuel class then defines which set of O/F membership functions to be used. The actual O/F approximation is then carried in the second step, which in this study is defined based on the highest membership degree. Similar to fuel approximation, each O/F class is assigned a numerical number from 1 to 5 with 0 being "Unknown". EQ (6.10) shows the formula for O/F class selection along with number assignment for each class.

$$Class(x) = Max\{\mu_0(x), \mu_1(x), \mu_2(x), \mu_3(x), \mu_4(x), \mu_5(x)\} \qquad \text{EQ (6.10)}$$

where Class(x) = class of output value x
x = feature output value
$\mu_0(x)$ = membership degree for the class unknown
$\mu_1(x)$ = membership degree for the class fuel rich
$\mu_2(x)$ = membership degree for the class rich-to-stoichiometry
$\mu_3(x)$ = membership degree for the class stoichiometry
$\mu_4(x)$ = membership degree for the class stoichiometry-to-lean
$\mu_5(x)$ = membership degree for the class lean

To test the O/F approximation, the same experiment run 15 is used. The aggregated class label output from the previous fuel classification will be used here to select the proper set of O/F membership functions. Figure 6.31 and 6.32 shows the actual key feature output values for run 15. Interestingly the trend of change is quite visible even at the feature output level for Blue Channel's Center of Mass about Y Axis.

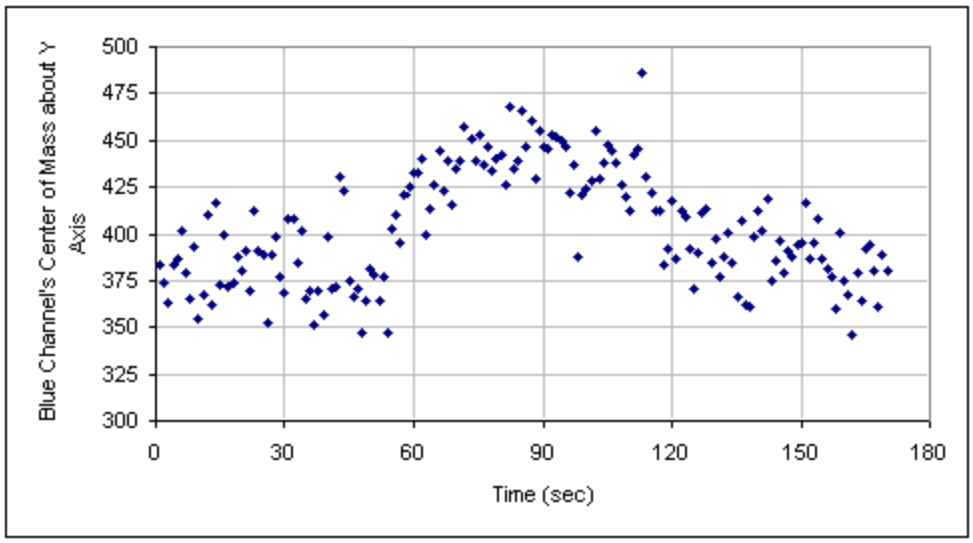

Figure 6.31 Blue Channel's Center of Mass about Y Axis Feature Output for Step Run

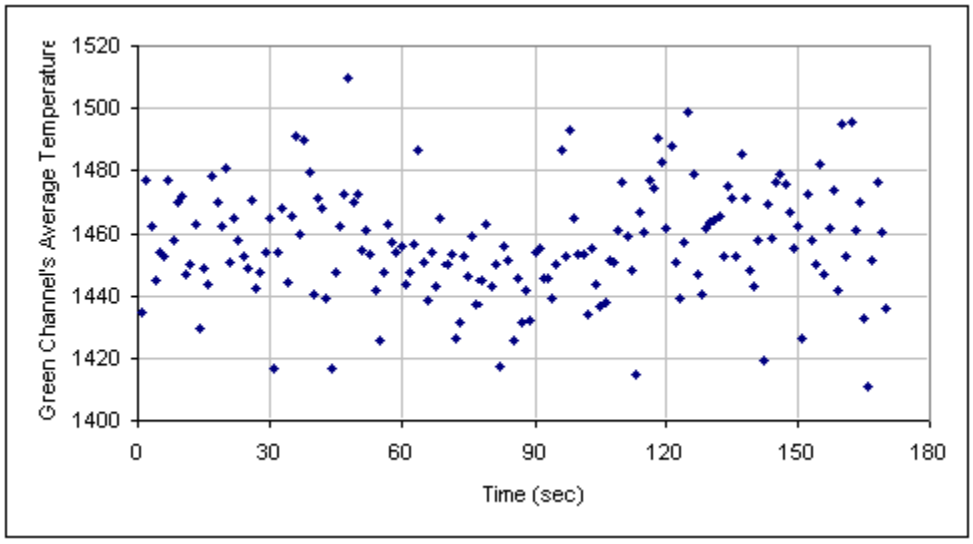

Figure 6.32 Green Channel's Average Temperature Feature Output for Step Run

Using EQ (6.10), the O/F classification output is as shown in Figure 6.33 and 6.34 for both key feature values. Similar to fuel classification, an ideal case of O/F class is created for classification assessment. Additionally, since the fuel classification itself contains inaccuracy, another set of O/F classification is carried on by using the ideal fuel class thus providing the ability to observe the true accuracy of the O/F classification itself. An ideal case is again introduced here so that some error assessment can be measured. It

depicts the expected trend based on the experiment description rather than the actual information from the furnace control since it is unavailable. It shows the trend from class "Fuel Rich" in 60 seconds, then change to "Fuel Lean" for another 60 seconds then return to "Fuel Rich". The O/F classification results are shown in Figure 6.35 and 6.36.

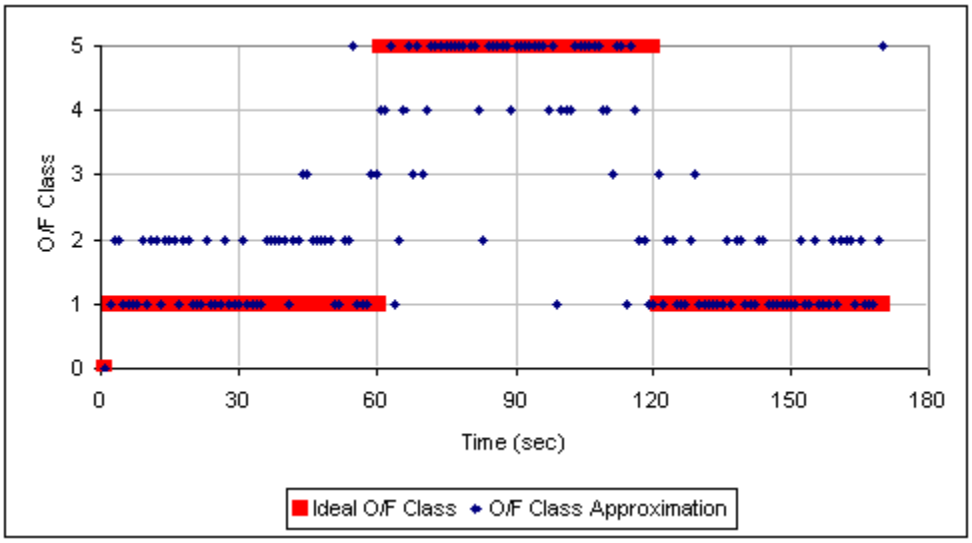

Figure 6.33 O/F Classification Output based on Blue Channel's Center of Mass about Y Axis

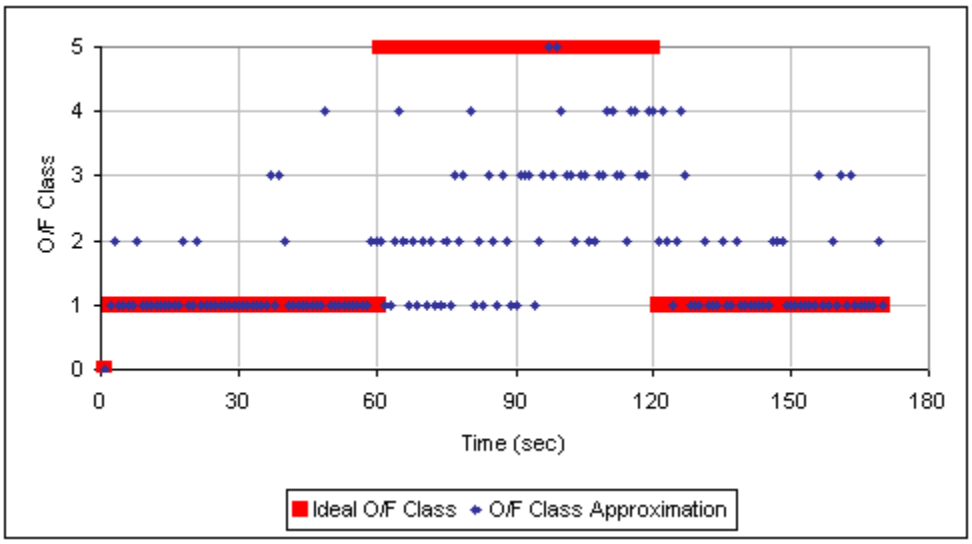

Figure 6.34 O/F Classification Output based on Green Channel's Average Temperature

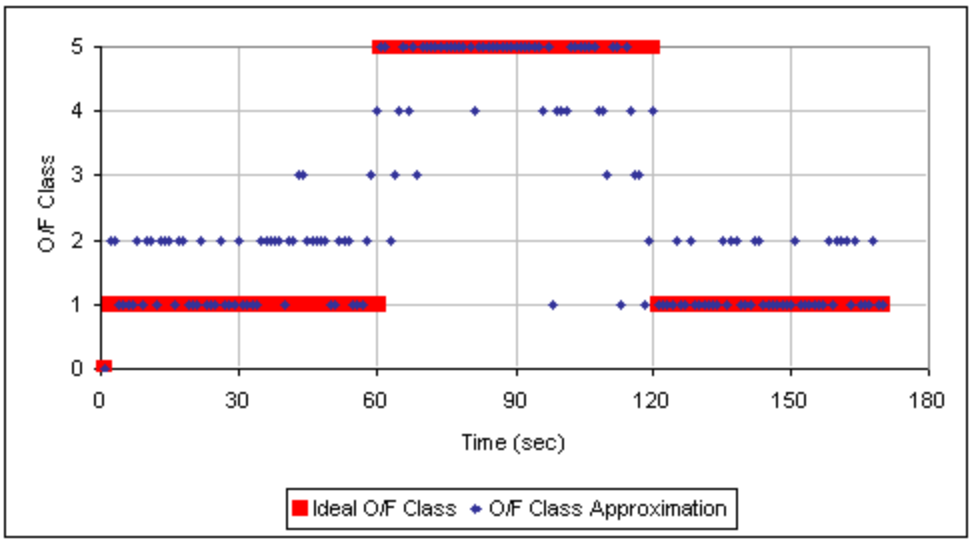

Figure 6.35 O/F Classification Output based on Blue Channel's Center of Mass about Y Axis using Ideal Fuel Class

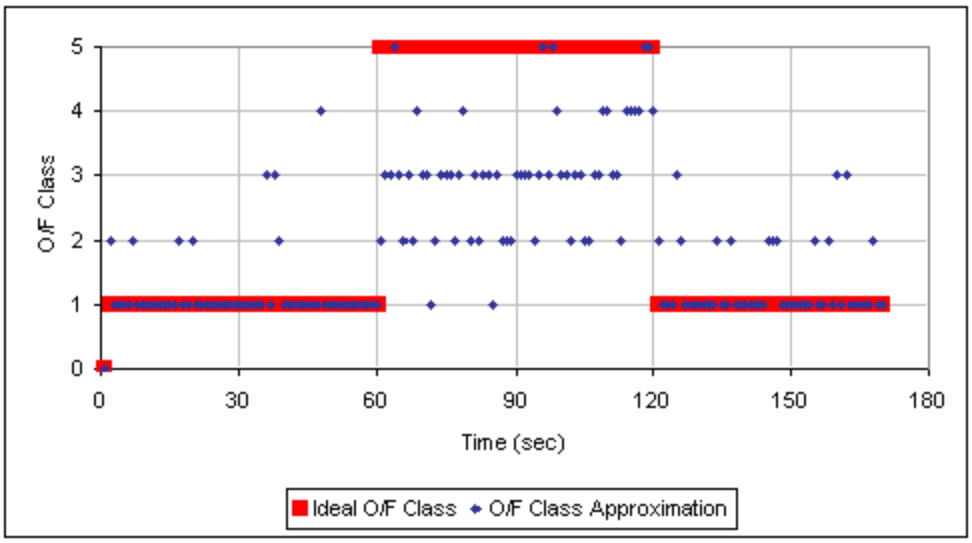

Figure 6.36 O/F Classification Output based on Green Channel's Average Temperature using Ideal Fuel Class

The classification results appear to have many misclassifications particularly if one compared it with the ideal case. Green Channel's Average Temperature particularly appears to provide the worst performance which is expected due to its membership function configurations. Similar to fuel classification case, the actual trend of change however still exists for both features although with varying qualities. It is particularly

very visible in Blue Channel's Center of Mass about Y Axis. Interestingly, using the ideal case of fuel class appears to have insignificant impact to the overall O/F classification for both features which indicates that the inaccuracies are independent of fuel classification.

Table 6.13 and 6.14 shows the error assessment for both features respectively. The error rate itself seems rather high for both features and at first might seem contradictory to their good performance during feature selection process. The main cause of the high error rate however is not because of the feature output themselves but also of the ideal case to which the assessment is compared with. For example, similar to fuel classification, there exists transition period from one O/F ratio to another which is not considered with the ideal case. This transition period appears to be different for both features with Green Channel's Average Temperature being longer. The length of transition time can be caused by two things. One is the temperature change in the flame takes longer time than the position of the combustion zone during the changes. Another is the quality of the membership function configurations. Particularly for Blue Channel's Center of Mass about Y Axis, it is very likely that many of the feature values falls around the range where the membership functions intersect. This can be seen from Figure 6.33 and 6.35 for the classification output where oscillations occur between class "Rich" and "Rich to Stoichiometry" and also between class "Stoichiometry to Lean" and "Lean".

Table 6.13 O/F Approximation Error Assessment using Blue Channel's Center of Mass about Y Axis

Fuel Class	Total Data (n)	Total Incorrect Classification (x)		Error Rate (x / n) * 100%	
		Using Approximated Fuel Class	Using Ideal Fuel Class	Approximated Fuel Class (%)	Ideal Fuel Class (%)
Unknown	1	0	0	0	0
Rich	109	51	47	46.8	43.1
Lean	60	25	21	41.6	35
Total		76	68	44.7	40

Table 6.14 O/F Approximation Error Assessment using Green Channel's Average Temperature

Fuel Class	Total Data (n)	Total Incorrect Classification (x)		Error Rate (x / n) * 100%	
		Using Approximated Fuel Class	Using Ideal Fuel Class	Approximated Fuel Class (%)	Ideal Fuel Class (%)
Unknown	1	0	0	0	0
Rich	109	27	21	24.8	19.3
Lean	60	58	55	96.7	91.7
Total	170	85	76	50	44.7

Table 6.15 and 6.16 shows a different assessment by combining class "Rich" and "Rich to Stoichiometry" into one class "Rich". Also, combine "Stoichiometry to Lean" and "Lean" into one class "Lean". One could consider this as being a measurement of

how far the flame condition is from the desired stoichiometry condition. This approach seems to reduce the amount of misclassifications as expected, particularly on errors caused by class oscillations. Especially for Blue Channel's Center of Mass about Y Axis, the error rate is reduced a lot more which indicates the original error rate is largely due to class oscillations.

Table 6.15 O/F Approximation Error Assessment using Blue Channel's Center of Mass about Y Axis

Fuel Class	Total Data (n)	Total Incorrect Classification (x)		Error Rate (x / n) * 100%	
		Using Approximated Fuel Class	Using Ideal Fuel Class	Using Approximated Fuel Class	Using Ideal Fuel Class
Unknown	1	0	0	0	0
Rich	109	8	4	7.3	3.7
Lean	60	12	10	20	16.7
Total	170	20	14	11.8	8.2

Table 6.16 O/F Approximation Error Assessment using Green Channel's Average Temperature

Fuel Class	Total Data (n)	Total Incorrect Classification (x)		Error Rate (x / n) * 100%	
		Using Approximated Fuel Class	Using Ideal Fuel Class	Using Approximated Fuel Class	Using Ideal Fuel Class
Unknown	1	0	0	0	0
Rich	109	9	6	8.3	5.5
Lean	60	49	45	81.7	75
Total	170	58	51	34.1	30

Based on the error assessment, it is concluded that Blue Channel's Center of Mass about Y Axis is a better feature to use for O/F approximation. Its performance however is not perfect; yet it appears to be quite promising. Further improvements in the approximation are possible as well particularly in the task of modeling the membership functions. Also, since it uses blue channel information which is also the case in fuel approximation, thus the overall flame image analysis can be done by using a single color channel alone which reduces the computational costs.

Another test is conducted for further assessment of the selected key feature's performance using experiment run 14. Similar to experiment run 15, run 14 has its fuel flow rate from 128 scfh to 96 scfh changes during the run. However, instead of an abrupt change, it is more of a gradual change resulting in a ramp-up effect that lasts for one minute. The run spanned approximately for 3 minutes. It starts with fuel flow rate at 128 scfh and after a minute it is slowly decreased manually by 1 scfh for every 2 seconds thus reaching 96 scfh in the next minute. Once it reaches 96 scfh, the flow rate is abruptly changed back to 128 scfh. The oxidizer flow is kept at constant throughout the whole experiment at 231 scfh.

Figure 6.37 shows the fuel flow rate classification result based on blue channel's Otsu threshold feature output which visually depicts the said ramp effect. The red lines on the plot are meant as a visual guideline for depicting general trend of the flow rate changes. Figure 6.38 depicts the desired trend according to the change made within the furnace control. Similar to run 15, run 14 provides a good test case for both fuel and O/F ratio classification assessment in terms of having fuel flow rates that are in-between the

known classes as well as providing insight to the key feature's sensitivity during a small incremental changes in fuel flow rate.

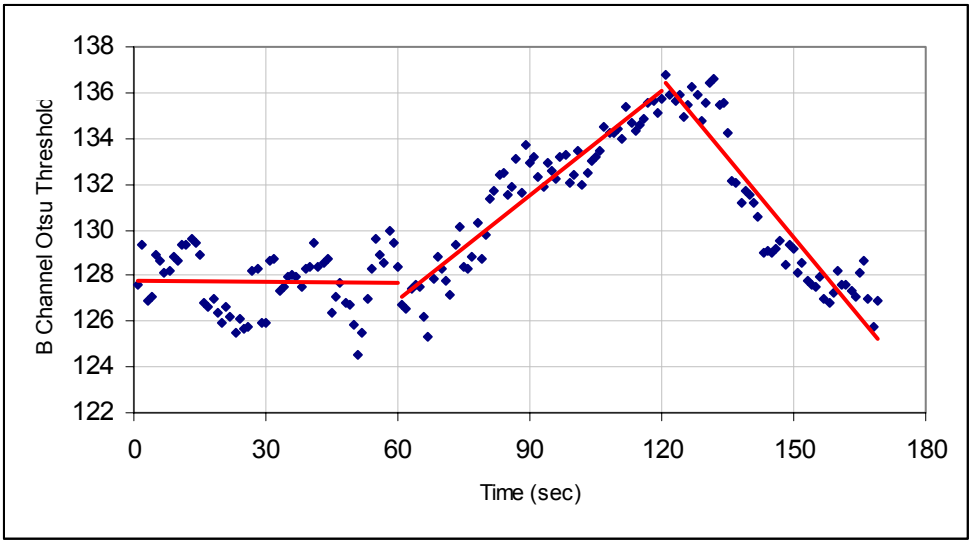

Figure 6.37 Experiment Run 14 with Fuel Flow Rate Changes

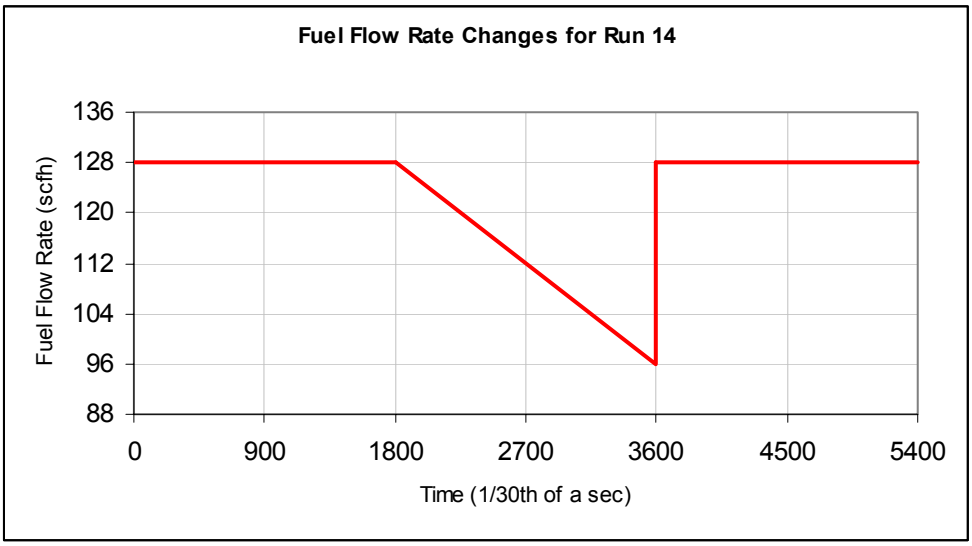

Figure 6.38 Experiment Run 14 with Fuel Flow Rate Changes

As shown in Figure 6.37 above, fuel classification using the Blue Otsu threshold follows the gradual changes that occur at the 2nd. Noticeably some fluctuations occur in the feature output during the 1st minute that gradually stabilizes particularly by the 2nd minute onward.

Interestingly as depicted by Figure 6.37, the abrupt change of the fuel flow rate from 96 to 128 scfh at the 2nd minute takes time to stabilize. This phenomenon is consistent with run 15 as well. This indicates the discrepancy between desired output based on the furnace control and the actual combustion do exist which can be caused by the furnace mechanism or the combustion process itself.

Figure 6.39 shows the flame analysis output, depicting the O/F ratio changes during the run using blue channel central of mass about Y axis as the key feature. The three colors are provided for visual guideline purpose to mark regions based on the 3 minutes span of the experiment run. Similar to run 15, there are some oscillations of classification particularly for neighboring classes. The oscillation occurs during all the 3 minute runs, even when the fuel classification output already stabilized at the 2nd minute. Nevertheless the overall trend of the classification, do depict the desired gradual changes from fuel rich situation in the 1st minute, the gradual change to fuel lean in the 2nd minute and then gradually back to fuel rich in the 3rd minute. It is observed that at the beginning of the ramp test during the fuel rich period the sensitivity is not as good as second half of the ramp which can be attributed to the small rate of changes.

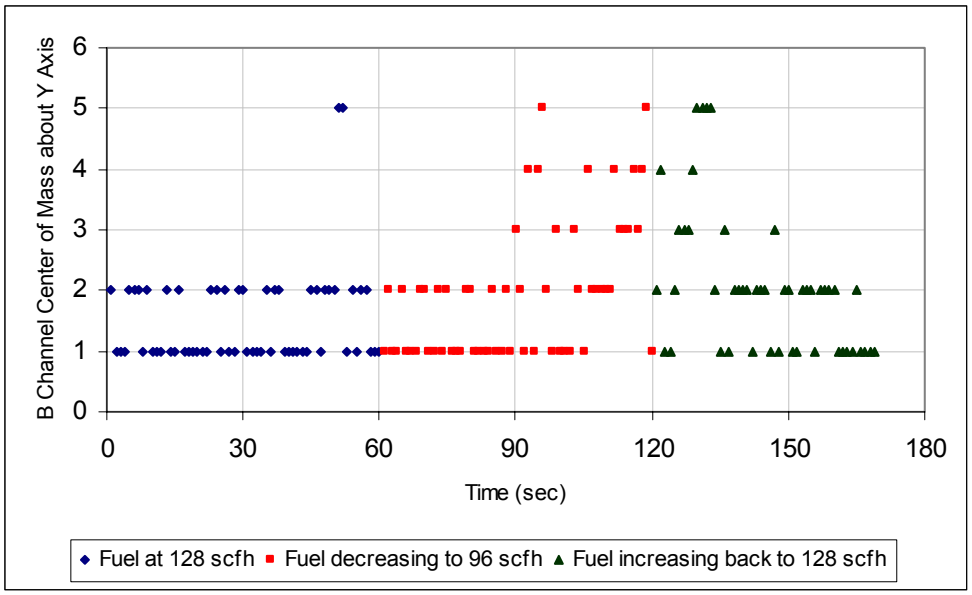

Figure 6.39 Flame Analysis Output for Experiment Run 14

It is therefore concluded that the strategy and methodology proposed in this chapter including the fuzzy system are feasible and provide reasonably acceptable results.

6.6 Implementation Summary

From the experimental results and findings in this study, the proposed system architecture as previously depicted in Chapter 1 (Figure 1.1), can be summarized and realized into eight main processes. This processes are summarized in Figure 6.40 below.

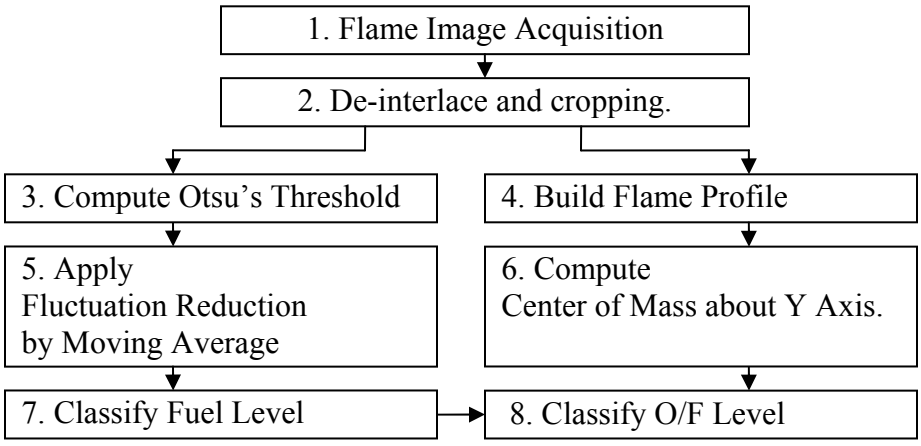

Figure 6.40 Finalized Process Flow of Proposed System Architecture

The finalized architecture is simulated using MatLab [75] and tested on a workstation using Intel P3 1.3GHz CPU [62] with 512MB RAM running Windows 2000 operating system [63]. For performance evaluation, each processed are timed based on processing 120 interlaced color flame images with 720x480 pixel resolutions. These images are acquired at 30 frames per second. Table 6.17 shows the task and pseudo code for each process along with the actual average time required to process one frame. Note that the images used are in the form of image files residing in the workstation.

Table 6.17 Processes Descriptions and Timing Summary

Process no.	Summary	Pseudo Code	Time (ms)
1	▪ Load flame images from hard drive. ▪ Extract B channel information from images.	01 for each image do 02 img = load_image() 03 imgB = extract_B_Chnl(img) 04 do process 2 05 end	23.84
2	▪ De-interlace image into two sub-images based on odd and even field. ▪ Crop sub-images as appropriate.	01set flag = 1 02 for each row of imgB 03 if (flag) 04 append row to imgB1 05 else 06 append row to imgB2 07 flag = 1 – flag 08 end 09 imgB1c = crop(imgB1) 10 imgB2c = crop(imgB2) 11 execute separate thread for 12 do process 3 (imgB1c, imgB2c) 13 do process 4 (imgB1c, imgB2c) 14 end	29.30
3	▪ Compute Otsu Threshold on sub-images based on EQ (3.1) to EQ (3.6).	01 otsu1 = applyOtsu(imgB1c) 02 otsu2 = applyOtsu(imgB2c) 03 do process 5(otsu1, otsu2)	77.1
4	▪ Build flame profiles for every 60 sub-images based on EQ (4.15). ▪ Apply intensity suppression for each completed flame profile based on EQ (3.8).	01 tmpImg += imgB1c + imgB2c 02 for every 60 sub-images do 03 imgFP = tmpImg / 60; 04 imgFPis = power(imgFP,4) 05 do process 6 (imgFPis) 06 end	23.8
5	▪ Apply moving average for latest 60 results from process 3 based on EQ (4.14).	01 put otsu1 to buffer 02 put otsu2 to buffer 03 remove 2 oldest data from buffer	0.4

		04 mvg_avg = mean(buffer) 05 do process 7 (mvg_avg)	
6	▪ Compute Center of Mass about Y Axis based on result from process 4 based on EQ (4.13)	01 result = compute(imgFPis) 02 do process 8 (result)	32.5
7	▪ Compute membership degree using functions based on EQ (6.1) and (6.4) using process 5's result. ▪ Determine fuel class from process 5 based on EQ (6.5) ▪ Update fuel class label buffer	01 μ0 = class_0(mvg_avg) 02 μ1 = class_1(mvg_avg) 03 μ2 = class_2(mvg_avg) 04 μ3 = class_3(mvg_avg) 05 μ4 = class_4(mvg_avg) 06 μ5 = class_5(mvg_avg) 07 μmax = max(μ0, μ1, μ2, μ3, μ4, μ5) 08 fuel_class = n where (μn == μmax) 09 fuel_classBuffer = update(fuel_class)	1.2
8	▪ Aggregate latest fuel class labels from process 7 based on EQ (6.6). ▪ Determine set of membership function parameters based on the aggregated fuel class label. ▪ Compute membership degree using functions based on EQ (6.1) using process 6's result. ▪ Determine O/F ratio class based on EQ (6.9) and (6.10).	01 aF_class = median(fuel_classBuffer) 02 load_OF_mf_params(aF_class) 03 μ0 = class_0(mvg_avg) 04 μ1 = class_1(mvg_avg) 05 μ2 = class_2(mvg_avg) 06 μ3 = class_3(mvg_avg) 07 μ4 = class_4(mvg_avg) 08 μ5 = class_5(mvg_avg) 09 μmax = max(μ0, μ1, μ2, μ3, μ4, μ5) 10 OF_class = n where (μn == μmax)	7.5

From this implementation, total time to classify fuel and O/F ratio can be obtained. For fuel classification, it takes process 1, 2, 3, 5 and 7 to complete. Thus it requires 146.24 ms per image frame. For O/F class, the total time to complete needs to take into account the existence of parallel processing. The bottleneck relies on the longer total processing time between path 3, 5 and 7 and path 4 and 6. The first is longer since the total time for 30 sets of path 3, 5 and 7 is 30 * 93.1 ms = 2.8 seconds while path 4 and 6 is 56.3 ms. Hence the total time for O/F ratio classification, depends on path 1, 2, 30 sets of path 3, 5, 7 and path 8 which is 2.9 seconds.

Assuming an input rate to the system of 30 frames per second, fuel classification can be achieved with no problem since the total time to process a frame is faster than the input rate. On the other hand, O/F classification which classifies every 30 images takes longer than 1 second thus a form of synchronization will be required to maintain proper flame analysis.

Improvement to the performance time for both classifications can be obtained by improving hardware capacity as well as software optimization.

7. CONCLUSION

System architecture for analyzing flame quality using a combination of image processing and machine learning methodology is proposed and examined in this study. The architecture is developed and evaluated using video footages of furnace flames with varying flow rate level of fuel and oxidizer intakes, acquired from a pilot-scale glass furnace. As shown by this study, the architecture has a high potential for monitoring combustion quality based on real-time flame image analysis that assesses its fuel flow rate and O/F ratio.

The proposed architecture consists of four main processes: image acquisition, pre-processing, feature extraction and finally flame image classification. Two separate processing paths or process configurations are examined for pre-processing and feature extraction processes. Each process configuration contains unique step of processing logics and are run in parallel. One configuration is designed for detection of changes in fuel flow rate and in turn its output becomes an input parameter for the second configuration for determining the O/F ratio. Based on the fuel flow rate and O/F ratio, one can derive the oxidizer flow rate and thus the full insight to the furnace flame's combustion status.

At the image acquisition process, two-dimensional furnace flame images are obtained from the furnace. The image acquisition device is an interlaced color CCD camera equipped with a 90° viewing angle lens, capable of acquiring uncompressed

video footage with 720 x 480 image resolutions and a frame rate of 30 frames per second. At this stage, each acquired image frame is deinterlaced to two sub-images to ensure the flame image integrity. Subsequently, stationary unwanted region such as the furnace wall and camera hole are removed from the image by manual cropping.

During the pre-processing stage the flame regions are first identified in every frame images. Two different strategies are proposed and tested for flame identification: automatic two-class image segmentation using Otsu threshold method and image enhancement by mapping function. Otsu threshold method is particularly valuable since not only it is proven to be capable of identifying the flame region, but also its output can be utilized as one of the feature to be analyzed. The thresholding method results in a crisp segmentation of the image into two classes: flame and non-flame. Image enhancement approach identifies the flame region by manipulating pixel intensity and is not limited by the two-class hypotheses as in the case of Otsu method. As discussed in chapter 3, each strategy has its own strength and usefulness for each process configuration.

Once the flame region has been identified, its features are computed during the feature extraction process. Set of prospective features are designed and proposed which are derived based on their feasibility in concept for quantifying flame image characteristics. These features evaluate the flame images based on their spatial and pixel intensity characteristic as discussed in Chapter 4. A total of nine features are examined in this study. Five are based on their typical inclusion in previous studies: area, average, variance, skew and kurtosis. Four new features are designed and proposed in this study: pseudo flame temperature, Otsu threshold, image entropy and center of mass about Y

axis. These features are computed separately for each red, green, blue, hue, saturation and value channel of each identified flame region within a flame image. Depending on the configuration, aggregations using moving or grouping average are applied to the feature output values which improve flame classification performance during flame analysis.

The feature extraction process involves large amount of computation due to the size of input data as well as the number of features computed. Feature selection process is introduced and discussed in Chapter 5 using decision tree classifier with wrapper method to select the best features for the flame image analysis and consequently reducing the amount of computation significantly. Two sets of key features are identified for both fuel and O/F ratio classification. These are Otsu's threshold level from blue channel and image entropy from value channel for classifying fuel flow rate. Average temperature from green channel and center of mass about y axis from blue channel are shown to be sensitive towards changes in O/F ratio. As previously discussed, these four key features are sensitive with respect to changes in both fuel flow rate and the O/F ratio. Through additional tests these four features are further reduced to two key features as discussed below.

Additional strategy is required to complete the flame image analysis process for monitoring fuel flow level and O/F ratio. Fuzzy system is proposed for the task due to its capability in accommodating uncertainty by using membership functions. These membership functions are modeled based on generalized bell formula, with its parameters derived based on the key features' output distribution characteristics as extracted from the known test cases. To test the fuzzy model, two experimental runs are used which contain

both fuel and oxidizer flow level outside the previously used test cases. In addition, each run contains varying level of fuel flow rates, hence, shedding light on the classification sensitivity in detecting flow rate changes. From this test, two key features provide promising performances for fuel and O/F ratio approximation respectively: blue channel's Otsu's threshold level and center of mass about y axis. Both features succeed in depicting changes between stoichiometry and non-stoichiometry flame condition for both test runs. Now, the architecture is more simplified with less computational effort as only blue channel is needed with only one feature for each classification.

A sample implementation based on the finalized system architecture is also provided. It provides both proof of concept, task summaries, as well as estimated computational cost for both fuel and O/F ratio classifications. The results show feasibility for real-time implementation in fuel classification. O/F ratio classification takes longer time, nonetheless it is still within acceptable limit. Both processes' performances can be improved further by better hardware and optimized software.

The test results ultimately show the feasibility of the proposed flame image analysis architecture. The classification rate may not be as high as expected as shown in Chapter 6. However this is due to its measured against an ideal situation which can be considered as overly pessimistic evaluation. For future work, a more objective ground-truth will also be needed in order to provide a more accurate performance evaluation.

The high speed of this promising paradigm for image-based flame analysis and classification and its relatively simple approach make it feasible for actual integration with an existing furnace control in a production environment. This task is certainly a sensible follow up and is recommended for future work.

Additional device enhancements are possible within the proposed architecture itself. One particular area of interest that can be crucial to the flame image analysis is the evaluation of different aspect of camera improvement. For example, a more detailed flame image can be obtained by using higher resolution progressive camera with faster acquisition rate. Also, multi-spectral camera with adjustable spectral sensitivity can provide further insight on the flame image visualization itself at different spectra. Naturally this implies an increase in the amount of data to be analyzed. To maintain the real-time analysis nature of the system, a dedicated hardware-based image processing tool or component may be necessary to enhance the performance speed for image acquisition, image pre-processing and feature extraction processes.

APPENDIX A Sample Feature Output for Run 15

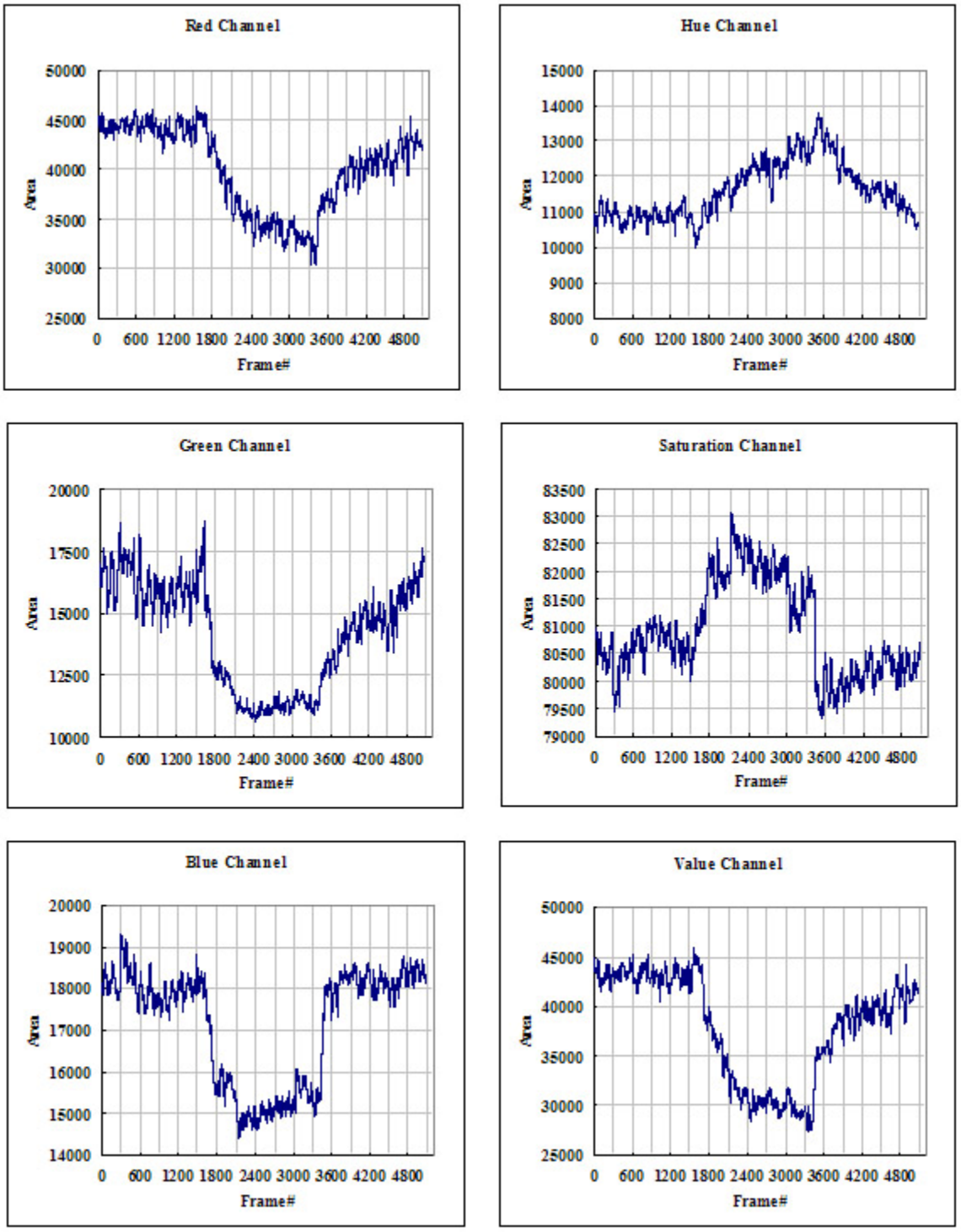

Figure 1 Set of Area Features from RGB and HSV channel for Step Change Experiment Run 15

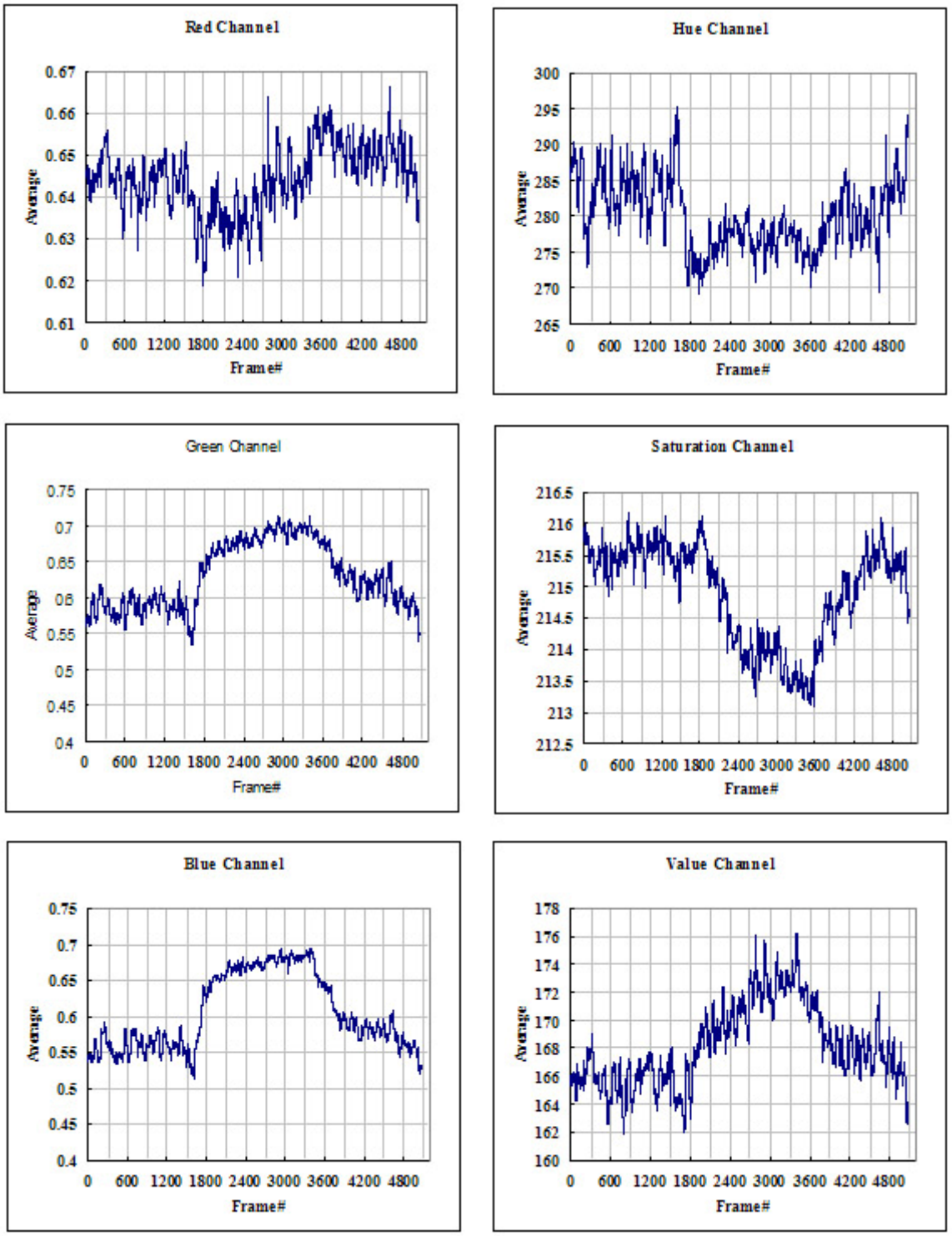

Figure 2 Set of Average Features from RGB and HSV channel for Step Change Experiment Run 15

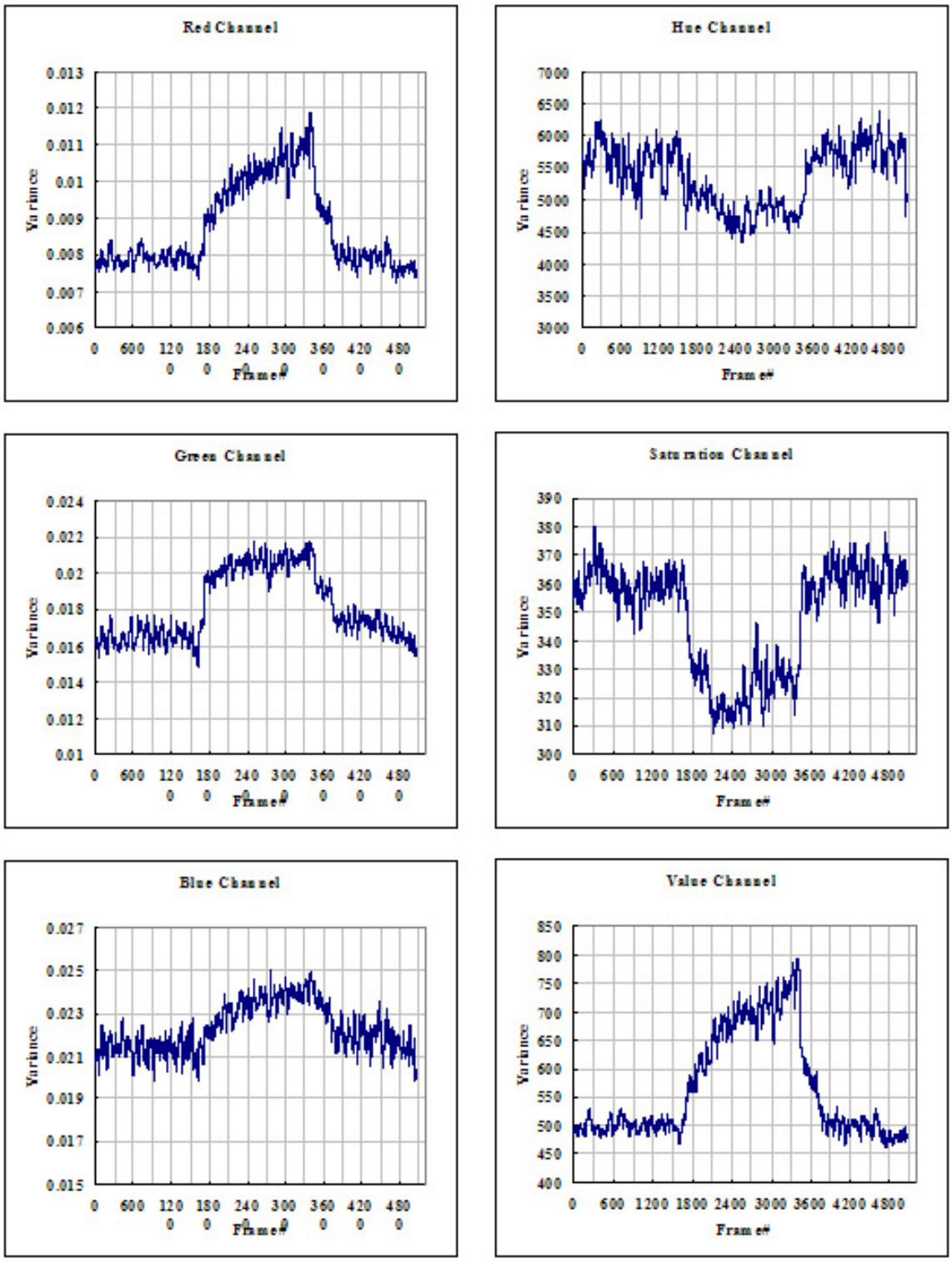

Figure 3 Set of Variance Features from RGB and HSV channel for Step Change Experiment Run 15

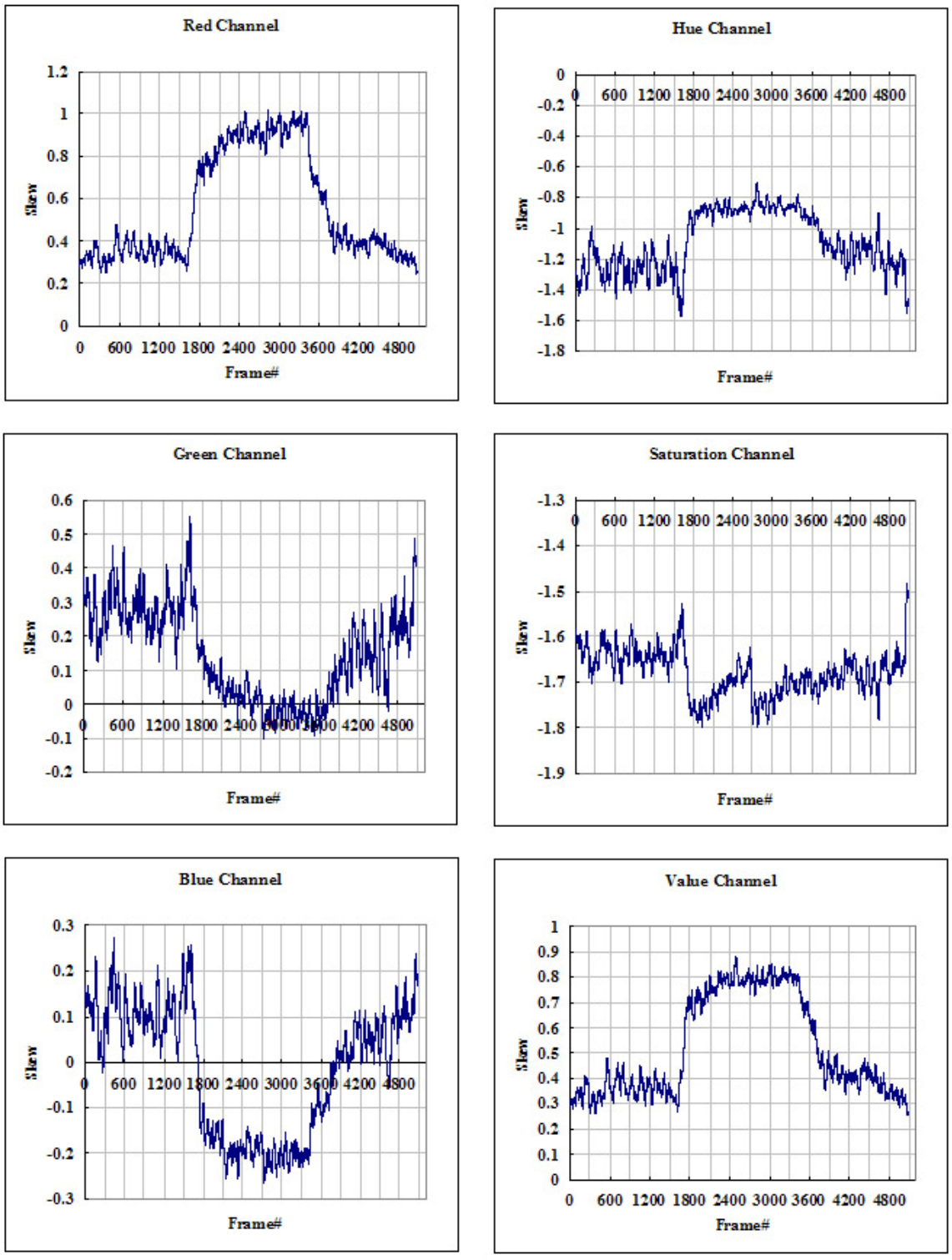

Figure 4 Set of Skew Features from RGB and HSV channel for Step Change Experiment Run 15

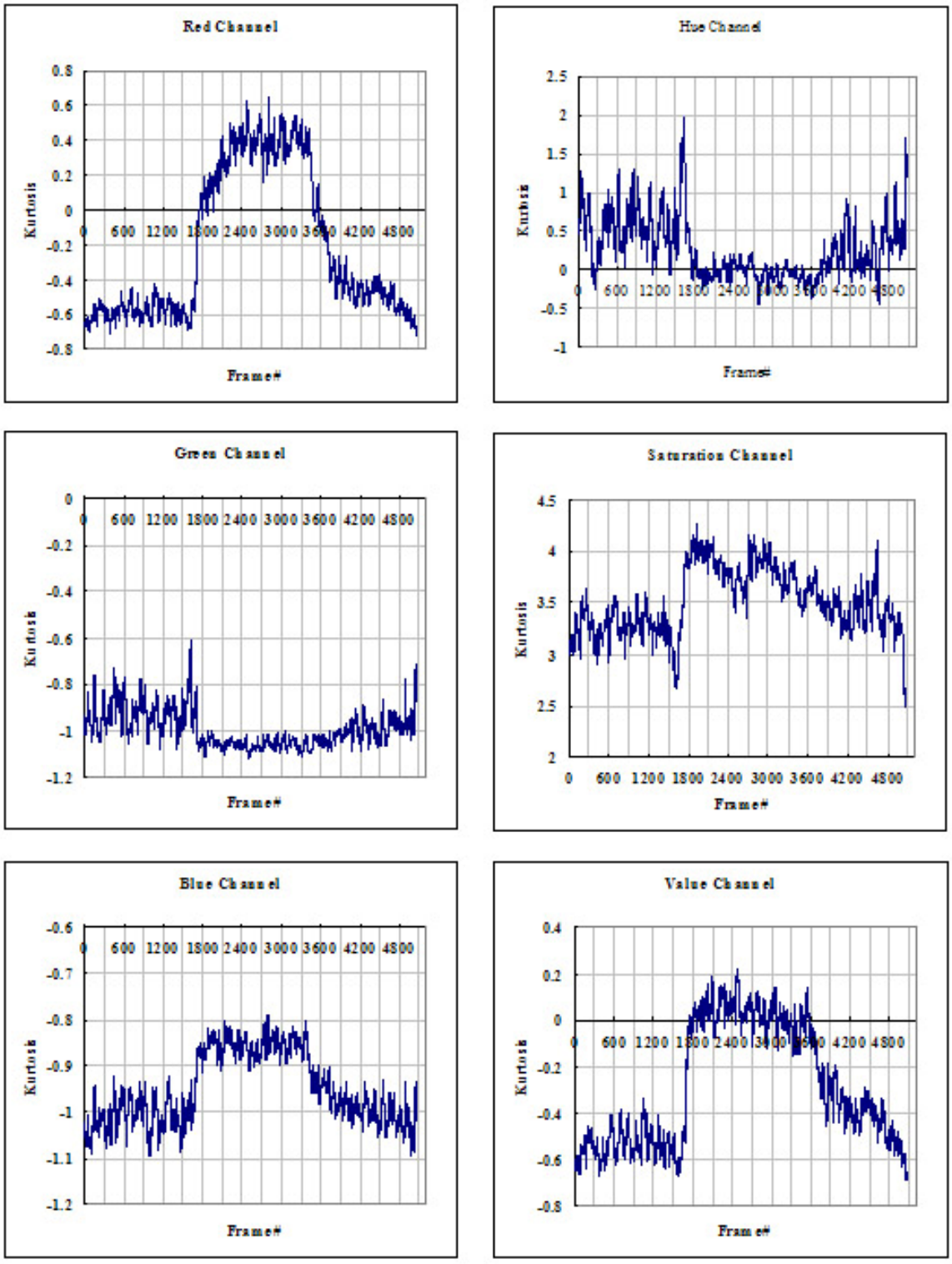

Figure 5 Set of Kurtosis Features from RGB and HSV channel for Step Change Experiment Run 15

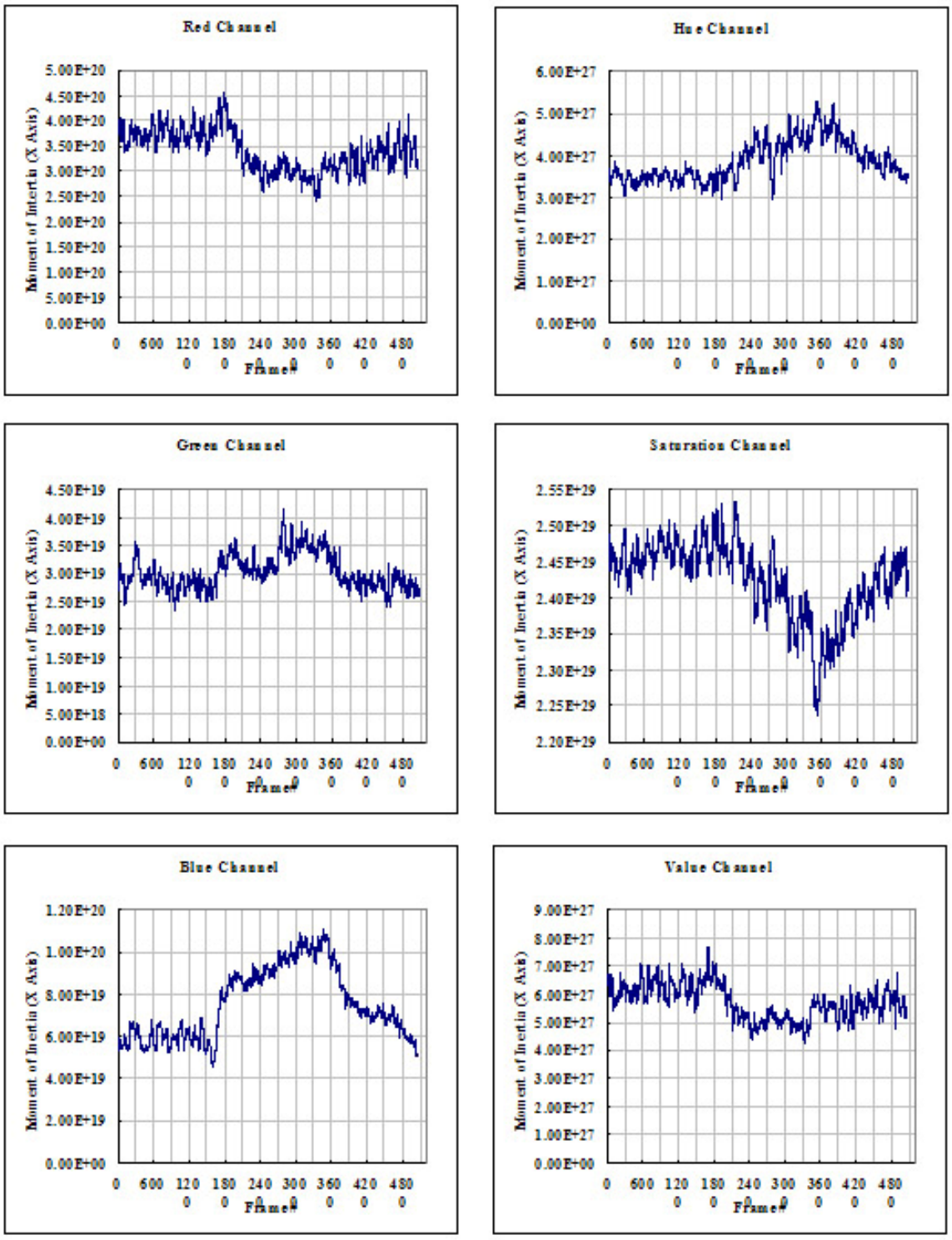

Figure 6 Set of X-axis Moment of Inertia Features from RGB and HSV channel for Step Change Experiment Run 15

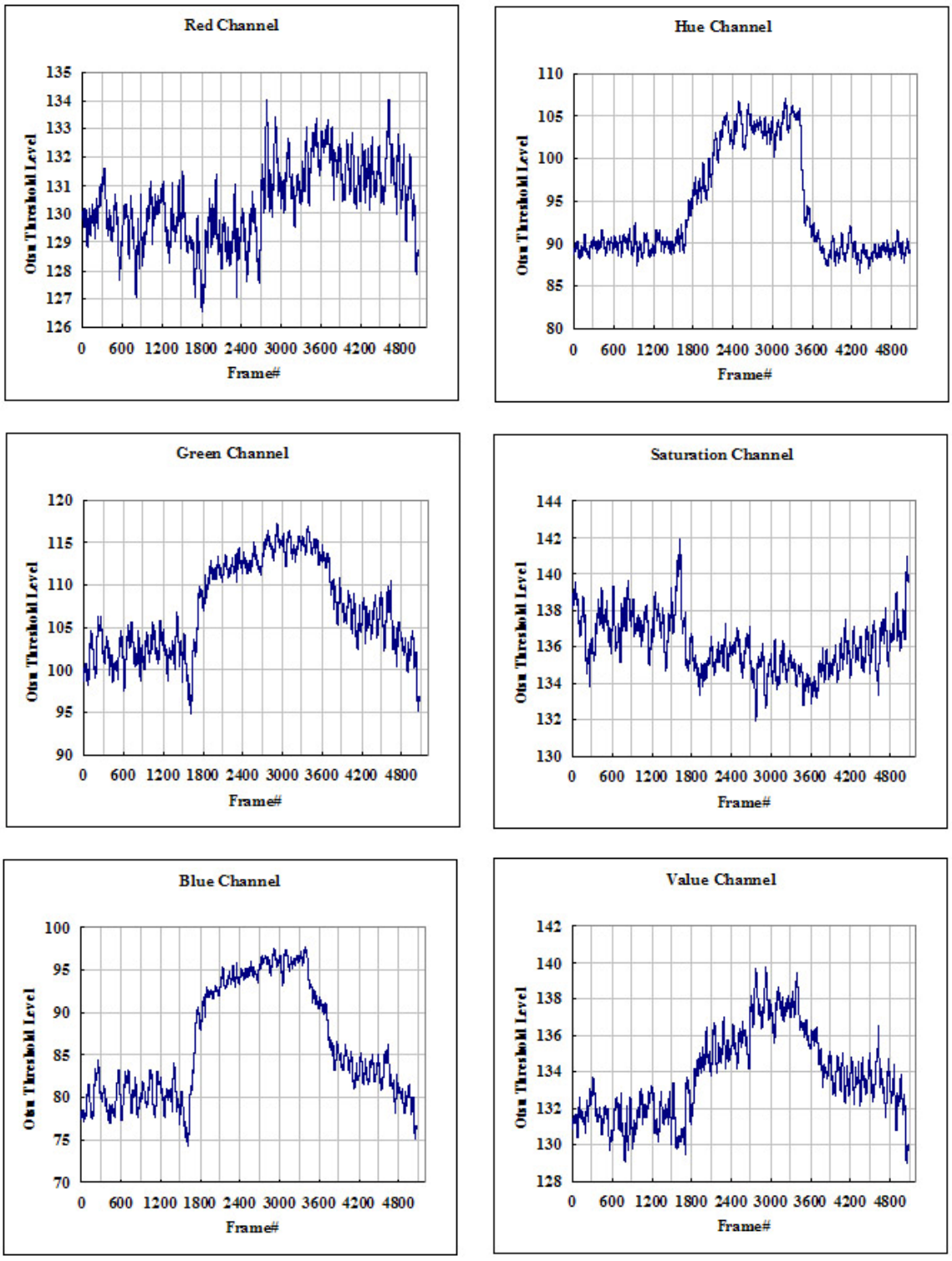

Figure 7 Set of Otsu Threshold Level Features from RGB and HSV channel for Step Change Experiment Run 15

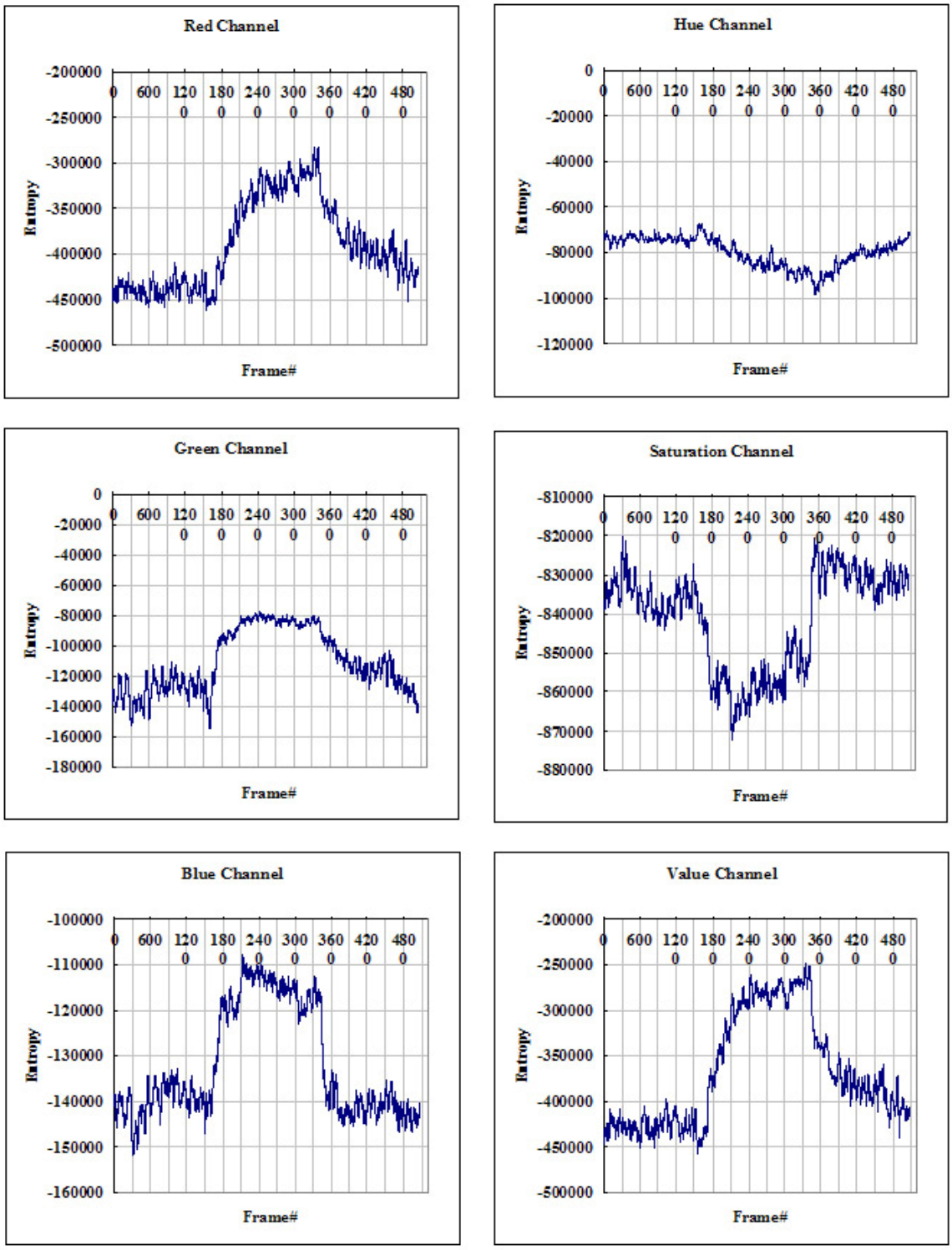

Figure 8 Set of Entropy Features from RGB and HSV channel for Step Change Experiment Run 15

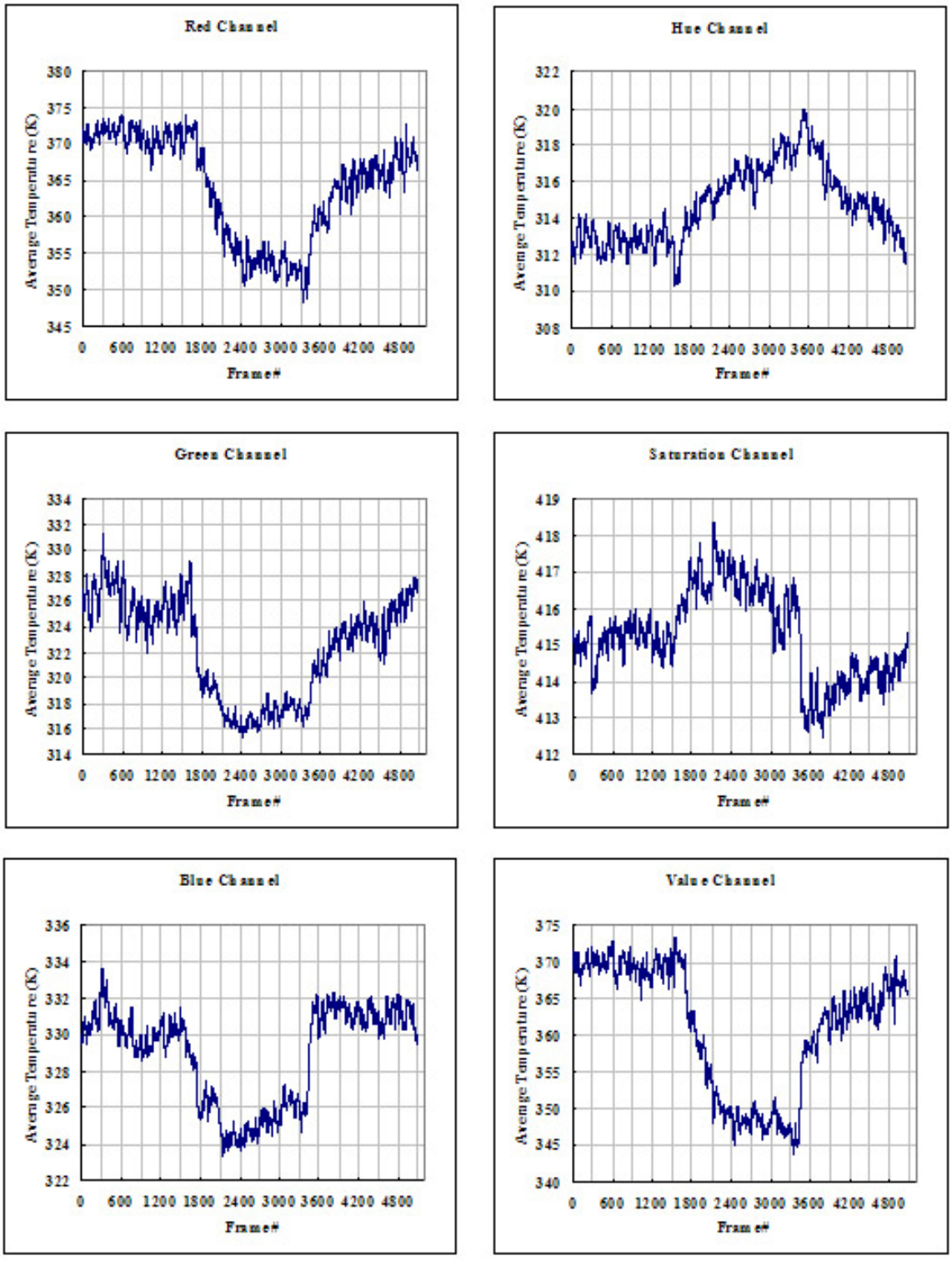

Figure 9 Set of Average Temperature Features from RGB and HSV channel for Step Change Experiment Run 15

APPENDIX B Panasonic GP KR-222 CCD Specification

- 1/2" interline transfer CCD with 768 (H) x 494(V) pixels
- 480-line horizontal resolution
- Minimum scene illumination of 3 lux at F1.4
- Signal-to-noise ratio of 50dB
- Digital signal processing circuit
- Electronic Light Control and Backlight Compensation
- C or CS-mount selectable
- S-VHS (Y/C) & Standard NTSC Composite output
- Selectable aperture level
- Auto Gain Control
- 12 Volt DC operation

Specification:

- Camera System: NTSC or PAL (GP-KR222E)
- Pick-up Device: 768 (H) x 494 (V) Pixels, interline transfer CCD
- Scanning Area: 525 lines/60 fields/30 frames horizontal 15.734kHz
- Scanning System: 2:1 interlace
- Synchronization: Internal
- Video Output: 1.0Vp-p NTSC composite / 75 ohms
- Horizontal Resolution: 480 TV lines
- S/N Ratio: 50dB (min.) (luminance S/N) (at AGC off, weight on)
- Minimum Illumination: 2 lux at f1.2 (3 lux at f1.4)
- AGC (Automatic Gain Control): Selectable on and off (approximately 14dB)
- White Balance: Selectable ATW and AWC (with white balance R/B VR)
- Aperture: Selectable - SOFT (off) / SHARP (on)
- Electronic Light Control: Equivalent to 1/60s - 1/15700s continuous variable
- shutter speed
- Lens Mount: Selectable C-mount and CS-mount
- Auto Iris Lens Type: DC Type Auto-Iris

- BLC (Backlight Compensation): Selectable normal and backlight control
- Y/C Out: Y out (1.0Vp-p/75 ohms)
- C out (0.286Vp-p/75 ohms burst level)
- Power Requirements: 10.8 to 16 Volts D.C.
- Dimensions: (excluding lens) 2 1/8"H x 2 5/8"W x 4 13/16"D
- Weight: 460g (1 lbs.)
- Operating Ambient Temperature: +14°F to +122°F

BIBLIOGRAPHY

[1] J.A. Barnar and J.N. Bradley, "Flame and Combustion (2nd edition),", Chapman and Hall, New York, 1995.

[2] J. Warnatz, U. Maas, and R.W. Dibble, "Combustion (3rd edition)," Springer, New York, 2001.

[3] A. Linan and F.A. Williams, "Fundamental Aspects of Combustion," Oxford University Press, New York, 1993.

[4] M.J. Saeger, "Spectroscopic Measurements in Flames for Glass Furnace Applications", Master thesis in Lehigh University, 2002

[5] H.D. Baker, M.E. Ryder, and N.H. Baker, "Temperature Measurement in Engineering Vol.I " John Wiley & Sons Inc, New York, 1953.

[6] L. Michalski, K. Eckersdorf, and J. McGhee, "Temperature Measurement," J.Wiley, New York, 1991.

[7] C. Romero, X. Li, S. Keyvan, and R.A. Rossow."Spectrometer-Based Combustion Monitoring for Flame Stoichiometry and Temperature Control," Applied Thermal Engineering, Vol. 25, 2005, pp.659-676.

[8] K.L. Cashdollar, "Three-wavelength Pyrometer for Measuring Flame Temperatures," Applied Optics, Vol.18, No.15, pp.2595-2597.

[9] R.A. Felice, "The Spectropyrometer – a Practical Multi-wavelength Pyrometer", the 8th Symposium on Temperature: Its Measurement and Control in Science and Industry, 2002.

[10] U.E. Meier, D. Wolff-Gassmann, J. Heinze, M. Frodermann, I. Magnusson, and G. Josefsson, "LIF Imaging of Species and Temperature in Technical Combustion at Elevated Pressures," Instrumentation in Aerospace Simulation Facilities, 18th International Congress, 1999, pp.701–710.

[11] G.S. Elliot, N. Glumac, and C.D. Carter, "Molecular Filtered Rayleigh Scattering Applied to Combustion," Measurement Science and Technology, 12 (2001), pp.452-456.

[12] D. Müller, W. Triebel, A. Bochmann, G. Schmidl, D. Eckardt, A. Burkert, J. Röper, and M. Schwerin, "Two-Dimensional Concentration and Temperature Measurements in Extended Flames of Industrial Burners using PLIF," Proceedings of the SPIE, Vol.5191, 2003, pp.66-74.

[13] W.Wojcik, T.Golec, A.Kotyra, "Combustion Assessment of Pulverised Coal and Secondary Fuel Mixtures Using the Optical Fiber Flame Monitoring System," Modern Problems of Radio Engineering, Telecommunications and Computer Science.Proceedings of the International Conference, Feb.24-28, 2004, pp.464–467.

[14] T.Shimada and T.Akiyama, "Spectroscopic Observation of Luminous Flames in an Industrial High Efficiency Test Furnace with Regenerative Combustion of Heavy Oil and Heat Analysis," Proceedings of 2000 International Joint Power Generation Conference, July, 2000, pp 1-6.

[15] J.Chen, P.Osborn, A.Paton, and P.Wall, "CCD Near Infrared Temperature Imaging in the Steel Industry," Industrial and Measurement Technology Conference, 1993, pp 299-303.

[16] M.Shimoda, A.Sugano, Y.Watanabe, T.Kimura and K.Tshiyama, "Prediction Method of Unburnt Carbon for Coal Fired Utility Boiler Using Image Processing Technique of Combustion Flame," IEEE Transactions on Energy Conversion, Vol.5, No.4, December 1990

[17] G. Lu, S. Siouris, Y.Yan, C.W.Wilson, and S.Cornwell, "Concurrent Measurement of Combustion Oscillation and Temperature of Multiple Flames in a Simulated Gas Turbine," Instrumentation and Measurement Technology Conference, Proceedings of the 21st IEEE , Vol.2 , 2004, pp.1112-1115.

[18] W.B.Baek, S.J.Lee, S.Y.Baeg, and C.H.Cho, "Flame Image Processing and Analysis for Optimal Coal Firing of Thermal Power Plant," Industrial Electronics, Vol.2, 2001, pp.928 –931.

[19] G.Szatvanyi, G.Duchesne, and G.Bartolacci, "Multivariate Image Analysis of Flames for Product Quality and Combustion Control in Rotary Kilns," Ind.Eng.Chem.Res., Vol.45, No.13, 2006.

[20] L.Bertucco, A.Fichera, G.Nunnari, and A.Pagano, "A Cellular Neural Networks Approach to Flame Image Analysis for Combustion Monitoring," Cellular Neural Networks and Their Applications, 2000.(CNNA 2000).Proceedings of the 2000 6th IEEE International Workshop on, 2000, pp.455-459.

[21] Z.Jaroszewicz, S.Y.Popov, and F.Wyrowski, "Combustion Assessment of Coal and Biomass Mixtures using Image Processing," Proceedings of SPIE, Vol.5954, September, 2005.

[22] M.G. Allen, C.T. Butler, S.A. Johnson, E.Y. Lo, and F. Russo, "Imaging Neural Network Combustion Control System for Utility Boiler Application," Combustion and Flame.Vol.94, no.1-2, 1993, pp.205-214.

[23] H. Renken, T. Bolik, Ch. Eigenbrod, J. Koenig, and H.J. Rath, "Application of a Digital High-speed Camera System for Combustion Research by using UV Laser Diagnostics Under Microgravity at Bremen Drop Tower," Proc.SPIE Vol.2869, 1997, pp.283-288.

[24] W. Fischer, and H. Burkhardt, "Three-dimensional Temperature Measurement in Flames by Multispectral Tomographic Image Analysis," Proc.of SPIE, Vol.1349, November 1990, pp.96-105.

[25] H. Fan, "Digital Analysis of Flame Images for a Natural Gas-Fired Furnace", Master Thesis, University of Missouri Columbia, May 2003.

[26] B. Jahne, "Image Processing for Scientific Applications," CPC Press, New York, 1997.

[27] W. Gunter, "Color Science: Concepts and Methods, Quantitative Data and Formulae," Wiley, New York, 1982.

[28] R.W.G. Hunt, "Measuring Color," Halsted Press, 2000.

[29] ISO 17321, "Graphic Technology and Photography – Colour Characterization of Digital Still Camera (DSCs) using Colour Targets and Spectral Illumination," March 9th 1999.

[30] S. Süsstrunk, R. Buckley, and S. Sven, "Standard RGB Color Space," Proceedings of IS&T/SID's 7th Color Imaging Conference, 1999.pp.127-134.

[31] R.S. Berns, "Principles of Color Technology, Third Edition," Wiley, New York, 2000.

[32] Panasonic KR222 camera Specifications
http://catalog2.panasonic.com/webapp/wcs/stores/servlet/ModelDetail?storeId=11201&catalogId=13051&itemId=67849&catGroupId=14872&displayTab=S&surfModel=GP-KR222&surfCategory=Discontinued

[33] H.Lee, "Introduction to Color Imaging Science", Cambridge, 2005.

[34] G.C.Holst, "CCD Arrays, Cameras, and Displays," SPIE Optical Engineering Press, Washington USA, 1998.

[35] K.Parulsi and K.Spaulding, "Color Image processing for Digital Cameras," Digital Color Imaging, CRC Press, 2003.

[36] Foveon X3 Technology Official Website
http://www.foveon.com/article.php?a=67

[37] R.Parenti, P.Verrecchia, G.Bosla and E.Pignone, “Industrialized Real-Time Flame Thermal Mapping System with Off-Line Correction of Spatial Error,” Industrial Electronics, Control and Instrumentation, 1994. IECON '94., 20th International Conference on , Vol.3 , 5-9 Sept.1994, pp.1977-1980.

[38] Lenox Borscope Official Website http://www.lenoxinst.com

[39] A.M. Tourapis, O.C.Au, and M.L.Liou, "Advanced DeInterlacing Techniques with the Use of Zonal Based Algorithms", to appear in Proc.of Visual Comm.and Image Proc., San Jose, CA, Jan'01, 2001.

[40] C.J. Kuo, C. Liao, and C.C. Lin, “Adaptive interpolation technique for scanning rate conversion,” IEEE Transactions on Circuits and Systems for Video Technology, Vol.6, No.3, June 1996, pp.317-321.

[41] T.Chen, H.R.Wu, and Z.H.Yu, “An Efficient Edge Line Average Interpolation Algorithm for Deinterlacing”, Proceedings of SPIE, Visual Communications and Image Processing 2000 (VCIP 2000), Vol.4067, No.3, Perth, Australia, 20-23 Jun’00, pp.1551-1558.

[42] R.C.Gonzalez and R.E. Woods, "Digital Image Processing", Addison-Wesley, New York, 2001.

[43] R.P. Nikhil and K.P. Sankar, "A Review on Image Segmentation Techniques," Pattern Recognition Vol.26, No.9, 1993, pp.1277-1294.

[44] P.K. Shaoo, et al., "A Survey of Thresholding Techniques", Computer Vision, Graphics and Image Processing, Vol.41, 1988, pp.233-260.

[45] N.Otsu, "A Threshold Selection Method from Gray Level Histograms," IEEE Trans.Systems, Man and Cybernetics, Vol.9, No.1, 1979, pp.62-66.

[46] W.L.Grosshandler, “The Effect of Soot on Pyrometric Measurements of Coal Particle Temperature,” Combustion and Flame, Vol.55, 1984, pp.59-71.

[47] W.L.Flower, “Optical Measurement of Soot Formation in Premixed Flames,” Combustion Science, Technology, Vol.33, 1983, pp.17–33.

[48] D.H. Rao and P.P. Panduranga, "A Survey on Image Enhancement Techniques: Classical Spatial Filter, Neural Network, Cellular Neural Network, and Fuzzy Filter," IEEE International Conference on Industrial Technology, 2006, pp.2821-2826.

[49] H. Witten, M. Neal, and G. Cleary, "Arithmetic Coding For data Compression," Communications of the ACM, Vol. 30, No. 6, June 1987, pp. 520-540.

[50] R.S. Ellis, "Entropy, Large Deviations, and Statistical Mechanics," Springer-Verlag, New York, 1985.

[51] H.C. Hottel and F.P. Broughton, “Determination of True Temperature and Total Radiation from Luminous Gas Flames,” Industrial and Engineering Chemistry (Analytical Edition), Vol. 4, No. 2, 1932, pp. 166-175.

[52] M. Planck, “Distribution of Energy in the Spectrum,” Annals of Physics, Vol. 4, No. 3, 1901, pp. 553-563.

[53] G. Lu, H.C. Bheemul and Y. Yan, “Concurrent Measurements of Temperature and Soot Concentration of Pulverized Coal Flames,” IEEE Instrumentation and Measurement Technology Conference, 2001, pp.1221-1225.

[54] G. Lu, Y. Yan, M. Colechin, and R. Hill, “Monitoring Of Oscillatory Characteristics of Pulverized Coal Flames through Image Processing and Spectral Analysis,” Instrumentation and Measurement Technology Conference, 2004. Proceedings of the 21st IEEE, Vol. 3, 18-20, May 2004, pp. 1801 - 1805.

[55] Y. Matsui, T. Kamimoto, and S. Matsuoka, “Study on the Application of the Two-color Method to the Measurement of Flame Temperature and Soot Concentration in Diesel Engines”, SAE, 1980.

[56] R.A. Rossow, "Blackbody Temperature Calculations from Visible and Near-IR Spectra for Gas-Fired Furnaces," Ph.D. dissertation in University of Missouri Columbia, 2005.

[57] D. Li, "Thermal Image Analysis using Calibrated Video Imaging," Ph.D. dissertation in University of Missouri Columbia, 2006.

[58] National Instruments LabVIEW Official Website http://www.ni.com/labview/

[59] MiniDV (IEC 61834) Standard Specification http://www.iec.ch/)

[60] Sony Camcorder Official Support Website http://esupport.sony.com/

[61] IEEE p1394 Working Group, "IEEE Std 1394-1995 High Performance Serial Bus," IEEE, 1995.

[62] Intel Official Website http://www.intel.com

[63] Microsoft Official Website http://www.microsoft.com

[64] Adobe Official Website http://www.adobe.com

[65] Y. Yuan and M.J. Shaw, "Induction of Fuzzy Decision Trees," Fuzzy Sets and Systems, Vol. 69, 1995, pp. 125–139.

[66] See5 Official Website http://www.rulequest.com/see5-info.html

[67] R. Kohavi and G.H. John, "Wrappers for Feature Subset Selection," Artificial Intelligence, Vol.97, 1997, pp. 273–324.

[68] I.S. Shaw, "Fuzzy Control of Industrial Systems : Theory and Applications," Kluwer Academic Publishers, 1998.

[69] M.G. Simões and M. Friedhofer, "An Implementation Methodology of a Fuzzy Based Decision Support Algorithm," International Journal of Knowledge-Based Intelligent Engineering Systems, Vol.1, No. 4, October 1997, pp. 267-275.

[70] L.A. Zadeh, "Fuzzy Sets," Information Control, vol. 8, 1965, pp. 338-353.

[71] M.R. Spiegel, "Theory and Problems of Probability and Statistics," McGraw-Hill, New York, 1992.

[72] G.J. Klir and B. Yuan, "Fuzzy Sets and Fuzzy Logic: Theory and Applications," Prentice Hall, 1995.

[73] E.T. Whittaker and G. Robinson, "The Method of Least Squares," Dover, New York, 1967.

[74] J.C. Ferguson, "Multi-variable Curve Interpolation," J. ACM, Vol. 11, No. 2, April 1964, pp. 221-228.

[75] Matlab Official Website http://www.mathworks.com/products/matlab

VITA

Handi Cokrojoyo was born on August 31st, 1976, in Jakarta, Indonesia. He received his Bachelor of Science degree in Computer Science from University of Wisconsin Madison, USA in 1998. He continued his education with main interest in image processing and computer graphic. He obtained Master of Science degree in Computer Science from University of Missouri Columbia in 2005. During the time, he was admitted into the PhD program as well in 2003 and involved with a join research program between Computer Science and Mechanical and Aerospace Engineering. His main research area is real-time image analysis application development utilizing image processing and machine learning implementation, for assessing combustion quality in glass furnace.